Efficient fatigue calculation via lumping block methods and the reliability for extreme wave conditions

Marten Heemskerk

Delft University of Technology

TU Delft

Efficient fatigue calculation via lumping block methods and the reliability for extreme wave conditions

by

Marten Heemskerk

Student Name	Student Number
Marten Heemskerk	4494229

TU Delft

Intecsea
Worley Group

Abstract

This thesis tests a lumping block method on accuracy in broad and narrow wave spectra. The method aims to construct a robust and efficient alternative for the computationally expensive time domain fatigue calculations of mooring lines in the early design stage of a floating offshore wind turbine (FOWT). A robust way of modelling must be applicable and reliable in all possible sea states, including extreme wavelengths, nonlinear waves, and dynamic amplification caused by the resonance frequencies. The method's reliability for different wave spectra is validated by comparing the proposed numerical lumped time-domain simulations with the original numerical time-domain simulations.

The lumping block method gives accurate damage results for narrow wave spectra. However, the model's reliability decreases when the broadening of a wave spectrum causes damage-increasing conditions, like outliers in wave periods and nonlinear waves. The lumped broad wave spectrum simulations underestimate a mooring line's structural damage, especially for wave periods above resonance. Moreover, the non-Gaussian wave-induced surge responses are the most critical parameter for reliable mooring line fatigue calculations. They must be considered for simplifying fatigue mooring line calculations in general. Furthermore, the non-Gaussian responses cause the underestimation of the proposed lumping block method for the broad wave spectra.

Nevertheless, the proposed method yields accurate but slightly conservative damage results and is robust and efficient in fatigue calculations for sea states corresponding to a narrow spectrum. Hence the lumping block method is safe and usable for significant parts of the North Sea since only middle or narrow spectra occur.

Chair member committee:	H.C. Seyffert
Committee members:	A. Coraddu, L. Pahlavan and G.D. Weymouth
Supervisor IntecSea:	Martijn van der Veer
Project Duration:	May 2022 - March 2023
Faculty:	Offshore and dredging engineering

Contents

1

Introduction

Since the beginning of the industrial revolution, humanity has caused an increase of CO_2 in the atmosphere. From 1750 the total amount of CO_2 increased from 280 ppm to 410 ppm in the 20^{th} century [56]. This increase of CO_2 causes an increase in the global temperature. To control the increase of CO_2, 20 countries signed in 2015 a global agreement at the United Nations Climate Change Conference, known as the Paris Agreement. This agreement sets a target for a maximum global temperature rise of 1,5°C. Moreover, these countries agreed to be carbon neutral in 2050, meaning a stable amount of CO_2 gasses in the atmosphere to achieve the maximum temperature rise [52].

An essential step to becoming carbon neutral is finding a solution for energy supply without a net release of CO_2. While early wind energy solutions depend on onshore wind turbines, offshore wind practices have increased in the previous decade. Offshore wind is promising because of the excellent wind conditions and the free space offshore. On the other hand, offshore structures' installation and maintenance costs are high. The global offshore wind power industry expects to double or even quadruple the total energy production in the coming decade. Figure 1.1a shows the expected growth in power production. The number of turbines is growing, and the capacity per turbine is increasing, resulting in a higher installed capacity [47].

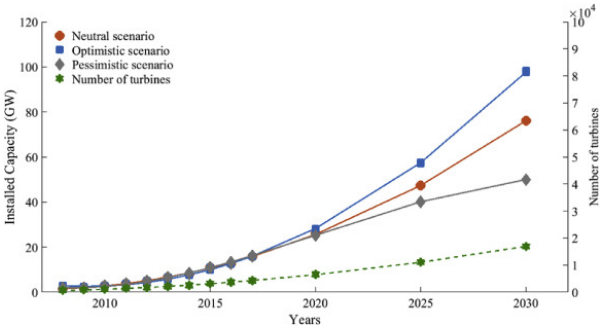

(a) Global trend growth offshore wind turbines due to increasing turbines and power production of the single turbines

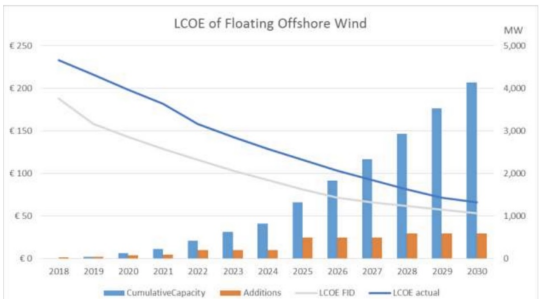

(b) Trend in cost reduction and power supply offshore wind turbines. The production and installation costs will decrease by 2-3 in the coming decade. LCOE: Levelized cost of energy

Figure 1.1: Trends in offshore wind [47]

Figure 1.2a shows two general concepts of offshore wind turbines, bottom-founded offshore wind turbines (BOWT) and floating offshore wind turbines (FOWT). Especially the North Sea is a very suitable place to install BOWT. The relatively small water depth and high wind speeds make the North Sea an economically feasible place to install BOWT. The need for offshore wind installation in deeper water increases because the total demand for green energy is still rising. From about 80 meters to several hundred meters of water depth, FOWT is the primary solution for renewable energy production.

Figure 1.1b shows the economic trend for a FOWT, the Levelized Cost of Energy (LCOE) more than halves in 2030 in comparison with 2020 [47]. The increasing power of a single turbine, in combination with technological development, causes this decreasing trend in the total cost for FOWT. The installed power of a single (offshore) wind turbine has increased to 15 MW and could grow to 20 MW in 2030. Gaining more knowledge about the technical part of offshore wind is critical for the economic feasibility of FOWT and its role as a key player in the energy transition.

Offshore wind structures
The industry developed various offshore wind turbines over the last decades. Figure 1.2a shows the most universal bottom-founded and floating models. Each model has specific properties and is suitable for different environmental circumstances. Essentially, the oil and gas industry developed most of these floating substructures. However, comparing the structural characteristics of FOWT constructions with oil and gas installations is irrelevant because of the contrasting properties of the top sides in terms of strength and material effects. In addition, the additional floaters provide static stability.

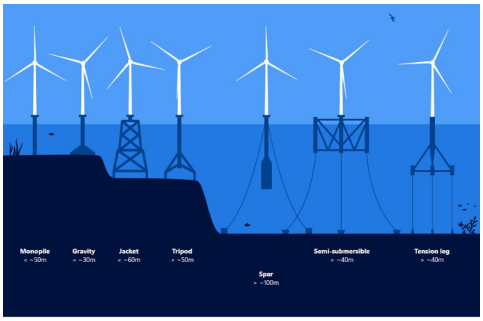

(a) Different types of offshore wind structures. Left to right: BOWT (4x) Monopile, gravity based, jacket, tripod, FOWT (3x) spar, semi-submersible, tension leg platform

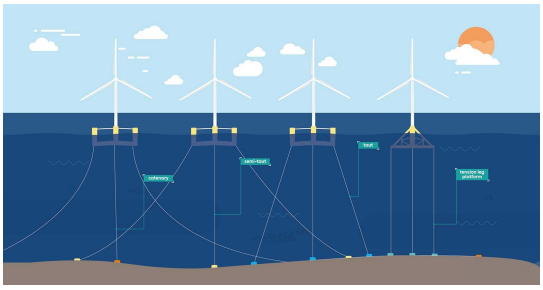

(b) Different configurations mooring line systems. Left to right: Catenary, semi-taut, taut, tension leg platform

Figure 1.2: Overview of offshore wind structures and mooring systems [14]

Figure 1.2a shows a wide variety of offshore wind energy constructions. The industry proposed a large set of technological solutions for every field of floaters. All have a bunch of components suitable for different environments. The case study of this thesis focuses on the Scotwind licensing round, which aims to install 25 GW offshore wind energy around Scotland. Intecsea's project for Scotwind consists of three different wind farms. Intecsea's client has applied for licenses for two of these wind farms, and both applications were granted. A wind farm is a set of wind turbines at the exact location with the primary goal of producing wind energy. Scotwind develops bottom-founded wind farms and floating wind farms using semi-submersibles as floaters [10].

Semi-submersible construction
This thesis focuses on semi-submersible floaters with a catenary mooring system. A triangle-shaped floater is the most frequently used semi-submersible foundation. Some concepts have three columns. Others have an additional column in the midpoint of the triangle. This case study uses a design which is numerically validated by the University of Maine [2]. Figure 1.3 shows this floater, specifically the "UMaine VolturnUS-S Semi-submersible Platform" concept. This configuration is remarkable since the wind turbine stands at a column at the midpoint of the triangle.

The active water ballast system improves the performance of the energy output. When the wind speed or direction changes, the active dynamic system adjusts the distribution of water among three active water ballasts to keep the axis of the wind turbine vertical, which is necessary to ensure the wind turbine's performance. This floating system has three catenary lines in combination with drag-embedment anchors, fairleads, and chains. The anchors moor the foundation to the seabed [2].

The following sections summarise the theoretical background and aim to justify the knowledge gap and the research question on a high level. The details can be found in chapter 2.

Fatigue limit states
The general design cycle of a FOWT is a limit state design-cycle approach with four different checks: ultimate -, fatigue -, accidental -, and serviceability limit states (ULS, FLS, ALS, and SLS). All four need to be satisfied before construction takes place. The ULS is the most critical limit state, while FLS accounts for more than 15% of the main events caused by breaching the fatigue limit state [21].

This thesis focuses on understanding the specifics of the FLS in mooring lines. In particular, the focus is on the fatigue limit state in mooring lines. FOWT will be exposed to multiple sea states during service life, causing fatigue damage. Because of the increasing size of turbines and the associated motions, fatigue damage, and therefore FLS, has become a guiding design criterion for FOWT. A sufficient and accurate fatigue assessment is essential.

For a fatigue load assessment in mooring lines, it is not sufficient to calculate the environmental loads and the resulting tensions during extreme events only, as the nature of fatigue is the accumulation of damage over time. A proper fatigue assessment requires the consideration of all relevant load scenarios over the expected lifetime of the system. Typically, this means a thorough investigation of the environmental conditions of the considered site. Furthermore, the total damage depends mainly on the environmental loads with a high probability of occurrence [35] [55].

An energy density spectrum describes the environmental conditions of waves by describing the energy level at specific wave frequencies. Roughly three spectrum states exist. Purely harmonic waves correspond to a Dirac delta energy function. The second spectrum is a modulated harmonic wave which matches a narrow wave spectrum, and the third spectrum has irregular waves described by a wide or broad spectrum. The broader the energy spectrum, the more frequencies have appreciable energy in the spectrum, resulting in a chaotic wave field. Subsequently, the components get out of phase, which results in more non-linear wave components and single outliers in wave period and - height [19].

Figure 1.3: UMaine VolturnUS-S platform is designed to support the IEA-15-240 RWT system. This type of structure is used for the case study [2]

A fatigue assessment for offshore structures can be done based on significant wave height H_s in combination with peak period T_p, the mode of the frequency spectrum. Both are presented in a wave scatter diagram. Each existing combination represents a different and unique load case. The three types of sea states (Dirac delta, narrow spectrum and broad spectrum) could have the same peak period. Although the sea states are incomparable, the input for the time simulations using in the fatigue assessment is the same. Moreover, greater fatigue damage occurs when the number of frequencies in the wave spectrum increases, concluding that a broad wave spectrum results in more total damage [5]. In addition, the fatigue damage of the mooring lines strongly depends on the dynamics of the floater, especially around the resonance peaks [55]. Environmental conditions like waves, wind and current influence the movements of the floater. Fundamental knowledge about waves is critical for predicting fatigue in mooring lines.

The offshore wind industry published only a limited number of articles on the effects of wave period or wave height on fatigue damage. Especially the impact of misinterpretations within these parameters is unknown. By comparison, the maritime industry studied these effects with great interest. An underestimation of the T_p of 10% leads to an uncertainty range of 50% to 30% underestimation of the fatigue in the mooring lines of a FPSO (Floating Production, Storage and Offloading platform) [45]. Although a FPSO and a FOWT are technically incomparable, this article shows the potential relevance of new research on interpreting wave period parameters for FOWT.

Simulations
Fatigue damage has been chiefly calculated using time - or frequency domain simulations. Mooring line damage typically uses time domain simulations due to the non-linear behaviour [13] [55]. Such a simulation is highly complicated and computationally expensive, considering all the different environmental load cases. When using a reasonably powerful computer, a complete dynamic coupled time domain simulation takes several days for a single turbine. Therefore, the industry is trying to reduce computing time. A solution is the lumping block method, which is a mathematical method that combines the original load cases into a smaller number of load cases which need to be considered in the assessment. The combined load cases have the same wave characteristics for structural fatigue damage as the original ones, resulting in fewer load cases to be simulated and decreased computational time.

Lumping block method
The methods of Jia [22], and Song [48] are very promising lumping block studies and reach an accuracy of ± 5% fatigue damage compared with the 'original' time domain simulation. With varying levels of certainty, these approaches make it possible to reduce the number of load cases by 25 to 200. Furthermore, the computational time reduces with the same factor.

However, these methods are simulated and tested in dominantly narrow-banded wave spectra, leaving the impact of the width of the wave spectrum unclear. The methods aim to construct a robust and efficient alternative for the computationally expensive time domain fatigue calculations. A robust way of modelling must be applicable and reliable in all possible sea states, including extreme wavelengths, non-linear waves, and dynamic amplification caused by the resonance frequencies.

In addition, the conclusions about the bounds of the lumping blocks are contradictory. Some studies state the bounds of peak periods when lumping have little or no influence on assessment accuracy [9]. In contrast, more recent studies indicate the choice of lumping block borders has a significant impact on the reliability of the lumping block methods [48] [20]. The explanation for the different conclusions probably lies in the stress spectrum and resonance peaks of the mooring lines.

The accuracy of a lumping block method depends significantly on the mooring line's stress spectrum. The stress or tension in a mooring line is a time-dependent variable. Moreover, it may have high amplification factors around the system's natural frequencies. The reliance on the wave period bounds probably depends on the natural frequencies of the floater. Since dynamic amplification influences fatigue damage, the relevance of accuracy caused by the impact of the boundary of the lumping period block should be correlated to the shape of the stress spectrum.

1.1. Knowledge gap

This research aims to investigate fundamental knowledge of fatigue in the mooring lines of a floating offshore wind turbine. Mooring line fatigue analysis is dominated by frequently occurring wave frequencies. Although floating wind turbines are a popular topic, it is unclear if the impact of single outliers in wave period or wave height on the damage should be considered. The effect of uncertainty in wave period with the corresponding wave load in modelling fatigue is unclear too. To understand fatigue in the mooring lines of floating offshore wind turbines, gaining fundamental knowledge is essential to learn about sea wave behaviour and the resulting forces and motions. Moreover, it should clarify their impact on modelling to discover the effect of these extreme environmental parameters.

For practical applications, the design heavily relies on simulations. The most basic, time or frequency domain simulations give good results but are respectively computationally expensive or unreliable for mooring lines. Lumping block methods are promising in saving computational time with reliable results to develop fatigue models. The challenge is finding a general way applicable to all broad wave spectra and scatter diagrams. It is important to note that a broad wave spectrum results in greater fatigue damage in a mooring line than a narrow wave spectrum, while the peak period T_p in these spectra could be the same.

Moreover, the lumping block method should be robust, efficient and accurate to reduce the computational time in fatigue damage calculations. The approach aims to slightly overestimate the fatigue damage, which means a maximum of 5% overestimation compared to the original time domain simulations, so the technique is conservative for engineering practices. Within this maximum range, the objective is an efficient technique, and the method focuses on an early design stage approach. The method of Song is the examined lumping block method.

Therefore, this thesis has two main objectives. The first goal is to test an existing reliable lumping block method in extreme sea conditions, focusing on outliers in wave periods and the irregularity of waves. A changing wave spectrum models this from a narrow spectrum to a broad spectrum. Besides testing a lumping block method, this thesis will indicate the multiplication factor appropriate to transform a wide range of frequencies into a regular wave with the same fatigue characteristics for fatigue life. This factor points out the relationship between different sea states and fatigue damage.

For the second goal, this thesis will explore the impact of the number of lumping blocks and the boundaries of these blocks. This method should discover fundamental knowledge about the effects of variations in the wave period, like extreme wave periods and the non-Gaussian behaviour of the response. Since dynamic amplification influences fatigue damage, the relevance of accuracy caused by the impact of the boundary of the lumping period block should be correlated to the shape of the stress spectrum.

2

Theoretical background

This chapter gives a technological background for the subjects of this thesis and a description of the knowledge gap. Section 1 discusses the waves and how they are described. Section 2.1 to 2.1.1 describes the linear theory necessary to describe the motions and forces on the floating platform. With the long-term wave statistics in 2.1.2 and wave spectra in section 2.1.4, the theory describes the input for the fatigue calculation.

Section 2 starts with a general description of fatigue in mooring lines, and section 2.2.1 to 2.2.5 explains how to fulfil a comprehensive fatigue assessment. Section 3 explains the relevance of lumping methods. Section 2.3.1 to 2.3.3 shows the possibilities of the developed methods and how to use them. Section 4 explains the dynamics of the floating platform. The environmental conditions are the most relevant input for this section.

Section 5 shows the relevant scenarios for fatigue damage in mooring lines. The main goal is to investigate the strengthening effects of fatigue in a FOWT and, specifically, the mooring lines. The last section 2.5.4 is about the technological background of the lumping block methods and the reliability in describing the dynamic response of the floater.

2.1. Wave theory

A typical sea surface elevation looks like figure 2.1. The total height consists of a summation of harmonic waves. Equation 2.1 shows this summation over different wave components i for wave elevation η. With N a large number of frequencies, $\underline{a}$ is the amplitude, and $\underline{\alpha}$ is the phase of a single wave. The line underneath both indicates them as a random variable. These parameters form the basis of the energy density spectrum [19]. Such a spectrum defines a random wave field consisting of several random frequencies with different probabilities. The contribution of a single frequency to the total variance is infinitely small because the spectral bandwidth of a single frequency is zero, which describes a single harmonic wave as a delta function at that frequency.

$$\eta(t) = \sum_{i=1}^{N} \underline{a}_i \cos(2\pi f_i t + \underline{\alpha}_i) \tag{2.1}$$

Moreover, the wave components are assumed not to affect one another, which is a realistic assumption for wind-generated waves [19]. Besides, this assumption guarantees linear wave theory.

The variance density spectrum

Equation 2.1 defines the amplitude model [19]. With this model, it is possible to derive the continuous variance density model, which is more relevant for practical use than the discrete amplitude model. To modify equation 2.1 into equation 2.3, the variance, $E\{\frac{1}{2}\underline{a}_i^2\}$, is distributed over frequency, f, with interval Δf_i. This is shown in equation 2.2.

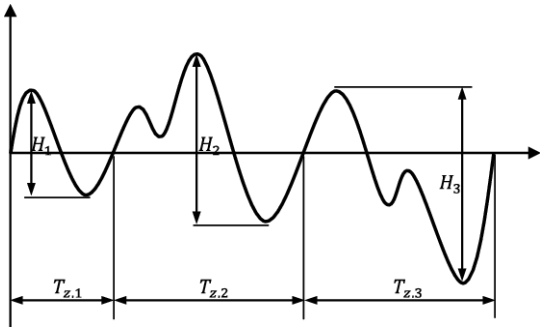

Figure 2.1: A random wave which defines a random wave height H and the zero crossing wave period T_z. The wave elevation η is the distance from the centre line to a crest or trough of a wave [19]

$$E^*(f_i) = \frac{1}{\Delta f_i} E\{\frac{1}{2}\underline{a}_i^2\} \tag{2.2}$$

Equation 2.2 is still discrete. To compose the continuous equation 2.3, the limit of the width of Δf_i is taken to zero. A spectrum analysis uses this transformation; sections 2.1.3 and 2.1.4 explain how. The Jonswap is the best-known practical example of variance density spectrum and is typically used in characterizing the North Sea [19].

$$E(f) = \lim_{\Delta f \to 0} \frac{1}{\Delta f} E\{\frac{1}{2}\underline{a}_i^2\} \tag{2.3}$$

2.1.1. Linear wave theory

Three parameters characterize a wave: height (H), period (T) and direction (θ). These parameters are visible in figure 2.2a. Equation 2.4 shows the dependency of location and time for a random wave. Where η is the elevation around the water line, k_i is the wave number of the i^{th} wave: $k_i = \frac{2\pi}{L_i}$. L_i is the wavelength of the i^{th} single harmonic wave component and ω_i is the wave frequency. x and y are the coordinates for the considered location. This equation defines the elevation at any moment in time and place. It is the origin of the derivation of wave speed and acceleration.

$$\eta(x, y, t) = \sum_{i=1}^{N} \sum_{j=1}^{M} \underline{a}_{i,j} \cos(\omega_i t - k_i x \cos(\theta_j) - k_i y \sin(\theta_j) + \underline{\alpha}_{i,j}) \tag{2.4}$$

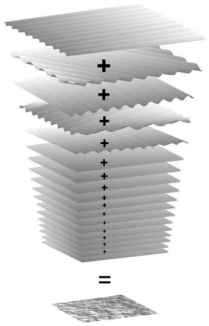

(a) A summation of a large set of harmonic waves summed to a realistic sea [42]

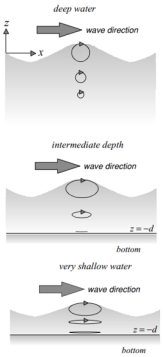

(b) Orbital movements from deep to shallow water, the orbital motion starts in circles and flattens when water becomes more shallow [19]

Figure 2.2: Motion of wave and wave particles

Equation 2.5 shows the potential theory (ϕ). $\frac{d\phi}{dx}$ results in the particle velocity u_x and the second derivative results in the acceleration a_x. d is the water depth, z is the vertical coordinate with 0 at mean sea level (MSL), and negative in the direction of the sea bed. These equations show different orbital

velocities, visible in figure 2.2b. In deep water, the wave particles move in circles. When water depth changes to intermediate water depth, first, the path will move to an oval shape path. When the water depth is shallow, the path flattens more and could become horizontal.

$$\begin{gathered}\phi = \frac{\omega a}{k}\frac{\cosh[k(d+z)]}{\sinh(kd)}\sin(\omega t - kx) \\ u_x = \omega a\frac{\cosh[k(d+z)]}{\sinh(kd)}\cos(\omega t - kx) \quad a_x = -\omega^2 a\frac{\cosh[k(d+z)]}{\sinh(kd)}\sin(\omega t - kx)\end{gathered} \tag{2.5}$$

These kinematics apply to every harmonic free and forced wave. The dispersion relationship in equation 2.6 relates the radian frequency ω and the wave number k. This relationship holds for every depth.

$$\omega^2 = gk\tanh(kd) \quad L = \frac{gT^2}{2\pi}\tanh\left(\frac{2\pi d}{L}\right) \tag{2.6}$$

Waves travel as a single wave or in groups. The phase speed is: $c_p = dx/dt = \omega/k = L/T$. Equation 2.7 derives the group speed from the dispersion relationship for an arbitrary water depth. The equation shows that long waves propagate faster than short waves.

$$c = \frac{g}{\omega}\tanh(kd) = \sqrt{\frac{g}{k}\tanh(kd)} \tag{2.7}$$

If, for example, two harmonic waves with different frequencies travel in the same direction, these waves will be in phase in some sections of the wave train and out of phase between those sections. This process consistently repeats itself, with travelling wave groups as a result. Figure 2.3 illustrates this phenomenon.

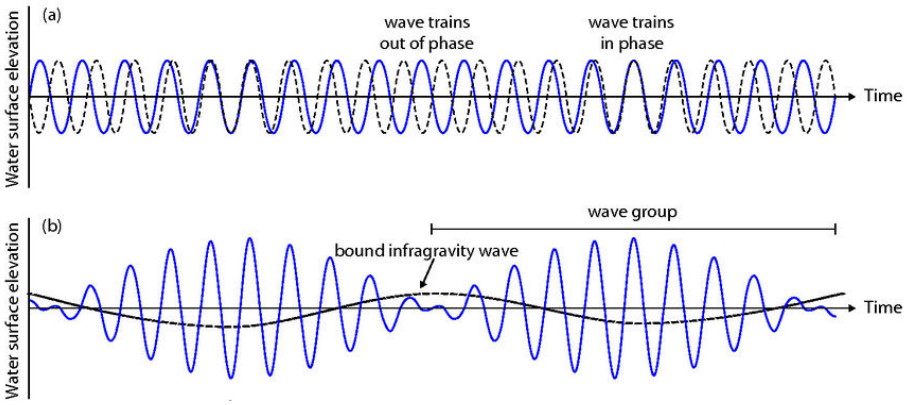

Figure 2.3: Single waves travelling in and out phase, resulting in damped or boosted waves, such a set of waves is a wave group. Moreover, the wave height and period change [11].

Wave pressure

Besides the hydrostatic Bernoulli pressure $p = \rho g z$, in which ρ is the density and g the gravitational acceleration, the waves create wave-induced pressure as expressed in equation 2.8. This pressure is in phase with the surface elevations and holds for linear wave theory, which explains the similarity with the orbital velocity in equation 2.5. The total pressure is essential for the environmental force calculation in section 2.4.

$$p_{wave} = \hat{p}_{wave}\sin(\omega t - kx) \quad with \quad \hat{p}_{wave} = \rho g a\frac{\cosh[k(d+z)]}{\cosh(kd)} \tag{2.8}$$

Wave characteristics

The characteristic wave parameters are an average set of single waves for characterising sea states in a wave record. A wave record measures the elevations of a sea state during a duration. The duration time for this record has two requirements: short enough to be stationary and long enough to obtain reliable averages. In a stationary process, the unconditional joint probability does not change as time changes, so the

mean and variance are constant with change in time. A period of 15 to 30 minutes is universally used [19].

For wave statistics, the significant wave height H_s is often used. Equation 2.9 defines H_s as the mean of the one-third largest wave heights in the wave record. Where j is the rank number of the wave, $j = 1$ indicates the rank of the lowest wave height of the highest one-third, and $H_{j=1}$ is the corresponding wave height of this wave.

$$\begin{aligned} H_{1/3} = H_s &= \frac{1}{N/3}\sum_{j=1}^{N/3} H_j \\ T_{1/3} = T_s &= \frac{1}{N/3}\sum_{j=1}^{N/3} T_j \end{aligned} \tag{2.9}$$

The wave period uses the same characteristic value. The significant wave period T_s is defined in equation 2.9 as the mean of the highest one-third wave periods in the wave record. Where j is the rank number of the wave. The time interval between two zero crossings is the zero crossing wave period, T_z [19]. For long-term wave statistics (section 2.1.2), a widely used parameter is the peak period: T_p. The peak period defines the frequency mode in the variance density spectrum.

When a sea surface elevation is a stationary Gaussian process, statistical characteristics are determined by the variance density spectrum $E(f)$. Equation 2.10 expresses the spectral moments of that specific spectrum.

$$m_n = \int_0^\infty f^n E(f)\, df \;\; for \; n = \ldots, -3, -2, -1, 0, 1, 2, 3, \ldots \tag{2.10}$$

It is possible to express T_z and H_s in terms of these spectral moments. This is done in equation 2.11 [19].

$$\begin{aligned} T_z &= 2\pi\sqrt{\frac{m_0}{m_2}} \\ H_s &= 4\sqrt{m_0} \end{aligned} \tag{2.11}$$

2.1.2. Long-term wave statistics

Wave statistics separate short-term statistics and long-term statistics. Short-term statistics express all the different wave profiles possible from a single wave spectrum. In contrast, long-term statistics predict all the different sea states the FOWT might experience over its lifetime. Long-term statistics are the leading parameter for a fatigue assessment. Section 2.2 explains fatigue damage as a time-varying parameter, where the more frequent sea states are more important than the extreme ones.

For long-term statistics, the conditions are not stationary. The basis for a long-term analysis is the characteristic values: H_s, T_p and the θ_{mean}. Typically, based on a 3-hour time interval, these values are derived. These parameters are presented in a wave scatter diagram in combination with the return period of each, like in figure 2.12.

A proper long-term wave analysis must fulfil two requirements. The time series must be statistically independent and distributed identically. In reality, this does not apply to a wave data set. For example, wave height is generally not independent. After all, a large wave height usually follows another large wave height.

To achieve statistical independence, consider only values with a sufficient separation in time. Practically, choose a single value per storm (3-hour time interval). A wave spectrum must be split into different spectra to satisfy the second condition. For example, another swell and wind wave spectrum solves this problem. This thesis uses a scatter diagram based on time series to evaluate fatigue damage.

2.1.3. Jonswap spectrum

The JONSWAP (JOint North Sea Wave Project) energy density spectrum is widely used to describe North Sea offshore waves. The Jonswap spectrum is an empirical relationship that defines the distribution of energy. Hasselmann et al. 1973 [18] concluded that a spectrum always develops with a longer fetch. It produces a sharper and higher peak for f_{peak}. The spectrum is a Pierson-Moskowitz spectrum multiplied by a peak enhancement factor. The shape is a summation of three energy sources: wind generation, non-linear wave-wave interactions (quadruplet) and dissipation (white-capping). Equation 2.12 describes the Jonswap energy spectrum, and figure 2.4 shows the developing spectrum. The energy peak and the high-frequency tail characterize this spectrum.

$$E_{JONSWAP}(f) = \alpha g^2 (2\pi)^{-4} f^{-5} \exp\left[-\frac{5}{4}\left(\frac{f}{f_{\text{peak}}}\right)^{-4}\right] \gamma_{peak}^{\exp\left[-\frac{1}{2}\left(\frac{f/f_{\text{peak}}-1}{\sigma}\right)^2\right]} \tag{2.12}$$

In which α and f_{peak} are the energy scale and the peak frequency. γ_{peak} is a peak-enhancement factor, and σ is a peak-width parameter, $\sigma = \sigma_a$ for $f \leq f_{peak}$ and $\sigma = \sigma_b$ for f > f_{peak} to account for the slightly different widths on the two sides of the spectral peak [18]. Figure 2.4 visualizes these parameters in the upper right corner. The numbers 5-11 correspond to different measurement stations, where a higher number is further offshore and, therefore, a longer fetch.

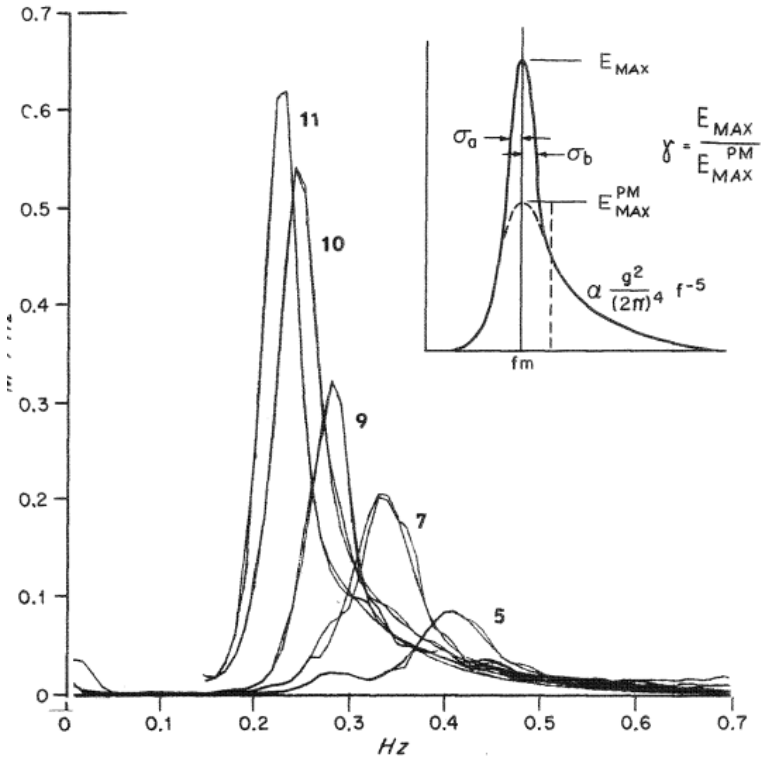

Figure 2.4: Jonswap spectrum defines different parameters f_m = peak period, σ, γ_{peak} and the Pierson-Moskowitz shaped tail for the higher frequencies. The numbers 5-11 correspond to a longer fetch resulting in a more developed spectrum [18].

Formula 2.12 has three varying shape parameters: Philips constant α, Peak-Enhancement factor γ_{peak} and width parameter σ, depending on different environmental conditions. The Philips constant varies for convenient values of environmental conditions in the range of 0.1 - 0.2. The peak-enhancement factor varies between 1 and 7. The width parameters are more or less the same. In conclusion, the Philips constant and peak-enhancement factor depend on the sea state, while the width parameter is more or less constant.

Peak-enhancement factor
The peak-enhancement factor determines the magnitude of the peak wave energy. Figure 2.5 shows the change in the spectrum for an increasing γ_{peak}, for a constant h_s and T_p [38]. When γ_{peak} increases, the spectral peak narrows. Therefore, the number of frequencies with appreciable energy negatively correlates to γ_{peak}.

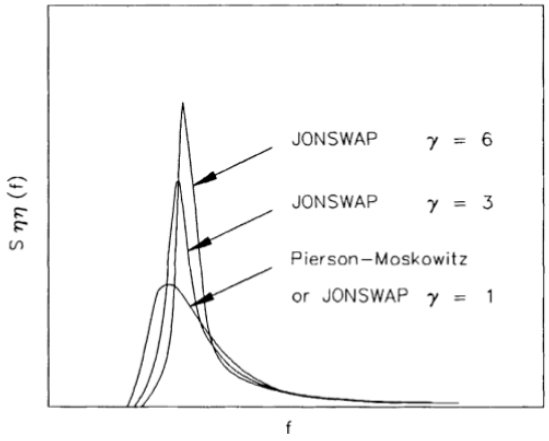

Figure 2.5: γ_{peak} in the Jonswap equation with constant H_s and T_p, $1 < \gamma_{peak} < 7$. The higher the gamma, the higher the energy at f_{peak}. $\gamma_{peak} = 1$, also known as the Pierson-Moskowitz spectrum, and describes an ocean wave spectrum, $\gamma_{peak} = 3.3$ expresses a typical Jonswap spectrum and $\gamma_{peak} = 6$ defines a narrow wave spectrum [38].

2.1.4. Impact wave spectrum on fatigue damage
Figure 2.6 shows three different energy density spectra where the degree of irregular waves increases from top to bottom. An energy density spectrum prescribes the environmental conditions of waves by relating the wave frequencies to the energy level of a single frequency. Roughly three spectrum states exist, purely harmonic waves corresponding to a Dirac delta energy function. A modulated harmonic wave matches a narrow spectrum, and the last spectrum consists of irregular waves coinciding with a broad spectrum. An irregular wave consists of many (harmonic) waves.

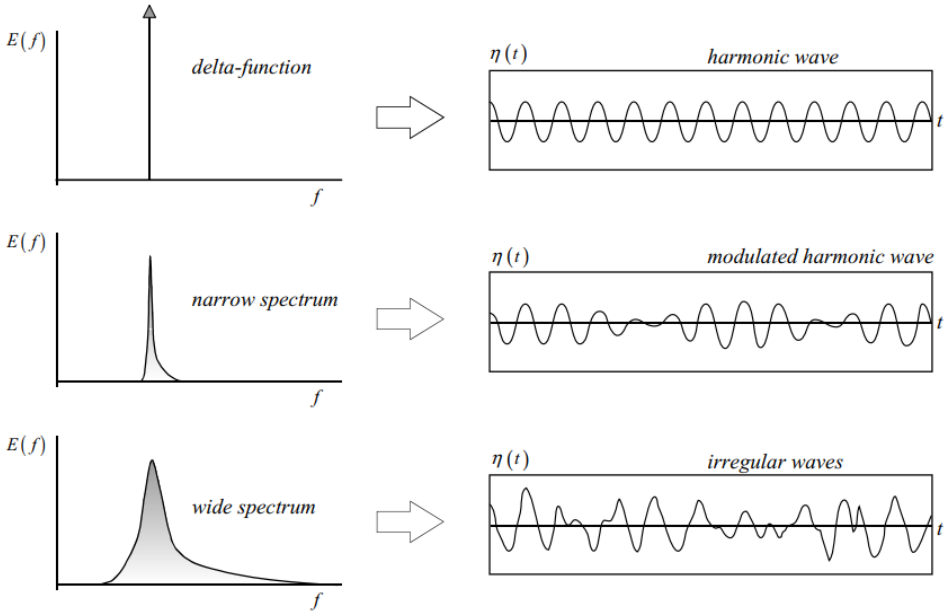

Figure 2.6: From top to bottom, starting with harmonic, more and more frequencies are present in the sea state. Resulting in an increasing broadness of the energy spectra. However, the peak period T_p remains the same [19].

The broader the energy spectrum, the more frequencies exist in the spectrum. Subsequently, the wave field becomes quite chaotic because the components in the time record get out of phase rather quickly. Resulting in more non-linear wave components and single outliers in wave period and - height. The 'broad' spectrum is the most developed and has the roughest circumstances. This thesis defines a broad spectrum as a spectrum with many frequencies resulting in non-linear wave components and more outliers in wave height or period.

When comparing sea situations, the spectrum differs, and the actual seas will be incomparable. Still, the peak period T_p remains the same since the peak period defines the frequency mode in the variance density spectrum. In addition, a fatigue assessment for offshore constructions is based on H_s in combination with T_p load cases for every wave train (3-hour wave state). Fatigue depends mainly on environmental conditions with a high probability of occurrence [50]. Besides wave height and - length, the irregularity of a wave also contributes to total fatigue. Irregular waves substantially affect the dynamic component of mooring tension despite the maximum tensile forces remaining the same regardless of wave irregularity [12]. However, a fatigue assessment uses the same parameter T_p, the frequency spreading within a wave train results in more significant total fatigue damage.

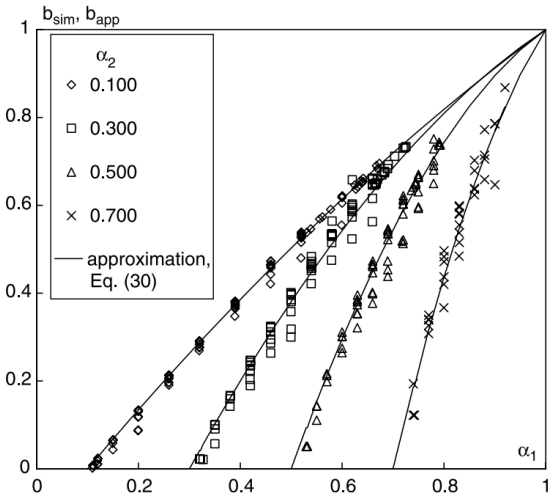

Figure 2.7: A higher damage is positively correlated to the factor α, α defines the total frequencies in an energy spectrum. b is the damage normalized by the expected damage caused by a changing wave spectrum. Showing that wave spectrum consisting of frequencies with appreciable energy results in a higher total damage [5].

Besides the input for a wave train, greater damage occurs when the number of frequencies in the total sea spectrum increases [5]. Figure 2.7 shows this increase in damage, where α defines the shape and the geometrical frequency distribution of a given spectrum, and the bandwidth parameters are defined as functions of the spectral moments in equation 2.10. b_{app} and b_{sim} relate α_1 and α_2 to the damage. Figure 2.7 clearly shows a strong dependence of damage on the α indices, showing that a broader wave spectrum results in a higher total damage [5].

2.2. Fatigue

Fatigue is the mechanism whereby cracks grow in a structure, which only occurs under fluctuating stress. Construction failure occurs in tensile stress areas when the reduced cross-section becomes insufficient to support the peak load without fracture [25].

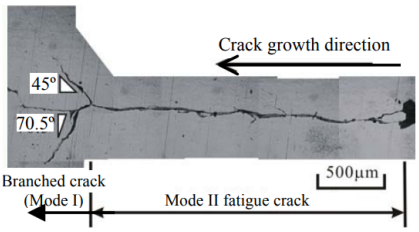

Figure 2.8: Fatigue crack profile, with the crack direction and internal angles [36]

Mooring lines in a FOWT construction will be exposed to multiple sea states during service life, causing fatigue damage. Because of the increasing turbine size and the associated motions, fatigue damage has become a guiding design criterion for FOWT. A sufficient and accurate fatigue assessment is essential.

2.2.1. Modeling of fatigue

A fatigue assessment is possible within the frequency - and time domain. A frequency domain simulation is faster and costs less computation time, making it a cheaper alternative. On the other hand, the frequency domain is less accurate than the time domain method, especially when coupled dynamic behaviour is highly non-linear. In particular, this is the case in severe sea states with non-linear waves, non-Gaussian excitation and for the mooring systems according to strongly non-linear motions [55]. With time domain simulations, it is possible to fulfil fully coupled dynamic analyses and to obtain the structural stress response. Because of the non-linear character of the mooring line, a time domain simulation is essential and indispensable for accurately calculating the fatigue damage in the long-term wave conditions.

A reliable damage calculation for long-term wave conditions must cover stochastic uncertainties. To reach such a fatigue assessment, every short-term sea state from a wave scatter diagram needs to be simulated several hundred times [55]. The following sections explain the procedure of a fatigue assessment.

2.2.2. Palmgren-Miner rule

A sea state causes random stresses at any time in a(n) (floating) offshore construction. Each stress cycle causes another degree of fatigue. Palmgren and Miner (P-M) developed a rule to couple the stress with the corresponding fatigue damage, known as the cumulative rule or P-M rule [32]. According to this rule: "the cumulative or total fatigue caused by different stress ranges is a linear summation of the individual fatigue damage from all of the considered stress ranges."

Equation 2.13 shows the dependency of the damage, d_i, in terms of the stress range S_i, with i a single cycle. Where $n_i(S_i)$ is the cycle number of the stress cycles, $N_i(S_i)$ is the cycle number that causes the fatigue failure. k_{sr} is the number of stress range intervals. In other words, the individual fatigue damage is equal to the ratio of the cycle number to the cycle number that causes a failure. D_a is the total damage. The total damage is cumulative of the single damage. Equation 2.13 shows this summation.

$$\begin{aligned} d_i &= \frac{n_i(S_i)}{N_i(S_i)} \\ D_a &= \sum_{i=1}^{k_{sr}} d_i = \sum_{i=1}^{k_{sr}} \frac{n_i(S_i)}{N_i(S_i)} \end{aligned} \tag{2.13}$$

$n_i(S_i)$ is determined with the rain-flow counting method in section 2.2.3. A S-N curve extrapolates the number of cycles to failure: $N_i(S_i)$, section 2.2.4 explains this procedure.

2.2.3. Rain flow count method

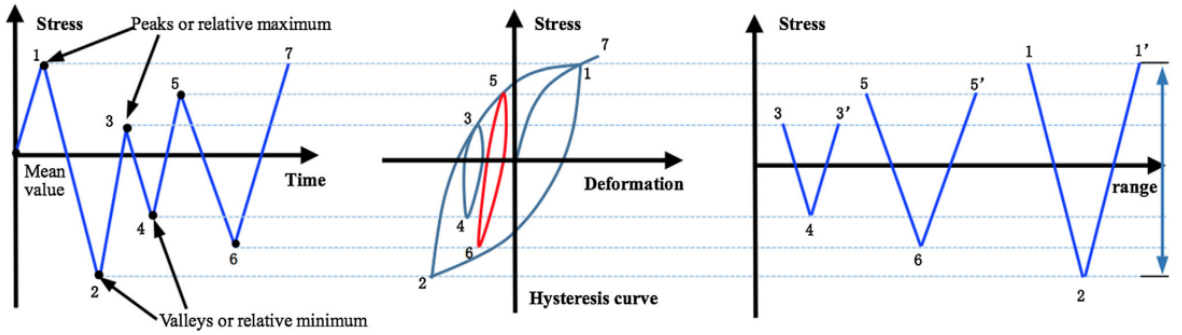

Figure 2.9: Counting algorithm: the rain flow method first indicates the maxima, secondly indicates the deformations and finally orders the critical stress cycles [48].

The environmental stresses cause a movement in the floating structure, resulting in the dynamic stress response in the mooring lines. The rain flow counting method converts these dynamic responses into stress ranges and the corresponding cycle number [43]. Figure 2.9 illustrates this algorithm. The stress range is the delta between two extremes (valley or peak). For a fatigue assessment, the largest cycles are the most critical. The algorithm identifies the essential cycles. The rain flow count method takes possible non-linear effects into account. The method is adequate and, for engineering practises, the most accurate [49].

2.2.4. S-N Curve

Figure 2.10 shows a two-segment S-N curve. The stress (σ or S) is plotted against the number of cycles, N, on a logarithmic scale. The high-stress ranges do not occur often and correspond to fewer cycles.

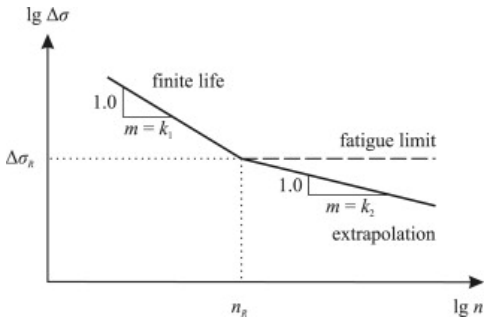

Figure 2.10: Two segment S-N curve with different directional coefficient after the critical fatigue point [29].

Equation 2.14 represents this line, where C and m are material-dependent values. C is the fatigue strength coefficient, and m is the fatigue strength exponent. A fatigue failure test determines these values, so this relation is empirical. Common values for mooring line fatigue are $m = 3$ or 5. Point n_R is the critical fatigue point, with another characteristic line [29].

$$\begin{gathered} N_i = C * \sigma_i^{-m} \\ n \leq n_R : m = k_1,\ C = A \wedge n > n_R : m = k_2,\ C = A \end{gathered} \tag{2.14}$$

2.2.5. T-N curve

T-N curves are used instead of S-N for a fatigue calculation in mooring lines. These curves have the same function unless the tension parameter is used instead of the stress parameter. Equation 2.15 shows the relation of the one-segment T-N line. The second addition to the S-N formula is the reference breaking strength (RBS). This parameter is also an empirical number.

$$N = C\left(\frac{T}{\text{RBS}}\right)^{-m}$$
$$\log_{10} N = \log_{10}(C) - m\log_{10}\left(\frac{T}{RBS}\right) \tag{2.15}$$

To express the effective tension in a mooring line for engineering practices, consider the tension at the mid-segment points and line ends. Effective tension (T_e) and wall tension (T_w) exist in a chain mooring line. No pressure terms apply in a chain. Therefore the resulting force in the chain is equal to the effective tension. Figure 2.11 shows this force balance for a mooring chain line.

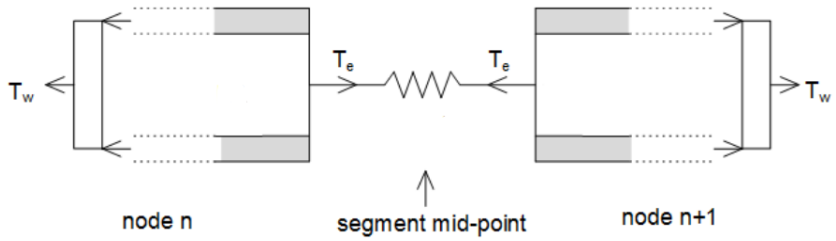

Figure 2.11: Force equilibrium: $T_e = T_w$ for chain mooring line in each node and no pressure [41].

2.3. Lumping load method

A sea state is translated into a wave scatter diagram for a fatigue assessment, as shown in figure 2.12. This North Sea scatter diagram has many combinations for H_s and T_p. This thesis defines this as a broad wave scatter diagram. Every combination represents another load case, and each H_s - T_p combination has a wave spectrum. From that spectrum, we could generate an infinite number of time series. A time domain simulation simulates a set of waves from a wave spectrum of every single combination of H_s and T_p. Section 2.1 describes the positive dependency between the number of frequencies of the sea state and the fatigue damage in the mooring lines.

H_s(m)	T_z(s)																	
	1.5	2.5	3.5	4.5	5.5	6.5	7.5	8.5	9.5	10.5	11.5	12.5	13.5	14.5	15.5	16.5	17.5	18.5
0.5	0	0	13	1337	8656	11,860	6342	1863	369	56	7	1	0	0	0	0	0	0
1.5	0	0	0	293	9860	49,760	77,380	55,697	23,757	7035	1607	305	51	8	1	0	0	0
2.5	0	0	0	22	1975	21,588	62,300	74,495	48,604	20,660	6445	1602	337	63	11	2	0	0
3.5	0	0	0	2	349	6955	32,265	56,750	50,991	28,380	11,141	3377	843	182	35	6	1	0
4.5	0	0	0	0	60	1961	13,543	32,885	38,575	26,855	12,752	4551	1309	319	69	13	2	0
5.5	0	0	0	0	10	510	4984	16,029	23,727	20,083	11,260	4636	1509	410	97	21	4	1
6.5	0	0	0	0	2	126	1670	6903	12,579	12,686	8259	3868	1408	422	109	25	5	1
7.5	0	0	0	0	0	30	521	2701	5944	7032	5249	2767	1117	367	102	25	6	1
8.5	0	0	0	0	0	7	154	979	2559	3506	2969	1746	776	277	84	22	5	1
9.5	0	0	0	0	0	2	43	332	1019	1599	1522	992	483	187	61	17	4	1
10.5	0	0	0	0	0	0	12	107	379	675	717	515	273	114	40	12	3	1
11.5	0	0	0	0	0	0	3	33	133	266	314	247	142	64	24	7	2	1
12.5	0	0	0	0	0	0	1	10	44	99	128	110	68	33	13	4	1	0
13.5	0	0	0	0	0	0	0	3	14	35	50	46	31	16	7	2	1	0
14.5	0	0	0	0	0	0	0	1	4	12	18	18	13	7	3	1	0	0
15.5	0	0	0	0	0	0	0	0	1	4	6	7	5	3	1	1	0	0
16.5	0	0	0	0	0	0	0	0	0	1	2	2	2	1	1	0	0	0

Figure 2.12: A random scatter diagram in the North Sea every cell defines a load case of a H_s and T_p.

The fully coupled dynamics in the time domain is a rather complicated and time-consuming execution. One option to reduce the computational time is simulating only the (highly) non-linear motion scenarios. However, considering mooring motions as non-linear, most load cases are significant and must be calculated. Consequently, no time reduction for the mooring line simulations can be obtained.

Another solution is using a lumping block method, an efficient method that combines the original sea scatter diagram load cases into a smaller number of load cases to consider. Each combined load case has many individual H_s - T_p combinations of the original scatter diagram. Compared to the original simulation, the lumping methods calculate an equivalent H_s and T_p for structural fatigue damage. This mathematical translation saves significant computation time by reducing the load cases of the original scatter diagram. Subsequently, the number of load cases in the time domain simulations reduces, hence the simulation time.

The challenge is to find a general method applicable to all broad scatter diagrams and possibly broad wave spectra. Moreover, it should be a robust, efficient and accurate method to improve the computational time in fatigue damage calculations. The approach aims to overestimate the fatigue damage slightly, so the technique is conservative for engineering practices. The method develops an early design stage approach.

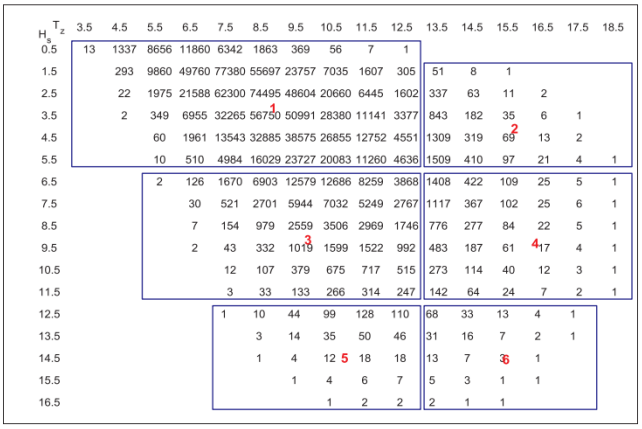

Figure 2.13: Six different lumping blocks from which an equivalent H and T must be calculated.

In general, the lumping block method (LBM) works as follows. The LBM uses equivalent H_s and T_p with similar fatigue damage to the original sea load cases. Figure 2.12 shows a random North Sea scatter diagram, with around 16 different T_p columns and 15 different H_s rows, so resulting in 240 load cases. Figure 2.13 shows six possible blocks. An equivalent H_s and T_p are calculated in each lumping block. The time domain simulations run only on these six combinations. The fact that these values should represent all other load cases within the corresponding block makes the values a parameterisation of reality. So this parameterisation reduces computational time by a factor of 40. But even a decrease from 240 original scatter diagram load cases to one equivalent combination of H_s and T_p is possible with reliable results [48] [53].

2.3.1. Early adopters

DNV, Det Norske Veritas [53], is a Norwegian classification engineering agency for the maritime and offshore industry. The organisation provides guidelines and requirements in risk management, quality and safety requirements and, among other things, fatigue calculations for various offshore structures. DNV judges calculation methods and decides if they are allowable. The organisation already sets the first requirement for the LBM in engineering practice, according to the DNV code:

"Fatigue damage resulting from a representative sea state should not be smaller than that contributed from the original sea states in the lumping block. The allowed DNV method sets the representative wave height into a wave height interval larger than the largest wave height in the lumping block. In addition, the representative wave period is set to a half wave period interval larger than the averaging of the wave period encompassed by the lumping block" [53].

Because this method does not consider the probability of occurrence and only works with maxima, the method extremely overestimates the damage. Equation 2.16 shows the approach for the DNV model. H_{srj} is the equivalent wave height, and T_{zrj} is the equivalent wave period. H_{skj} and T_{zkj} are the significant wave height and period of the k^{th} original sea state. The $max[]$ function indicates the maximum wave height in the corresponding original block. ΔH_s and ΔT_z are the interval of the significant wave height and period [53].

$$\begin{aligned} H_{srj} &= \max_{1 \le k \le n_j} [H_{skj}] + \Delta H_s \\ T_{zrj} &= \frac{\sum_{k=1}^{n_m} T_{zkj}}{n_m} + \frac{\Delta T_z}{2} \end{aligned} \tag{2.16}$$

In cooperation with DNV, Sheehan [46] proposed an improved method by combining the largest wave height with the representative wave period as the probabilistic average of the wave periods. But this research also disregards the probability of the occurrence of sea states. Mittendorf [33] developed a lumping method by lumping all the sea states with the same wave height with an average wave period. Burton [7] lumped all the same wave periods and determined the equivalent wave height based on a relation between the probability of wave height and the fatigue slope. These methods are over-conservative, unreliable for a variation in H_s and T_p or only applicable for a single situation.

2.3.2. Jia

Jia [22] set up a new method based on Burton and Mittendorf and is the first method not dependent on the block range of H_s and T_p. The method slightly underestimates the fatigue damage. Moreover, the technique is not sensitive to the number of blocks and predicts fatigue with a 95% certainty [22]. Still, Jia's method underestimates the mooring line damage of a FOWT by 5% compared to the original time domain simulations.

Jia's model adopts the linear wave theory. Therefore, it does not include non-linear wave motions, though the model has a reliable accuracy for OFWT [48]. The model has been made for OWT, like jackets or jack-ups [22].

Equation 2.17 shows the equivalent wave height, period and probability. Jia expresses the fatigue proportional to the m^{th} power of the original wave significant wave height, H_{skj}. m is the slope parameter of the S-N curve. Along with the probability of the original sea state, p_k and the likelihood for the representative blocked sea state, p_{rj}.

$$H_{srj} = \left(\frac{\sum_{k=1}^{n_j} H_{skj}^m \, p_k}{p_{rj}} \right)^{1/m} \quad T_{zrj} = \frac{\sum_{k=1}^{n_j} T_{zkj} \, p_k}{p_{rj}}$$
$$p_{rj} = \sum_{k=1}^{n_j} p_k \tag{2.17}$$

2.3.3. Song

Song based his theory on the work of Jia. The study proposed a first method [49] whereby the spectral moments of the original sea states are weighted. The theory is, in essence, robust and accurate. However, the method's accuracy decreases significantly when the number of original sea states in the blocks increases.

The second method of Song [48] is based on the assumption that the fatigue is proportional to the i^{th} power of the spectral wave energy, which is called the 'spectral moments equivalence' (SME). The accuracy is even better than the first method, slightly conservative and not sensitive to the number of blocks. However, the study only validates the method for a narrow wave spectrum [48].

$$D_{a_k} = m_{0k}^{\zeta m}$$
$$D_{a_j} = \sum_{k=1}^{n_j} D_{a_k} \, p_k = \sum_{k=1}^{n_j} m_{0k}^{\zeta m} \, p_k \tag{2.18}$$

This method is based on the cumulative fatigue damage, D_{a_k}, of the cumulative sea state in equation 2.18. This damage function depends on the spectral wave energy, m_{0k}, to the power of ζm. m is the slope parameter from the $S-N$ or $T-N$ curve, and ζ is an exponent linking spectral wave energy to the cumulative damage. Song uses γ in the paper [48]. Since γ_{peak} is a leading variable in this thesis, ζ will be used instead of γ to prevent confusion. For a square FOWT: $\zeta = 0.67$ [48]. Multiplying the damage by the probability p_k calculates the cumulative fatigue damage resulting from the original sea states in the j^{th} lumping block. n_j stands for all the sea states in the j^{th} lumping block in this equation.

$$D_{a_{rj}} = m_{0rj}^{\zeta m} \, p_{rj} \tag{2.19}$$

According to equation 2.17 and 2.18, the fatigue damage contributed from the equivalent spectral wave energy of a representative sea state can be given in equation 2.19. Where m_{0rj} represents the equivalent spectral wave energy of the j^{th} representative sea state [48]. Rewriting equation 2.19 and combining with equation 2.18, results in the expressions for m_{0rj} and m_{2rj}.

$$\begin{aligned} m_{0rj} &= \left(\frac{\sum_{k=1}^{n_j} m_{0k}^{\zeta m} p_k}{p_{rj}} \right)^{\frac{1}{\zeta m}} \\ m_{2rj} &= \left(\frac{\sum_{k=1}^{n_j} m_{2k}^{\zeta m} p_k}{p_{rj}} \right)^{\frac{1}{\zeta m}} \end{aligned} \tag{2.20}$$

In equation 2.21, the spectral moments are combined with the statistical correlation from section 2.1.1. The equivalent significant wave height and wave period formula can be determined [48].

$$\begin{aligned} H_{srj} &= 4.00 \beta_j \sqrt{m_{0rj}} \\ T_{zrj} &= 2\pi \sqrt{\frac{m_{0rj}}{m_{2rj}}} \end{aligned} \tag{2.21}$$

Where β_j is a correction factor related to the significant wave height and fatigue. The correction factor β_j should be considered as the influence of the s-n curve slope to keep the dimensional consistency. The factor β_j and ζ are the main points of improvement between the first [49] and the second method [48] of Song. Section 2.5.4 explains these variables theoretically.

$$\beta_j = (n_j)^{\frac{1}{4mn_j}} \tag{2.22}$$

2.4. Dynamic response of a FOWT

Section 2.2 introduces the fatigue dependency of different stress cycles. The mooring systems' stress cycles arise from the floating platform's motions. This section explains the wave loads. After discussing the wave stresses, section 2.4.2 explains the restoring forces. The concluding remark is the sum of all the different forces in the equation of motion.

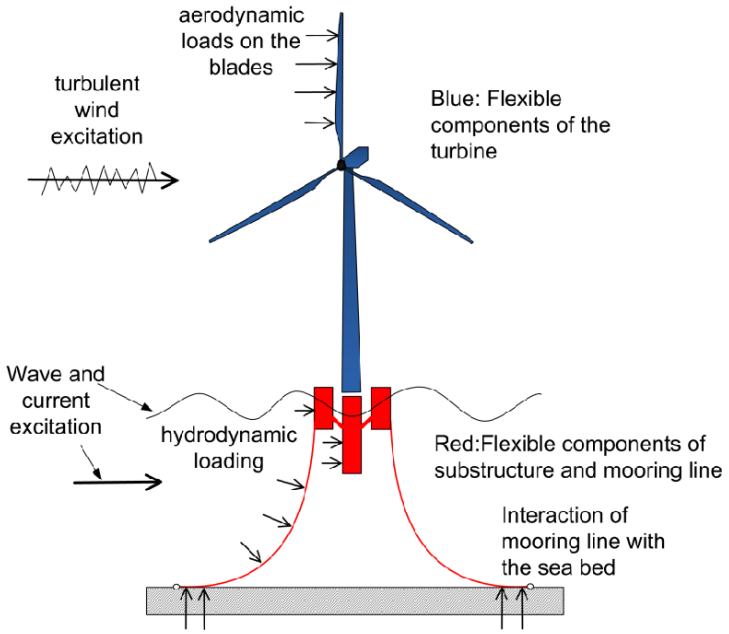

Figure 2.14: Environmental forces on a FOWT, waves, wind and current. The waves are the leading forces, followed by the wind. The current has the lowest impact on the dynamic response [31].

2.4.1. Environmental loads

Three main forces expose to a FOWT are the waves, wind and current. Figure 2.14 shows these different forces. These forces are time-dependent and oscillate due to natural and site-specific circumstances. The time dependency makes the fatigue damage dependent on these forces. Since the FOWT is only exposed to wave loads in the case study, these loads are explained. The impact of the assumptions in the case study is discussed in section 5.5

Wave loads

The acceleration and velocity of a wave depend on the time and place, as shown in section 2.1.1. The corresponding forces for a slender construction can be calculated with the Morison equation [34]. Equation 2.23 shows the calculation for the total force, $f(z)$. The total force depends on a drag component ($f_d(z)$) and an inertia component ($f_i(z)$). ρ is the water density, C_d the drag coefficient, C_m the inertia coefficient and D the diameter. $u(z)$ and $\dot{u}(z)$ are the water particle velocity and acceleration. Because of the shape of a wave, the maximum wave-particle acceleration is always 90° ahead of the velocity. The maximum force is, therefore, the vector addition of the two load components.

$$f(z) = f_d(z) + f_i(z) = \frac{1}{2} * \rho * C_d * D * u(z) * |u(z)| + \frac{\pi}{4} * \rho * C_m * D^2 * \dot{u}(z) \tag{2.23}$$

Since the maximum force consists of vector addition, the force could be drag or inertia-dominated. This domination is the case when one of the components is significantly larger than the other. The Keulegan-Carpenter number provides a set of rules to indicate if a component dominates one. Equation 2.24 shows these rules. A structure is inertia dominated when $KC < 3$ and drag-dominated when $KC > 45$ [24].

$$KC = \frac{u_{max} T}{D} = \frac{\pi H_{max}}{D} \tag{2.24}$$

The use of the Morison equation is only possible when the construction is slender. A structure is slender when the slenderness ratio is higher than 12, as shown in equation 2.25. This relation divides the effective length (L_{eff}) by the least radius of gyration, r. In addition, I is the moment of inertia, and A is the area.

$$\lambda = \frac{L_{eff}}{r} = \frac{L_{eff}}{\sqrt{\frac{I}{A}}} > 12 \tag{2.25}$$

A semi-submersible is a typical non-slender structure, whereas transfer functions must be used to calculate the motions according to the wave force. These transfer functions are called RAOs: response amplitude operators. Different RAOs exist, for example, a force or response RAO. A force RAO consists of a pair of numbers. These numbers define the force and moments of the floater. A response RAO relates the amplitude of the floater response to the amplitude of the wave and phase, which defines the timing of the floater response relative to the wave.

A RAO for linear forces can be assembled into an equation of motion. See equation 2.26. x is the motion of the rigid body, and ω is the frequency. M is the mass and inertia matrix, $A(\omega)$ is the added mass matrix, $B(\omega)$ is the linear damping matrix, C is a stiffness matrix, and $F(\omega)$ is the wave force.

$$[M + A(\omega)]\ddot{x} + B(\omega)\dot{x} + Cx = F(\omega) \tag{2.26}$$

The force is proportional to the incoming wave: $\zeta = \zeta_a e^{i\omega t}$, with ζ_a the wave amplitude. To calculate the RAO, assume $x = ae^{i\omega t}$. As a result, equation 2.27 gives the RAO. In this equation, F_0 is the force per wave height. Figure 4.5 displays the RAO for this thesis.

$$RAO(\omega) = \frac{a}{\zeta_a} = \frac{F_0}{C - (M + A(\omega))\omega^2 + iB(\omega)\omega} \tag{2.27}$$

2.4.2. Mooring loads

Floaters use different mooring systems to ensure the desired place of the floater. Several mooring systems are possible to withstand all environmental forces. Figure 1.2b gives an overview of four mooring types. Generally, two configurations are possible: catenary, used in this thesis, and taut mooring systems.

Catenary mooring lines

A catenary system is a flexible line suitable for deeper water depths. Usually, the line's material is chain or steel. The net-own weight, in combination with the buoyancy of the line, creates the restoring force. Equation 2.28 describes the shape of the line by parameter z. The maximum horizontal displacement, x_{max}, is reached at $z = h$, where h is the water depth.

$$\begin{aligned} z &= \frac{F_x}{w}\left[\cosh\left(\frac{w}{F_x}x\right) - 1\right] \\ x_{max} &= \frac{F_x}{w}\cosh^{-1}\left(\frac{hw}{F_x} + 1\right) \end{aligned} \tag{2.28}$$

The variable S gives the total suspended cable length. Equation 2.29 describes S, w defines the line weight in water, and F_x is the governing horizontal force. The corresponding force in the mooring line is the $F_{z,max}$ [30].

$$\begin{aligned} S &= \frac{F_x}{w}\sinh\left(\frac{w}{F_x}x\right) \\ F_{z,max} &= w * S = F_x \sinh\left(\frac{w}{F_x}x_{max}\right) \end{aligned} \tag{2.29}$$

2.4.3. Hydromechanics

In figure 2.15a, the vertical force equilibrium of a floater is visible. The Archimedes principle describes this equilibrium: The upward buoyant force for a (floating) object equals the displaced fluid (or gas) weight. Figure 2.15b shows the rotational equilibrium. When the wind turbine is in stable equilibrium and the wind turbine is subjected to a force, the floater heels by this created moment. This heeling leads to some heel angle ϕ. Because of the heel ϕ, the centre of buoyancy shifts to B_ϕ and the buoyancy force acts from the new point. This new point of engagement creates a moment which opposes the angle ϕ, and the floating systems shifts to the original state [23].

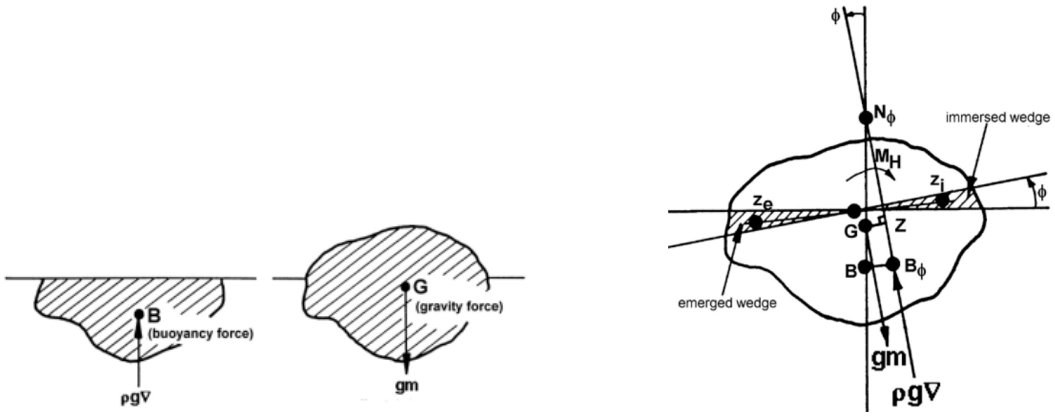

(a) Definition of centres and forces in a floating structure. The vertical equilibrium buoyant force equals the gravity force causing the floating mechanism.

(b) Heeling moment in a floating structure, the increasing couple when the heeling angle increases

Figure 2.15: Forces and moment in a random floating structure [23]

2.4.4. Equation of motion

A floating wind turbine has six different degrees of freedom. Figure 2.16 gives the names and directions. Three motions are translation motions, and the three others are rotation motions. The equations of motion describe the motions of a floating wind turbine. Equation 2.30 represents the general form of the EOM for any floating object. This 6-DOF equation expresses every direction independently [23].

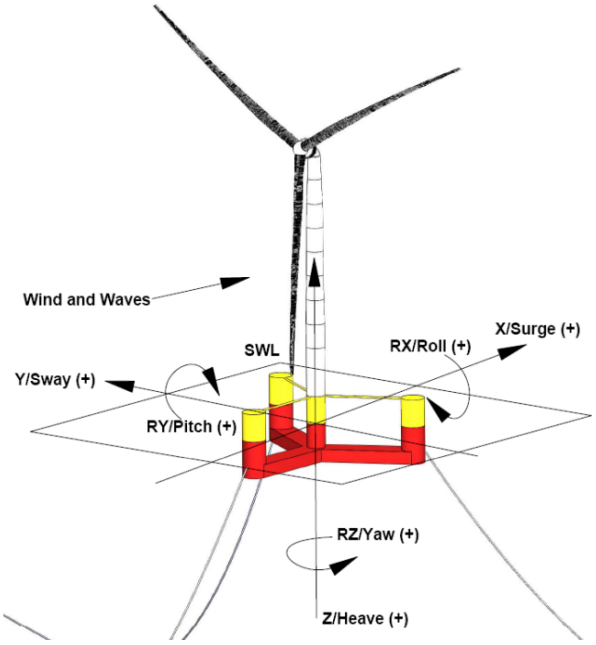

Figure 2.16: Reference frame FOWT that defines the direction of movement of sway, pitch, heave, yaw, surge and roll [2]

$$\begin{gathered}[M + A(\omega)]\ddot{x} + B(\omega)\dot{x} + Cx = F_{total}(\omega) \\ F_{total} = F_{wave} + F_{wind} + F_{current} + F_{mooring} + F_{hydromechanics}\end{gathered} \tag{2.30}$$

In this equation, M, A, B, and C are all [6x6] matrices which denote the: mass + inertia, added mass, linear damping and stiffness, respectively. x is a [6x1] motion vector containing the motion for each degree of freedom. $\ddot{x}$ and $\dot{x}$ are the first and second-time derivatives of the displacement and, therefore, form the acceleration and velocity. F_{total} is the [6x1] force vector, which contains all the external forces and moments described in section 2.4.1 to 2.4.3. This formula expresses the displacements at any moment in time.

2.4.5. Stress spectrum mooring chain

Floating systems are subjected to dynamics by waves caused by wave frequency (WF) motions. Moreover, the system is also subjected to low-frequency (LF) motions. Newman [39] derived an approach to calculate the second-order wave force caused by LF. Equation 2.31 expresses the diagonal components of the quadratic transfer function (QTF), also known as the mean wave drift force. The LF force is calculated with equation 2.32.

$$H^{(-2)}(\omega_i, \omega_j) \cong \frac{1}{2}\left[H^{(-2)}(\omega_i, \omega_i) + H^{(-2)}(\omega_i, \omega_j)\right] \tag{2.31}$$

$$F^{(-2)}(\omega_d) = \sum_{|\omega_i - \omega_j| = \omega_d} a_i a_j H^{(-2)}(\omega_i, \omega_j) \tag{2.32}$$

Equation 2.33 gives the motions for the LF, and equation 2.34 shows the WF motions originated by the wave spectrum. The total platform motion, $M(\omega_F)$ is the sum of $M^{(-2)}(w_L)$ and $M^{(1)}(\omega)$.

$$M^{(-2)}(w_L) = \frac{F^{(-2)}(\omega_L)}{T_F^1(\omega_L)} \cdot T^{(1)}(\omega_L) \tag{2.33}$$

$$M^{(1)}(\omega) = T^{(1)} \cdot \sqrt{2S(\omega)\, d\omega} \tag{2.34}$$

To calculate to total force, $F(\omega_f)$, $M(\omega_F)$ is calculated with the stiffness K in equation 2.35.

$$F(\omega_f) = K \cdot M(\omega_F) \tag{2.35}$$

The mooring line stress $R_S(\omega_F)$ is proportional to the dynamic amplification factor and the total force. This is shown in equation 2.36.

$$\begin{gathered}\alpha_d(\omega_F) = \frac{1}{\sqrt{1 - \left(\frac{\omega_f}{\omega_0}\right)^2 + \left(2\zeta\frac{\omega_f}{\omega_0}\right)^2}} \\ R_S \sim F(\omega_f)\alpha_d(\omega_F)\end{gathered} \tag{2.36}$$

In conclusion, the stress spectrum is proportional to the power of the mooring line stress, as shown in equation 2.37.

$$S_S(\omega_F) = \frac{1}{2}\frac{R_s^2(\omega_F)}{d\omega} \tag{2.37}$$

2.5. Fatigue in a floating wind turbine

2.5.1. fatigue in tower, floater and blades

Floating wind turbines are a relatively new concept for energy production, and technical development is essential for the feasibility of floating offshore wind turbines. Different studies have already contributed to describing the fatigue behaviour of a floating wind turbine. Kvittem et al. [26] did a long-term fatigue assessment with time domain simulations for a semi-submersible. The study showed that blade passing frequency resonance in the tower and the pitch motion of the platform are the most significant contributors to fatigue damage in the tower and pontoon. Also, the misalignment of wind and waves contribute to a high level of fatigue on the platform. Other contributing scenarios for fatigue are:

- Wave length corresponds to wave forces with 180° phase difference on the columns of the floater.
- Resonance peaks for heave for the floater.
- Tower 3P wake loads, 3P defines the number of times the blades pass the tower in a single cycle.
- Harmonics of drag forces close to flexible structural modes, most relevant is the 3ω for the tower.
- Turbulence at lower wind speeds for blades and tower.
- Rated wind speed for the maximum thrust force on the rotor.

The dynamics of the mooring lines impact the fatigue in different parts of the wind turbine, like the shaft, blades and tower. The mooring lines are attached at a large radius from the platform centre in the semi-submersible. This provides a restoring arm for the pitch and roll rotations. Consequently, the additional damping of the dynamic model decreases the platform rotations, with high fatigue in the rotor and lower fatigue damage in the tower [3].

2.5.2. Kurtosis and skewness of the stress spectrum of a mooring line

Kurtosis expresses the 'peakedness' of the probability distribution, and the skewness characterizes the asymmetry of the distribution according to the normal distribution. Figure 2.17 shows positive and negative values of both parameters. For simplicity of fatigue calculations, a Gaussian distribution of the mooring line tension is assumed in many lumping method studies. It is essential to understand the shortcomings of that assumption.

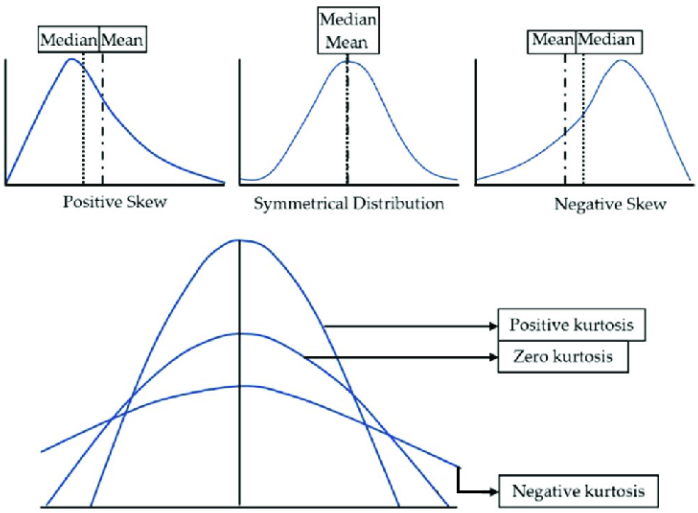

Figure 2.17: Definition of kurtosis and skewness. The distribution is Gaussian if the kurtosis value is 3 and the skewness is 0. A longer tail at the right occurs for positive values. For negative values, the tail at the left is longer. Negative kurtosis gives a broader distribution with more outliers. Positive values give a sharper distribution with fewer outliers [55].

The kurtosis and skewness coefficients of the mooring line tension are closely related to the sea states. Figure 2.18 shows the impact of the Gaussianity for varying H_s and T_z. It turns out that the parameters significantly affect the Gaussian nature of the mooring line tension [28].

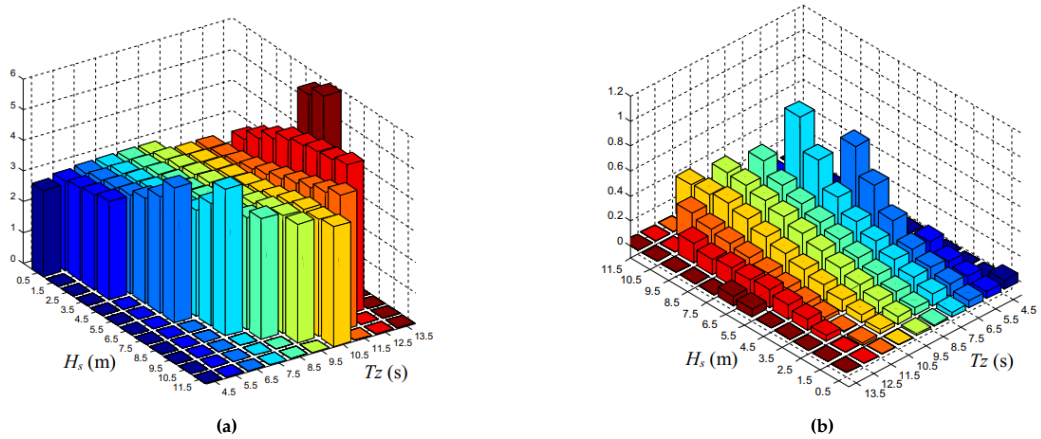

Figure 2.18: Kurtosis and skewness coefficients of mooring line tension for 73 sea states. Figure (a) is the kurtosis, and (b) is the skewness. Plot against the significant wave height H_s and zero crossing period T_z [28].

Figure 2.18a illustrates that for an increasing H_s and T_z, the kurtosis coefficient grows, and therefore, the peak of the mooring line tension distribution gets sharper. Furthermore, the kurtosis is more sensitive for the T_z than the H_s. Figure 2.18b indicates a positive skewness for every combination, resulting in a line tension with a longer tail to the right compared to the normal distribution. Moreover, for a constant T_z, the skewness increases with an increasing H_s. For an unvarying H_s, the skewness is inversely proportional to a varying T_z.

Moreover, based on the kurtosis and skewness, mooring lines follow different long-term distributions for fatigue damage. Compared to time domain simulation, a modified gamma distribution best fits a Catenary mooring system in deep waters.

2.5.3. Mooring line fatigue

The line dynamics and tensions are the main contributors to fatigue damage. In particular, the floater surge resonance motions and considerable contribution comes from the wave frequency range when a wave height is large. This results in maximum tensions around rated wind speed [3] [55]. Below rated wind speed, the fatigue level is primarily governed by wind forces. Above rated wind speed, the contribution of waves increases. The large wave heights and periods appear to impact the fatigue most. But when there are small waves, the wind gives the most impact [55]. This is independent of the platform type and mooring system configuration. Mooring systems can have different configurations. The fatigue life of different types of mooring systems is almost the same as long as their static stiffness is similar. The reason arises because of the same dynamic response [17].

Section 2.5.2 expresses the kurtosis and skewness compared with a normal distribution. The kurtosis becomes sharper for higher H_s and T_p values and could lead to more significant damage because of the higher probability of higher tensions. The skewness right tail could result in more line damage but counts only for the increasing H_s values and not for outliers in T_z because the skewness becomes lower for a longer period. Note: these conclusions are compared to a fatigue assessment based on line tension with a normal distribution but not absolute values.

For the catenary mooring system in deep water, the mooring line tension responses are typically non-Gaussian and wide-banded random processes due to the drag force exerted on the mooring lines and the geometrical non-linearity of the lines. Moreover, the second-order wave drift force causes non-linear motions of the floater [39], resulting in correlated tensions. Besides, the deeper the depth, the more non-Gaussian nature of the tension [28]. Therefore, the Rayleigh distribution based on the narrow-banded assumption and the Weibull distribution does not apply to fatigue damage assessment of the mooring lines. Besides, the line tension of the taut mooring system has better Gaussianity due to the weaker geometric non-linearity of the taut mooring system. [28].

When wave heights increase, the waves will become steeper and more non-linear. The linear wave theory underestimates the tension response for large waves. For large waves, the non-linear wave effects become significant for mooring line tension and must be considered. For mooring line tension, the surge is governing, while floater heave, pitch motion, tower base bending moment and pontoon axial force are less sensitive to the non-linear wave effect [55].

Fatigue is directly proportional to an increase in wave height [50]. This could indicate that extreme values significantly contribute to total fatigue damage. Figure 2.19 shows the significant impact of fatigue damage from environmental conditions with a high probability of occurrence. For a fatigue load assessment, it is not sufficient to calculate the loads during extreme events only, as the nature of fatigue is the accumulation of the damage over time. A proper fatigue assessment requires the consideration of all relevant load scenarios over the expected lifetime of the system, and typically this means a thorough investigation of the environmental conditions of the considered site [35] [55] [26].

Besides wave height and - length, the irregularity of waves also contributes to total fatigue. Irregular waves substantially affect the dynamic component of mooring tension despite the maximum tensile forces remaining the same regardless of wave irregularity [12].

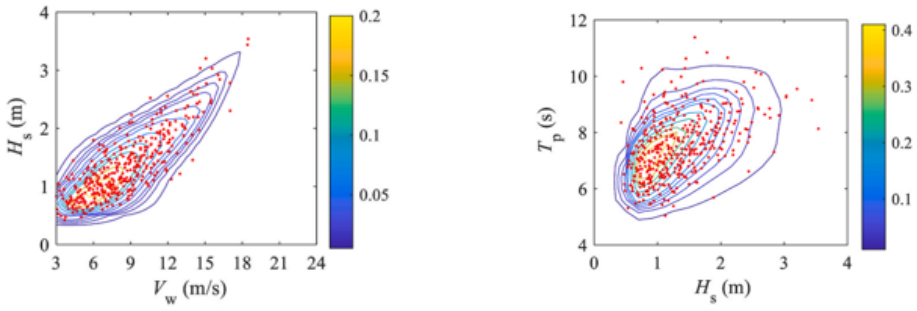

(a) Fatigue caused by wind speed and wave height

(b) Fatigue caused by wave height and wave period

Figure 2.19: Fatigue plotted against different load cases for three different variables in the mooring lines of a FOWT, H_s: significant wave height, T_p: significant wave period, V_w: mean wind speed. The right bar indicates the intensity of the fatigue damage. The greatest fatigue impact arises from the most frequent combinations of environmental forces [50].

For a comprehensive fatigue assessment, wind and waves should be considered. Equations of motion include many non-linear forces. For the tower, non-linear forces are vicious- and aerodynamic damping. Moreover, the catenary mooring line movements are excited by non-linear forces. Due to these non-linearities, one cannot treat the wind and wave loads on the structure separately. All combinations of wind and wave loads must be analysed individually [26].

2.5.4. Dynamic response and lumping methods

With section 2.5.3, an explanation for the mooring line fatigue damage is given. However, finding a theoretical-based lumping block method is not the goal of most reviewed studies. Due to the different non-linear dynamic coupling fatigue loads, a purely theoretical-based lumping method is complicated [48]. This section indicates the governing variables of the lumping block methods to create an accurate lumping block method.

Low amplitude cycles and high amplitude cycles have a significant influence on fatigue damage [44] [16]. Small significant wave heights produce low amplitude cycles of fatigue damage, while sea states with high significant wave heights lead to high amplitude cycles of fatigue damage. Without the low and high amplitude of the cycles, the representative sea state will underestimate the total damage. In a robust lumping method, the created underestimation must compensate. A correction factor which correlates the fatigue damage to the spectral wave energy should correct it. In section 2.3.3, this correction factor is given as ζ. The factor ζ couples the spectral wave energy to the corresponding damage [48].

Another important correction factor is the probability, p_k, in equation 2.38. As described in section 2.5.3 and figure 2.19, the main contribution to fatigue comes from waves that occur most frequently: The spectral moments of representative sea states are the weighted average spectral moments of original sea states.

$$
\begin{aligned}
m_{0rj} &= \left(\frac{\sum_{k=1}^{n_j} m_{0k}^{\zeta m} p_k}{p_{rj}} \right)^{\frac{1}{\zeta m}} \\
m_{2rj} &= \left(\frac{\sum_{k=1}^{n_j} m_{2k}^{\zeta m} p_k}{p_{rj}} \right)^{\frac{1}{\zeta m}}
\end{aligned}
\tag{2.38}
$$

The proposed lumping block methods are simulated and tested in dominantly narrow-banded wave spectra, leaving the impact of the width of the wave spectrum unclear. The methods aim to construct a robust and efficient alternative for the computationally expensive time domain fatigue calculations. A robust way of modelling must be applicable and reliable in all possible sea states, including extreme wavelengths, non-linear waves, and dynamic amplification caused by the resonance frequencies.

In addition, the conclusions about the bounds of the lumping blocks are contradictory. Some studies state the bounds of peak periods when lumping have little or no influence on assessment accuracy [9]. In contrast, more recent studies indicate the choice of lumping block borders significantly impacts the reliability of the lumping block methods [48] [20]. The explanation for the different conclusions probably lies in the mooring lines' stress spectrum and resonance peaks.

A lumping block method depends significantly on the mooring line's stress spectrum. The stress or tension in a mooring line is a time-dependent variable. Moreover, it has a high amplification factor around the natural frequencies. The dependence of the wave period bounds likely depends on the natural frequencies of the floater. Since the dynamic amplification influences the fatigue damage, the relevance of accuracy caused by the impact of the boundary of the lumping period block should be correlated to the shape stress spectrum.

2.6. Research gap and questions

This thesis aims to investigate fundamental knowledge about fatigue in the mooring lines of a floating offshore wind turbine. Mooring line fatigue analysis is dominated by frequently occurring wave frequencies. Although floating wind turbines are a popular topic, it is unclear if the impact of single outliers in wave period or wave height on the damage should be considered. The effect of uncertainty in wave period with the corresponding wave load in modelling fatigue is unclear too. To understand fatigue in the mooring lines of floating offshore wind turbines, gaining fundamental knowledge is essential to learn about sea wave behaviour and the resulting forces and motions. Moreover, it should clarify their impact on modelling to discover the effect of these extreme environmental parameters.

For practical applications, the design heavily relies on simulations. The most basic, time or frequency domain simulations give good results but are respectively computationally expensive or unreliable for mooring lines. Lumping block methods are promising in saving computational time with reliable results to develop fatigue models. The challenge is finding a general way applicable to broad wave spectra and scatter diagrams. Or to determine the bounds when these methods are not applicable. It is important to note that a broad wave spectrum results in greater fatigue damage in a mooring line than a narrow wave spectrum, while the T_p in these spectra could be the same. This leads to the main research question of this thesis:

> *What are the accuracy bounds of a lumping block method when considering resonance periods, probability of sea state occurrence, large wave height and periods, and narrow and broad wave spectra?*

The lumping block method should be robust, efficient and accurate enough to reduce the computational time in fatigue damage calculations. The approach aims to slightly overestimate the fatigue damage, which means a maximum of 5% overestimation compared to the original comprehensive time domain simulations. Hence, the technique should be safe for engineering practices. The objective is an efficient method appropriate for the early design stage approach within this maximum range. The method of Song is the examined lumping block method.

In addition to the main question, we focus on three sub-questions. For the first one, we want to know which main H_s and T_p components contribute in a narrow-banded wave scatter diagram to the fatigue in a mooring line. Besides testing a lumping block method, we will indicate the multiplication factor appropriate to transform an irregular sea into a regular wave with the same fatigue characteristics for fatigue life.

1 *Does the proposed simulation method of Song aim to transfer a narrow banded wave spectrum into a single harmonic wave with equivalent properties for fatigue in a mooring line?*

This question answers topics about time reduction, the possibilities to decrease the number of time simulations, the total simulation time reduction and the reliability of the proposed methods. In addition, it indicates what the practical application is.

The second sub-question is about broad wave spectra. The first goal is to test an existing reliable lumping block method in extreme sea conditions.

2 *What is the impact of a more broad wave spectrum with non-linear waves on the reliability of the chosen concept for different boundaries of the lumping period?*

In answering the second sub-question, the method's reliability in extreme sea conditions is tested, focusing on outliers in wave period, non-linearities and irregularity of waves. The wave input must be a changing wave spectrum from a narrow spectrum to a broad spectrum. The effect of spreading in wave periods is analyzed by changing the input data for the mooring line design. This way, more knowledge about the effects of variations in the wave period, like extreme wave periods and the non-Gaussian behaviour of the response, should be discovered. In addition, the representative sea states should indicate the fatigue damage represented per wave sea state. Since dynamic amplification influences fatigue damage, the relevance of accuracy caused by the impact of the boundary of the lumping period block should be correlated to the shape of the stress spectrum.

The third sub-question should include a reliability check around the resonance peak of the floater:

3 *Is the lumping block method reliable for wave periods around the resonance peak?*

The answer clarifies how strongly the choice of wave parameters influences the estimated dynamic performance of the FOWT. Besides, it answers if the wave frequencies act in the range of the natural surge frequency and show the effect of misrepresenting these parameters.

Research questions
To summarize the previous section, the central question of this thesis is: What are the accuracy bounds of a lumping block method when considering resonance periods, probability of sea state occurrence, large wave height and periods, and narrow and broad wave spectra?

To answer the main question, three sub-questions need to be answered. Sub-question 2 is the leading sub-question for the answer to the main question and receives the focus.

1. Does the proposed simulation method of Song aim to transfer a narrow banded wave spectrum into a single harmonic wave with equivalent properties for fatigue in a mooring line?
    - This question answers topics about time reduction, the possibilities to decrease the number of time simulations, the total simulation time reduction and the reliability of the proposed methods. In addition, it indicates what the practical application is.
2. What is the impact of a more broad wave spectrum with non-linear waves on the reliability of the chosen concept for different boundaries of the lumping period?
    - By differentiating the boundaries in the period range, the effect of spreading in T_p is analyzed for the mooring line design. In addition, the fatigue damage can be accurately represented per wave sea state.
3. Is the lumping block method reliable wave periods around the resonance peak?
    - This clarifies how strongly the choice of wave parameters influences the estimated dynamic performance of the FOWT. Besides, it answers if the wave frequencies act in the range of the natural surge frequency and show the effect of misrepresenting these parameters.

3

Methodology

To answer the research questions, several general steps must be taken. Section 3.1 explains the time domain fatigue calculation procedure. After that, the system parameters are determined, such as damping, simulation nodes and the resonance peaks of the mooring lines. These data put the results of the research questions into perspective. Finally, the details are explained per sub-question.

3.1. Time fatigue domain assessment

For the fatigue calculation of mooring lines, it is essential to use time domain simulations. This section explains the procedure. First, make a numerical model of the wind turbine and its mooring lines. After that, simulate the time domain line movements based on generated wave data. The wave data corresponds to a Jonswap spectrum and uses all the load cases from the scatter diagram in figure 3.4.

With this information, the dynamic analysis is made of the FOWT to obtain the tension response. The stress ranges and the corresponding cycle numbers are obtained with the rain flow count algorithm. Then the correct T-N curve is used for the maximum number of possible cycles. Figure 3.1 visualizes the whole procedure. Simulating for the complete scatter diagram and the lumped simulations are comparable since the lumped method gives representative values for H_s and T_z.

$$\begin{aligned} D_a &= \sum_{i=1}^{k_{sr}} \frac{365 \times 24 \times 3600 \times p_k}{T_k} \frac{n\left(S_i\right)}{N\left(S_i\right)} \\ D &= \sum_k D_a = \sum_k \sum_i \frac{365 \times 24 \times 3600 \times p_k}{T_k} \frac{n\left(S_i\right)}{N\left(S_i\right)} \end{aligned} \tag{3.1}$$

Equation 3.1 shows the annual calculation of the total damage on behalf of the individual fatigue damage from all of the considered stress ranges. p_k is the occurrence probability of k^{th} sea state. This equation divides the annual damage by the duration time of the k^{th} sea state: T_K. Finally, the total damage for long-term conditions is obtained by summing D_a overall sea states in the scatter diagram. Ultimately, the damage is summed up until the total lifespan of 25 years is reached.

3.1.1. Numerical model

This thesis uses OrcaFlex to model the fatigue, corresponding dynamic forces, and damping in the mooring lines [13]. The University of Maine created and validated a numerical model, the "UMaine VolturnUS-S Semisubmersible Platform", which will be used in the case study [2]. Chapter 4 explains the details of the case study, including the numerical model.

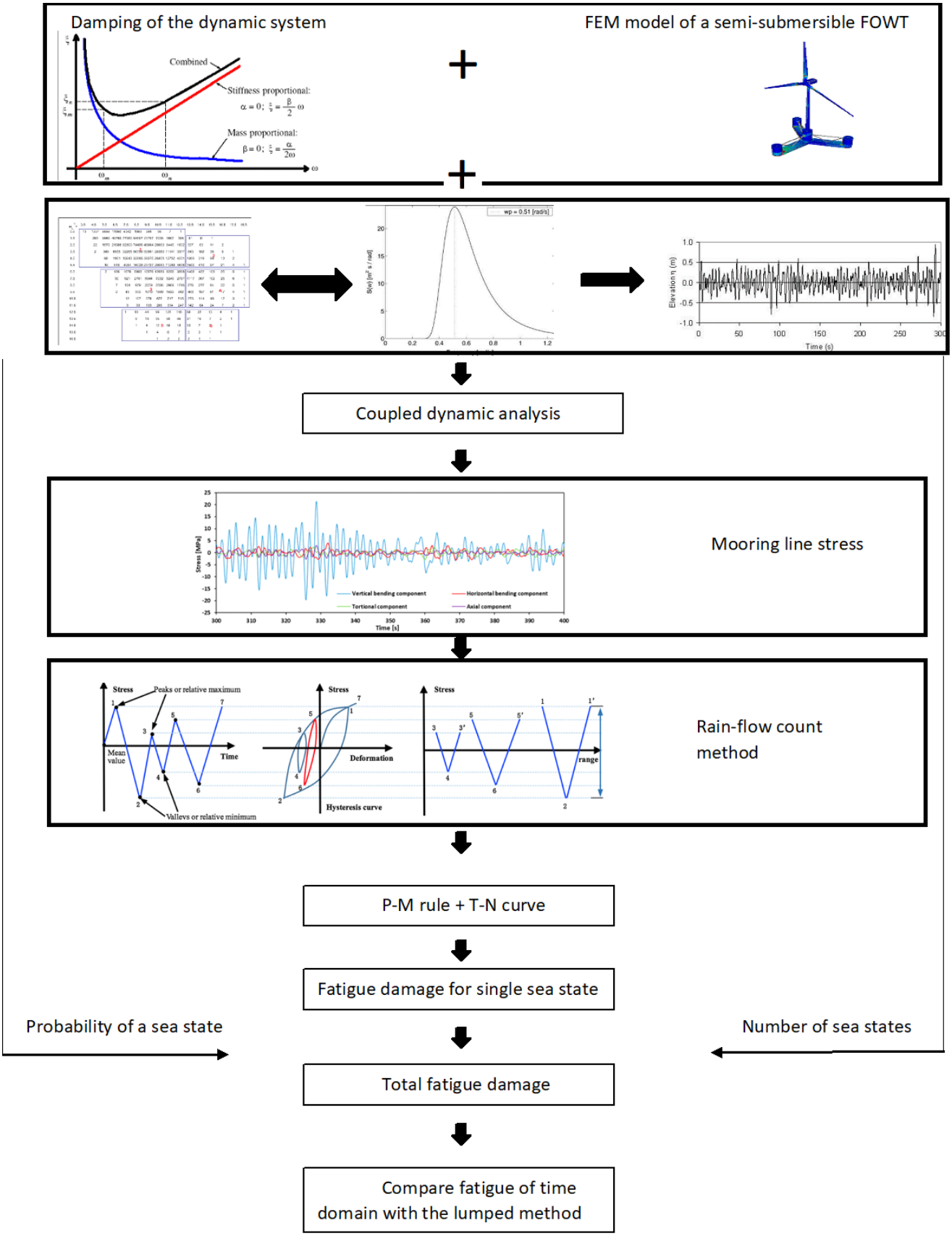

Figure 3.1: Procedure of the time domain simulations for the original and lumped cases. The main goal of this study is to compare both.

3.1.2. Wave data

The simulation uses wave trains as wave data input. Each wave train defines the direction and has its spatial and time origins. The spatial start is specified relative to the global frame, and the time origin is specified relative to the global time origin. A Jonswap spectrum defines the wave trains.

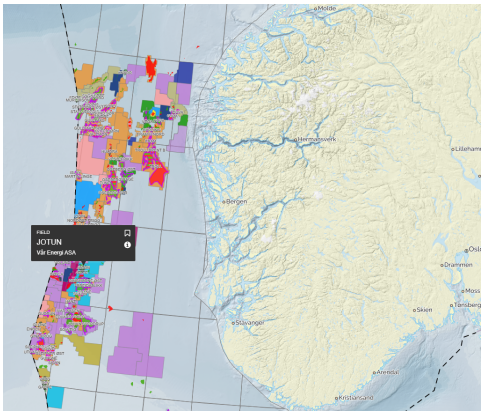

Figure 3.2: Location of the passive Jotun oil field. An oil well on the southwest coast of Norwegian. The water depth is 125 m. Deep water and intermediate conditions apply at this place [40].

Jotun field

Figure 3.2 shows the location of the data input, the Jotun field. Although the Scotwind projects are not located near this site, and since the goal is verifying the proposed model, only relevant wave conditions matter. The water depth near the Jotun field is 125 m. The diagram contains measurement data extrapolated to 100-year wave data, and the data set does not account for swell. The input data is shown in figure 3.4 and contains wave height, period and the probability of each combination/load case. The wave height is indicated by the significant height H_s. The wave period is described by the mean zero crossing period T_z.

Each wave train uses H_s and T_z as input from the scatter diagram, specified in figure 3.4, leading to 196 unique load cases. For the time domain simulations, T_p must be used to set up the Jonswap spectrum. Myrhaug and Kjeldsen link T_p and T_z via de spectral moments and shape parameters [37], such that H_s and T_z are the input parameters. In addition, other shape parameters are kept constant, $\sigma_1 = 0.07$ and $\sigma_2 = 0.09$. Figure 3.3 shows the impact of a varying peak enhancement factor for a constant T_p and T_z. This thesis let the peak enhancement factor differ between $\gamma_{peak} = 1$, 3.3 and 6 while keeping the same total energy.

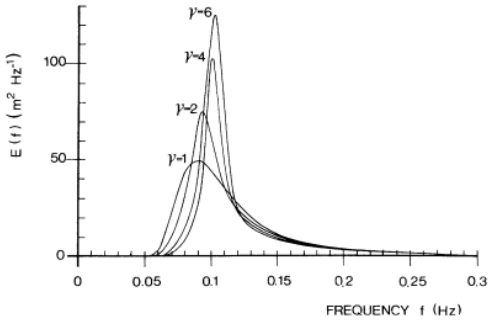

(a) Shape of the Jonswap spectrum for $H_s = 7\ m$ and the T_z is held constant.

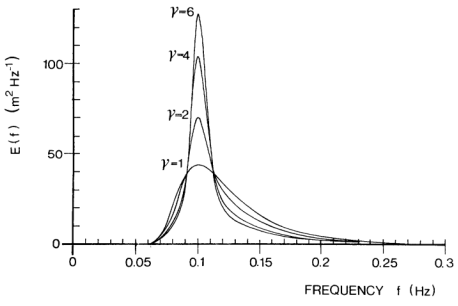

(b) Shape of the Jonswap spectrum for $H_s = 7\ m$ and the T_p is held constant.

Figure 3.3: Jonswap spectrum constant for T_z and T_p [8].

3.1.3. Simulation time

For a proper dynamic simulation, the simulation time of each series must have sufficient run time. The simulation period defines two consecutive stages. The main simulation stage(s) usually start with a build-up stage, during which wave and turbine motions are smoothly ramped up from zero to full size.

The case study uses a build-up time of 10 s or the time of one wavelength if this is more prolonged. The simulation time of a single load case is 3600 s with a time step of 0.1 s, which is at least 1/10th of the shortest natural period of motion for any degree of freedom in the model. The simulations cover the frequency range between 0.02 Hz and 1.0 Hz, which experts indicate as sufficient.

Hs \ Tz	3.5	4.5	5.5	6.5	7.5	8.5	9.5	10.5	11.5	12.5	13.5	14.5	15.5	16.5
0.5	0.00%	0.13%	0.87%	1.19%	0.63%	0.19%	0.04%	0.01%	0.00%	0.00%	0.00%	0.00%	0.00%	0.00%
1.5	0.00%	0.03%	0.99%	4.98%	7.74%	5.57%	2.38%	0.70%	0.16%	0.03%	0.01%	0.00%	0.00%	0.00%
2.5	0.00%	0.00%	0.20%	2.16%	6.23%	7.45%	4.86%	2.07%	0.64%	0.16%	0.03%	0.01%	0.00%	0.00%
3.5	0.00%	0.00%	0.03%	0.70%	3.23%	5.68%	5.10%	2.84%	1.11%	0.34%	0.08%	0.02%	0.00%	0.00%
4.5	0.00%	0.00%	0.01%	0.20%	1.35%	3.29%	3.86%	2.69%	1.28%	0.46%	0.13%	0.03%	0.01%	0.00%
5.5	0.00%	0.00%	0.00%	0.05%	0.50%	1.60%	2.37%	2.01%	1.13%	0.46%	0.15%	0.04%	0.01%	0.00%
6.5	0.00%	0.00%	0.00%	0.01%	0.17%	0.69%	1.26%	1.27%	0.83%	0.39%	0.14%	0.04%	0.01%	0.00%
7.5	0.00%	0.00%	0.00%	0.00%	0.05%	0.27%	0.59%	0.70%	0.52%	0.28%	0.11%	0.04%	0.01%	0.00%
8.5	0.00%	0.00%	0.00%	0.00%	0.00%	0.10%	0.26%	0.35%	0.30%	0.17%	0.08%	0.03%	0.01%	0.00%
9.5	0.00%	0.00%	0.00%	0.00%	0.00%	0.03%	0.10%	0.16%	0.15%	0.10%	0.05%	0.02%	0.01%	0.00%
11	0.00%	0.00%	0.00%	0.00%	0.00%	0.01%	0.04%	0.07%	0.07%	0.05%	0.03%	0.01%	0.00%	0.00%
12	0.00%	0.00%	0.00%	0.00%	0.00%	0.00%	0.01%	0.03%	0.03%	0.02%	0.01%	0.01%	0.00%	0.00%
13	0.00%	0.00%	0.00%	0.00%	0.00%	0.00%	0.00%	0.01%	0.01%	0.01%	0.01%	0.00%	0.00%	0.00%
14	0.00%	0.00%	0.00%	0.00%	0.00%	0.00%	0.00%	0.00%	0.01%	0.00%	0.00%	0.00%	0.00%	0.00%
15	0.00%	0.00%	0.00%	0.00%	0.00%	0.00%	0.00%	0.00%	0.00%	0.00%	0.00%	0.00%	0.00%	0.00%
16	0.00%	0.00%	0.00%	0.00%	0.00%	0.00%	0.00%	0.00%	0.00%	0.00%	0.00%	0.00%	0.00%	0.00%
17	0.00%	0.00%	0.00%	0.00%	0.00%	0.00%	0.00%	0.00%	0.00%	0.00%	0.00%	0.00%	0.00%	0.00%

Figure 3.4: All sea states in the scatter diagram and the corresponding probabilities. T_z is the mean wave period on the horizontal axis, and H_s is the significant wave height on the vertical axis. The white cells are zero cells. The coloured ones have a nonzero value. Yellow indicates a low value; green indicates a higher value. The frame highlights T_z and H_s combinations, which highlight the most frequent load cases, with a combined probability of 91% concerning the total scatter diagram.

3.2. The system

Before simulations can start, understanding the system's behaviour is critical for interpreting the results. First, the difference in the system's damping with and without rotating blades. After that, the number of nodes in the mooring lines is determined based on a trade-off between simulation time and sufficient representation of the forces. Finally, mapping the resonance frequencies for the mooring lines is essential for the total damage. The results and the figures are in section 5 and appendix A.

3.2.1. Damping coefficients

The rotation of the blades provides a damping component for the total movement of the system with an order of magnitude of 10%. A free decay test is performed to determine the difference in damping for rotating blades with a rotational speed of 5 rpm and a parked wind turbine. This is a test in which an initial displacement is given to the floater, and then the time series of the movements are measured for both situations. With equation 3.2, the damping coefficient, ξ, is calculated. x_0 and x_1 are the successive positive or negative peaks in the time series.

$$\xi = \frac{\delta}{\sqrt{\delta^2 + (2\pi)^2}} \quad \text{with:} \quad \delta = \ln \frac{x_0}{x_1} \tag{3.2}$$

In this test, the turbine is excited 30 m in the sway and surge direction, 10 m in the heave direction and 10° in the roll and pitch direction. The damping coefficient is expressed in percentages. A higher rate means faster damping. With a damping of 100%, the movement is completely damped out within a single cycle.

3.2.2. The number of nodes

The number of nodes strongly depends on the non-linear motions of the systems. If the non-linearities in the system are not substantial, fewer simulation points result in accurate results, reducing the overall simulation time required. The number of nodes depends on the sea climate and the type of floater, but no rule of thumb exists. Therefore, a sensitivity study must clarify the number of nodes needed to minimize the number. A general overview of nodes in a mooring line is given in figure 3.5.

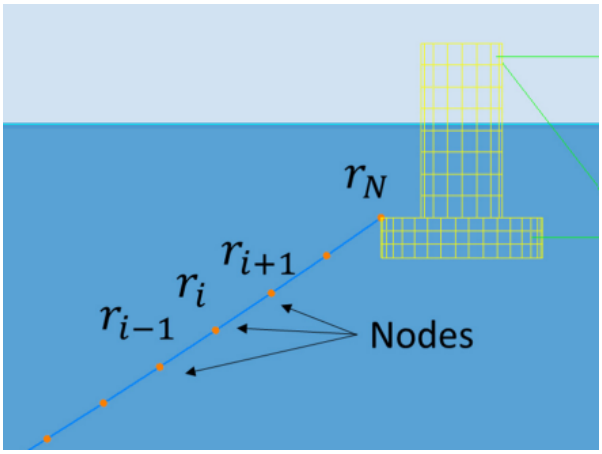

Figure 3.5: Nodes in a mooring line of a floating wind turbine depending on the wave climate and the type of floater. A sensitivity study must define the number of nodes in the lines [41].

To model the mooring lines properly, nodes are applied in the mooring lines, and section 4.2 shows the details of the nodes. The nodes model the movements of the line, subsequently, the forces of the line. When increasing the number of nodes, more calculation points exist. Consequently, the reliability of the simulation increases. The downside is a comprehensive calculation resulting in longer simulation time. The goal of the sensitivity study is to find an optimum between the calculation time and the reliability of the calculation.

To find an optimum number of nodes, the time series of the floater is simulated for the same wave spectrum. A Jonswap spectrum with a simulation time of 3600 s and parameters $H_s = 2\ m$, $T_p = 9\ s$ is used due to the resonance of this period and the corresponding maximum forces (see section 5.1). Figure 3.6 shows a time series of one of the simulations. These plots are made for a different number of nodes, looking at the differences in the average tension and the maximum tension.

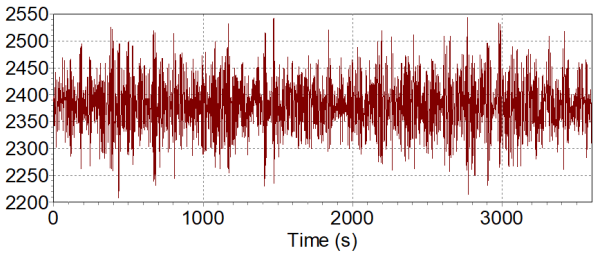

Figure 3.6: Time series of the tensions in the mooring over the time s. The y-axis displays the effective tension in kN. This is the time series of the upper part of the mooring line, which expires the highest forces.

3.2.3. Response spectrum of the mooring lines

The tension spectra of the mooring lines are of great relevance for the reliability of the lumping methods. At a constant wave height ($H_s = 2\ m$), regular waves with different periods are subjected to the floater. Starting with a wave period of 1 s, and increasing with 1 s to 20 s is reached. This way, the impact of a single frequency is simulated. The peaks in the different spectra indicate the mooring line resonance frequencies.

3.3. Number of lumping blocks

The distribution of the lumping blocks in a wave scatter diagram could be divided randomly. For this thesis, a lumping block is discretized, starting in the top left corner and moving to the bottom right corner with the same amount of rows and columns, making each block a square. The next block starts after the boundaries of the previous block, so no overlap exists, and each sea state is transferred into a lumping block. This way of lumping is chosen since a set of rules is needed for comparing the reliability of different amounts of lumping blocks. Furthermore, this way of lumping is always the same, making it easy to use for engineering practices. In addition, with this method, the sub-questions about resonance and extremes can be answered. All the different lumping blocks used in this study are summarized in table 3.1.

Table 3.1: Different lumping blocks with corresponding original sea states

Number of blocks	Original sea states
57	2 x 2
29	3 x 3
14	5 x 5
8	7 x 7
4	10 x 10
1	18 x 18

Figure 3.7 shows an example of naming the blocks, specifically 4 lumping blocks with 10 x 10 original cells as the input for the lumping block. Block_{11} is the block on the first row and first column, block_{12} is the first row and second column etc. Each block is made up of an equal division of original sea states. Block_{11} and block_{12} cover different cells. Block_{11} ecloses 100 (10 x 10) cells and block_{12} 90. If the number of cells from the scatter diagram doesn't line up in the grid of the blocks, in this case, a 10 x 10 grid, the blocks at the edges of the scatter diagram consist of fewer original cells.

	1.5	2.5	3.5	4.5	5.5	6.5	7.5	8.5	9.5	10.5	11.5	12.5	13.5	14.5	15.5	16.5	17.5	18.5
0.5	0.000000000	0.000000000	0.000013002	0.001337210	0.008657359	0.011861862	0.006342996	0.001863293	0.000369058	0.000056009	0.000007001	0.000001000	0.000000000	0.000000000	0.000000000	0.000000000	0.000000000	0.000000000
1.5	0.000000000	0.000000000	0.000000000	0.000293046	0.009861548	0.049767814	0.077392151	0.055705746	0.023760730	0.007036105	0.001607252	0.000305048	0.000051008	0.000008001	0.000001000	0.000000000	0.000000000	0.000000000
2.5	0.000000000	0.000000000	0.000000000	0.000022003	0.001975310	0.021591390	0.062309783	0.074506698	0.048611632	0.020663244	0.006446012	0.001602252	0.000337053	0.000063010	0.000011002	0.000002000	0.000000000	0.000000000
3.5	0.000000000	0.000000000	0.000000000	0.000002000	0.000346054	0.006956092	0.032270066	0.056758911	0.050999007	0.028384456	0.011142749	0.003377530	0.000843132	0.000182009	0.000035005	0.000006001	0.000001000	0.000000000
4.5	0.000000000	0.000000000	0.000000000	0.000000000	0.000060019	0.001961308	0.013545127	0.032890164	0.038581057	0.026859217	0.012754002	0.004551715	0.001309206	0.000319010	0.000069011	0.000013002	0.000002000	0.000000000
5.5	0.000000000	0.000000000	0.000000000	0.000000000	0.000010002	0.000510080	0.004984783	0.016031517	0.023730726	0.020086154	0.011261768	0.004636728	0.001509237	0.000410004	0.000097015	0.000021003	0.000004001	0.000001000
6.5	0.000000000	0.000000000	0.000000000	0.000000000	0.000002000	0.000126020	0.001670262	0.006904084	0.012580975	0.012687992	0.008260297	0.003868607	0.001408221	0.000422066	0.000109017	0.000025004	0.000005001	0.000001000
7.5	0.000000000	0.000000000	0.000000000	0.000000000	0.000000000	0.000030005	0.000521082	0.002701424	0.005944933	0.007033104	0.005249824	0.002767434	0.001117175	0.000367058	0.000102016	0.000025004	0.000006001	0.000001000
8.5	0.000000000	0.000000000	0.000000000	0.000000000	0.000000000	0.000007001	0.000043007	0.000979154	0.002559402	0.003506551	0.002969466	0.001746274	0.000776122	0.000277043	0.000084013	0.000022003	0.000005001	0.000001000
9.5	0.000000000	0.000000000	0.000000000	0.000000000	0.000000000	0.000002000	0.000012002	0.000332052	0.001019160	0.001599251	0.001522239	0.000992156	0.000483076	0.000187029	0.000061010	0.000017003	0.000004001	0.000001000
10.5	0.000000000	0.000000000	0.000000000	0.000000000	0.000000000	0.000000000	0.000003000	0.000107017	0.000379060	0.000675106	0.000717113	0.000515081	0.000273043	0.000114018	0.000040006	0.000012002	0.000003000	0.000001000
11.5	0.000000000	0.000000000	0.000000000	0.000000000	0.000000000	0.000000000	0.000001000	0.000033005	0.000133021	0.000266042	0.000314049	0.000247039	0.000142022	0.000064010	0.000024004	0.000007001	0.000002000	0.000001000
12.5	0.000000000	0.000000000	0.000000000	0.000000000	0.000000000	0.000000000	0.000000000	0.000010002	0.000044007	0.000099016	0.000128020	0.000110017	0.000068011	0.000033003	0.000013002	0.000004001	0.000001000	0.000000000
13.5	0.000000000	0.000000000	0.000000000	0.000000000	0.000000000	0.000000000	0.000000000	0.000003000	0.000014002	0.000035005	0.000050008	0.000046007	0.000031005	0.000016003	0.000007001	0.000002000	0.000001000	0.000000000
14.5	0.000000000	0.000000000	0.000000000	0.000000000	0.000000000	0.000000000	0.000000000	0.000001000	0.000004001	0.000012002	0.000018003	0.000018003	0.000013002	0.000007001	0.000003000	0.000001000	0.000000000	0.000000000
15.5	0.000000000	0.000000000	0.000000000	0.000000000	0.000000000	0.000000000	0.000000000	0.000000000	0.000001000	0.000004001	0.000006001	0.000007001	0.000005001	0.000003000	0.000001000	0.000001000	0.000000000	0.000000000
16.5	0.000000000	0.000000000	0.000000000	0.000000000	0.000000000	0.000000000	0.000000000	0.000000000	0.000000000	0.000001000	0.000002000	0.000002000	0.000002000	0.000001000	0.000001000	0.000000000	0.000000000	0.000000000

Figure 3.7: Example of 4 lumping blocks which show the naming of the lumping blocks, block_{11} is the block on the first row and first column, block_{12} first row and second column etc.

3.4. Subquestions

Sections 3.1 to 3.3 set the conditions for the research questions, this section focuses on the steps to answer the questions and outline the differences.

Sub-question 1: Does the proposed simulation method of Song aim to transfer a narrow banded wave spectrum into a single harmonic wave with equivalent properties for fatigue in a mooring line?
A Jonswap spectrum defines the narrow-banded spectrum with a peak enhancement factor of 6. Figure 3.3 shows $\gamma_{peak} = 6$ as a concentrated and narrow spectrum. Resulting in less spreading in wave frequencies and predominantly linear waves.

Initially, the base case is run according to the current way of simulating, in which the fatigue damage of the complete scatter diagram is calculated with time domain simulations. Based on this, the total damage is calculated, as described in section 3.1. The proposed method determines each block's H_{srj} and T_{srj}. This is done for 57, 29, 14, 8, 4 and 1 lumping block(s). The lumped fatigue damage is calculated based on time-domain simulations for these values. The damage from the lumping block method is compared to the initial time domain calculations to assess reliability.

Sub-question 2: What is the impact of a more broad wave spectrum with non-linear waves on the reliability of the chosen concept for different boundaries of the lumping period?
A varying Jonswap spectrum defines the wave input for the scatter diagram for the second sub-question. The broad spectra cause more outliers for the wave period. At the same time, a narrow band spectrum could trigger the resonance more. The shape parameters γ_{peak} and α modify the number of frequencies in the spectrum. γ_{peak} is the best parameter to vary because it directly impacts the low and high-frequency tail. The low frequencies are most relevant for this thesis. To see the impact of γ_{peak}, α must change to keep H_s constant. Barltrop and Adams developed an equation for α, equation 3.3 shows how this is done [38].

$$\alpha = 603.9 \left(\frac{H_s * f_p^2}{g} \right)^{2.036} (1.0 - 0.298\ ln(\gamma_{peak})) \tag{3.3}$$

The factor γ_{peak} varies between 1, 3.3 and 6. To cover a broad, regular, and narrow sea spectrum. Then the procedure is repeated, as in question 1, to test the reliability of each.

Sub-question 3: Is the lumping block method reliable for wave periods around the resonance peak?
Checking the reliability of the resonance blocks, the scatter diagram is divided into 57 blocks. The 5^{th} block in the row encloses the resonance frequencies. The reliability of the resonance is estimated at the lumping block level.

4

Case study

This case study verifies the proposed method. This section defines the spatial arrangement of the tower, floater and mooring lines to specify the frame of this study. The wind turbine is an 'IEA Wind 15-Megawatt Offshore Reference Wind Turbine' designed by Gaertner et al. 2020 [15]. The tower supports the nacelle mounted upon the University of Maine (UMaine) Volturn US-S reference semi-submersible platform [2]. The Scotwind floating wind farm elaborates on this type of structure.

4.1. Wind turbine configuration

Tower and floater

The technical report of 'UMaine VolturnUS-S Reference Platform' defines the floater in detail [2]. Figure 4.1 shows the general arrangement of the turbine and platform. The foundation is the most frequently used semi-submersible recognizable by a triangle outer-shaped, four-columned structure. This configuration is remarkable since the wind turbine stands at a column at the midpoint of the triangle. After installation, the platform has a draft of 20 meters with a 15-meter freeboard.

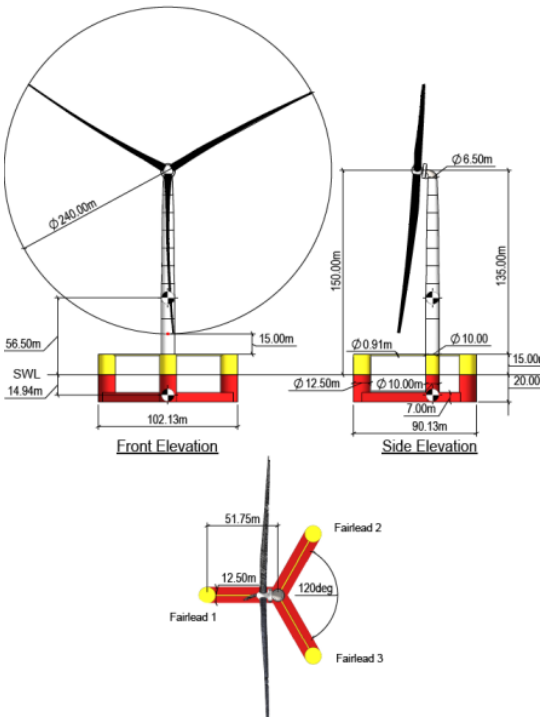

Figure 4.1: This is the arrangement for the UMaine VolturnUS-S Reference Platform, the floater used for the case study [2].

Mooring system
A total of 3 mooring lines moor the floating system. Each line is connected at the fairlead to one of the platform's three outer columns 14 m below the SWL. The lines use a 'R3' chain with a nominal diameter of 185 mm. The anchors are spaced equally by 120° in the surge-sway plane. The maximal offset in this reference plane is 25 m. Figure 4.2 shows the mooring configuration.

Table 4.1 summarizes parameters for the floating system or the corresponding fatigue calculation. [2] gives a total overview of the floating design and the parameters for the fatigue calculation.

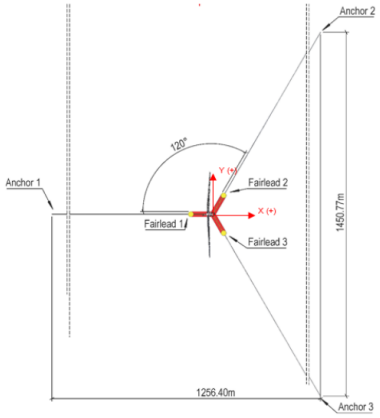

(a) Mooring line arrangement. Spacing between the three mooring lines and their allocation of place concerning the reference frame of the FOWT.

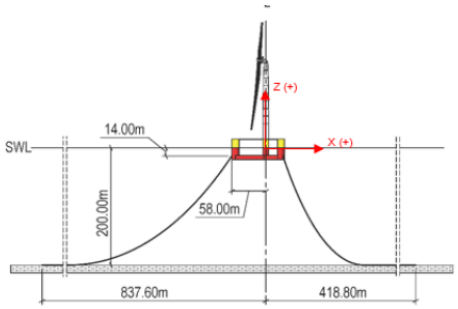

(b) View perpendicular to the SWL of the FOWT and shows the maximum - horizontal displacement x and vertical displacement z.

Figure 4.2: The floater has three catenary mooring lines that keep the wind turbine in place, with a maximum offset of 25 m caused by LF cycles [2]

4.2. Numerical model

Tower and floater
The turbine is modelled with a finite element method (FEM). The prescribed dimensions of the turbine are captured in the numerical model to simulate the motions of the floater. Orcina published the model of this specific wind turbine [2]. The model can move in six degrees of freedom. The mooring lines are attached to the pontoons with a 45° corner, and the mooring lines are modelled as an external stiffness matrix in the floater dynamics. Figure 4.3 shows the model.

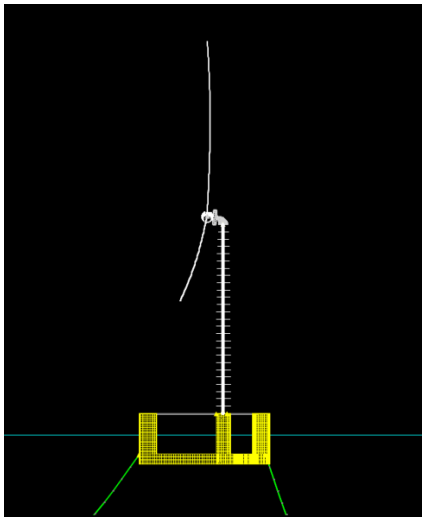

Figure 4.3: The numerical model of the 15 MW wind turbine developed by the university of Maine and the corresponding floater. Every stripe shows a different node in the tower, blades, and floater of mooring lines. For this thesis, only the nodes of the lines will be used [2].

Table 4.1: Most important parameters for the floating system and the fatigue calculation [2].

Parameter	Mooring system type	Line Type	Line Breaking strenth	Chain diameter	Slope tn curve (t)
Unit	-	-	Kn	mm	-
Value	Chain catenary	R3 studlees mooring chian	22.286	185	3

Mooring lines
Figure 4.4 shows how the mooring lines are modelled into a finite element model as a set of nodes attached to springs. The model segments only model the axial and torsional properties of the line. The other properties (mass, weight, buoyancy etc.) are all lumped into the nodes, as indicated by the arrows in the figure above.

A node is a short straight nod representing two half segments. Figure 4.4 shows each line segment is divided into two halves. The related properties like mass, weight and buoyancy are divided this way. Forces and moments are applied at the node. The bending properties of the line are represented by rotational spring dampers at each end of the segment, between the segment and the node. Since different stiffness values can be specified, the line does not have axial symmetry [13].

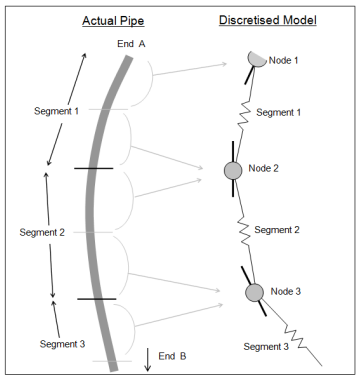

Figure 4.4: With this model, the mooring lines are modelled in OrcaFlex. A line is modelled as rods attached with springs [13].

4.3. Dynamics of the floater

The floating dynamics impact the mooring damage to a great extent. The technical report of the University of Maine did calculations for the dynamics of the floater [2].

First order transfer functions
Figure 4.5 shows the first-order wave excitation coefficients concerning wave frequency for a wave heading of 0°. The left picture shows the frequencies with a high excitation for surge and heave. The right image illustrates the corresponding phase. The maxima and minima arise at the same frequencies for the low frequencies.

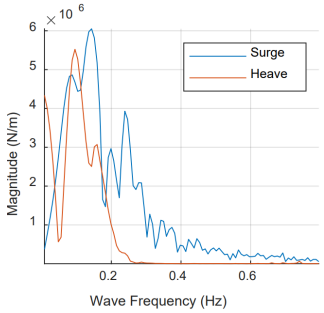

(a) Magnitude of first-order wave translational excitations of the floater for a wave heading of 0°. With a maximum for the surge: 6 Mn/m around 0.18 Hz

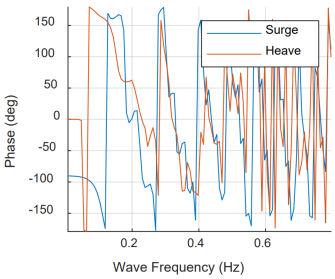

(b) Phase of first-order wave translational excitations of the floater for a wave heading of 0°.

Figure 4.5: RAO for surge and heave of the floating platform [2]

5

Results

This thesis tests a lumping block method on accuracy in broad and narrow wave spectra as described in section 2.2. The method aims to construct a robust and efficient way for the time domain fatigue calculations of mooring lines in the early design stage of a FOWT. A robust way of modelling must be applicable and reliable in all possible sea states, including extreme wavelengths, non-linear waves, and resonance frequencies. Recent studies show the method's good accuracy, and applicability for a North Sea Jonswap spectrum [48].

This thesis varies the broadness of the wave spectrum driven by peak enhancement factor γ_{peak} = 1, 3.3 and 6, resulting in broad, middle and narrow spectra, as shown in section 2.1.3 and section 3.1.2. Moreover, the different wave spectra result in different extreme wavelengths, non-linear waves and dynamic amplification caused by the resonance frequencies. To investigate the effect on the method's reliability and applicability in all sea states. The method's reliability for different wave spectra is validated by comparing the proposed numerical lumped time-domain simulations with the original numerical time-domain simulations.

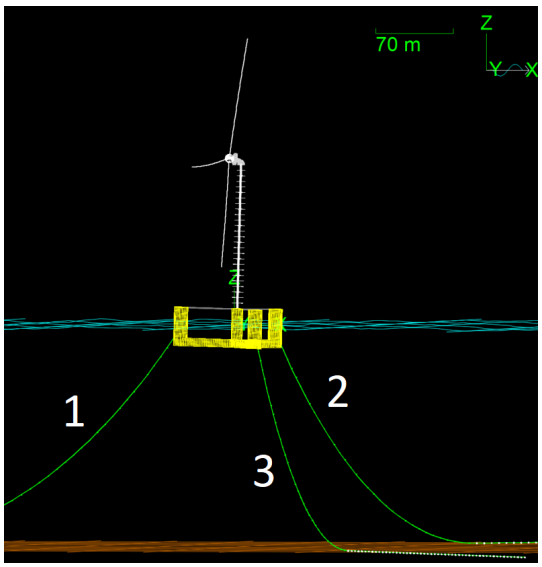

Figure 5.1: Side view for the mooring line arrangement. The figure defines the names/numbers of the mooring lines. The waves travel purely in the x-direction. Mooring line 1 stands right against the waves, mooring lines 2 and 3 at an angle of 60° compared to the x-axis. Lines 2 and 3 are loaded symmetrically and thus have exactly the same damage.

Characteristics like aerodynamic damping, the number of mooring line nodes and the resonance frequencies are simulated to understand the systems' behaviour in section 5.1. Secondly, the fatigue damage for different time domain simulations with varying peak enhancement factors is presented

in section 5.2. Section 5.3 shows the calculation of ζ. The reliability of the lumping block method for different peak enhancement factors is presented in section 5.4, besides showing the reliability of resonance lumping blocks and concluding with the lumping methods' pitfalls.

This thesis assumes the turbine is not exposed to windspeed or current, so only the accuracy of damage calculations caused by wave impact is investigated. Furthermore, the waves travel only in the x-direction. Moreover, the turbine is parked during the simulations. These assumptions are discussed in section 5.5. Figure 5.1 shows in the top right the system's reference. In addition, the figure defines the numbering of the mooring lines. Mooring line 1 stands right against the waves, mooring lines 2 and 3 at an angle of 60° compared to the x-axis.

5.1. The system

It is essential to understand the system to put the results in perspective. To this end, the differences between the aerodynamic damping of a wind turbine with and without a rotating rotor are first examined. The line dynamics and tensions are the main contributors to fatigue, see section 2.5.3. Hence the damping impacts the damage significantly. In the second section, a sensitivity study tests the number of nodes needed in the mooring lines for reliable results. The last section indicates the resonance periods at which the mooring lines expire the most damage. Appendix A shows the detailed graphs of the damping and resonance periods.

5.1.1. Damping coefficients

This section shows the difference in damping for a rotating wind turbine with a rotational speed of 5 rpm and a parked wind turbine with a free decay test for both situations. In this test, the turbine is excited 30 m in the sway and surge direction, 10 m in the heave direction and 10° in the roll and pitch direction. Appendix A.1 shows all the figures. Each direction of movement shows two figures, first the time series of movement and second the damping ratio at an amplitude, both for a rotating and nonrotating rotor. The results show less damping for nonrotating blades. Since the case study uses a parked turbine, the wave-induced damage found will, in reality, be lower than in this case study.

The two most noticeable differences are the surge and pitch movements. Figure 5.2 defines the pitch damping coefficient as 2.5% higher for surge motions with rotating blades compared to the case without rotation and almost no difference for sway motions. Figure 5.3 shows that the damping ratio is 10% higher for the pitch rotation, such that the pitch rotation after 100 seconds is almost damped, which is visible in appendix A. There is practically no difference in damping for roll. The last two figures in appendix A show the heave movement. Nearly no difference between the situations is measured.

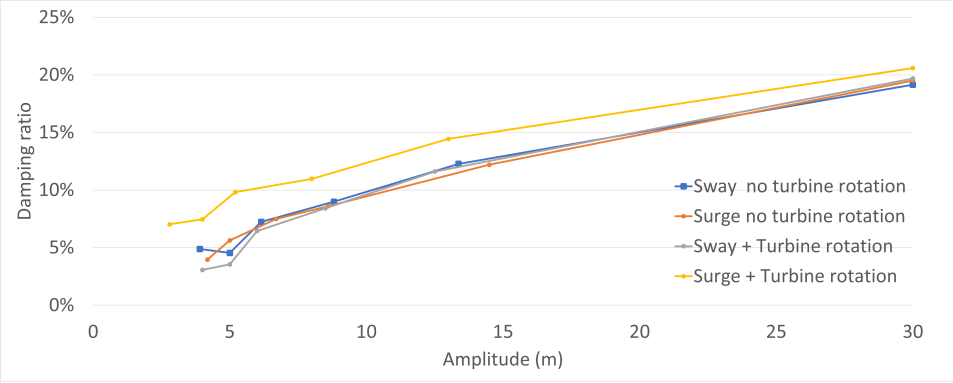

Figure 5.2: Damping coefficients of sway and surge after a 30 m excitation. The damping coefficient for surge motion is 2.5% higher for a rotating rotor than nonrotating blades.

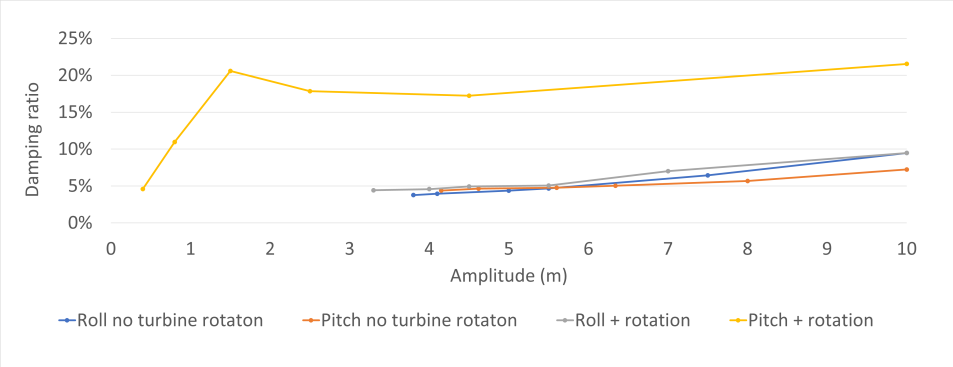

Figure 5.3: Damping coefficients of roll and pitch after a 10° rotation. The damping coefficient for pitch motion is 2.5% higher for a rotating rotor than nonrotating blades.

5.1.2. Number of nodes

The nodes model the movements of the line and, subsequently, the forces of the line. Section 4.2 shows the details of the nodes. With this sensitivity study, this section aims to find an optimum between the calculation time and the reliability of the calculation. For 10 different cases, the time simulations are made. Figure 5.4 shows the normalized values for the simulated cases for mooring line 1, as the values for mooring line 2 are similar. The case with 1700 nodes is the reference case because it accounts for the maximum number of nodes possible in OrcaFlex.

Figure 5.4 shows the maximum, mean and minimum normalized forces for different nodes in the mooring line. This figure visualizes force results around 1 for 49 and 57 nodes. Looking in detail at the difference between 49 and 57 nodes, 49 nodes slightly underestimate the tensions, especially the maximum values. Therefore the case study simulations are done with a node every 15 meters (57 nodes) to ensure tensions are not over conservative and ensure the minimum simulation time.

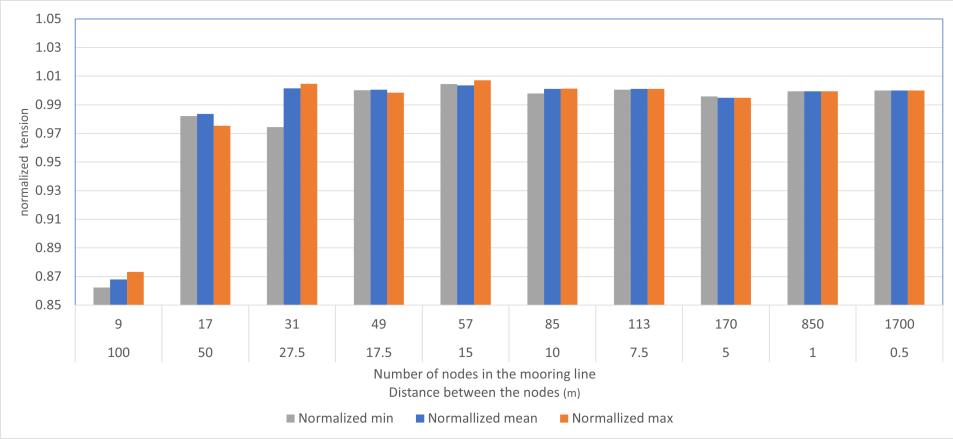

Figure 5.4: The normalized values for the maximum, mean and minimum values according to a 1-hour time series at the midpoint. The case with 1700 nodes is the reference case because it accounts for the maximum number of nodes possible in OrcaFlex.

5.1.3. Response spectrum of the mooring lines

The resonance peaks are of great relevance for the reliability of the lumping methods. Figure 5.5 shows the maximum tensions for each wave period in the mooring lines. The highest peaks in the tension spectrum occur for 9 and 10 s, which are the resonance periods in the x-direction! In the case study, the waves with these periods will contribute most to the total damage. Figure 5.5 shows the maximum tensions for each wave period. The corresponding tension spectra are given in appendix A.2.

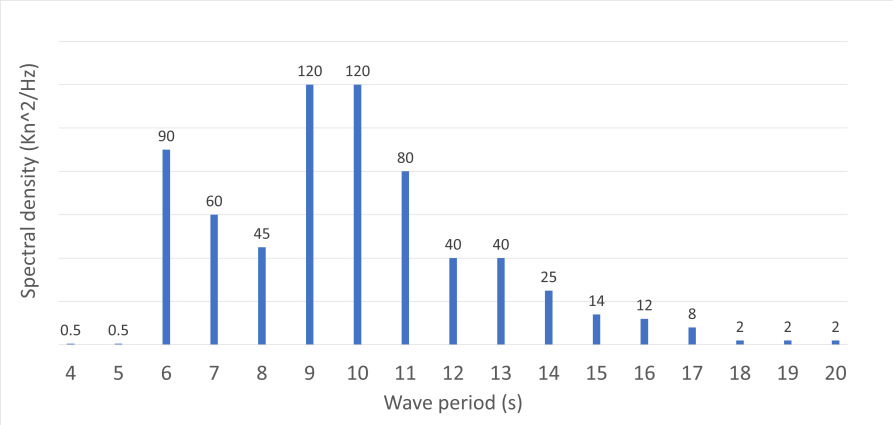

Figure 5.5: For the different periods, the corresponding maximum tension from the tension spectrum. The maximum peaks lay around 120 e^3 Kn^2/Hz, for $T = 9$ s and 10 s. The spectral density values are not the exact values but are rounded up.

5.2. Time domain fatigue assessment

This section describes the most governing load cases for fatigue damage, a combination of the probability of occurrence and the corresponding dynamics. In addition, these sections show how the damage ratio within the scatter diagram changes for different peak enhancement factors, γ_{peak}.

5.2.1. Probability

Figure 5.6 presents the input for the fatigue time domain calculation and zooms on the most frequently occurring sea states. This section accounts for 91% of the probability of the total scatter diagram.

Hs \ Tz	3.5	4.5	5.5	6.5	7.5	8.5	9.5	10.5	11.5	12.5	13.5	14.5	15.5	16.5
0.5	0.00%	0.13%	0.87%	1.19%	0.63%	0.19%	0.04%	0.01%	0.00%	0.00%	0.00%	0.00%	0.00%	0.00%
1.5	0.00%	0.03%	0.99%	4.98%	7.74%	5.57%	2.38%	0.70%	0.16%	0.03%	0.01%	0.00%	0.00%	0.00%
2.5	0.00%	0.00%	0.20%	2.16%	6.23%	7.45%	4.86%	2.07%	0.64%	0.16%	0.03%	0.01%	0.00%	0.00%
3.5	0.00%	0.00%	0.03%	0.70%	3.23%	5.68%	5.10%	2.84%	1.11%	0.34%	0.08%	0.02%	0.00%	0.00%
4.5	0.00%	0.00%	0.01%	0.20%	1.35%	3.29%	3.86%	2.69%	1.28%	0.46%	0.13%	0.03%	0.01%	0.00%
5.5	0.00%	0.00%	0.00%	0.05%	0.50%	1.60%	2.37%	2.01%	1.13%	0.46%	0.15%	0.04%	0.01%	0.00%
6.5	0.00%	0.00%	0.00%	0.01%	0.17%	0.69%	1.26%	1.27%	0.83%	0.39%	0.14%	0.04%	0.01%	0.00%
7.5	0.00%	0.00%	0.00%	0.00%	0.05%	0.27%	0.59%	0.70%	0.52%	0.28%	0.11%	0.04%	0.01%	0.00%
8.5	0.00%	0.00%	0.00%	0.00%	0.00%	0.10%	0.26%	0.35%	0.30%	0.17%	0.08%	0.03%	0.01%	0.00%
9.5	0.00%	0.00%	0.00%	0.00%	0.00%	0.03%	0.10%	0.16%	0.15%	0.10%	0.05%	0.02%	0.01%	0.00%
11	0.00%	0.00%	0.00%	0.00%	0.00%	0.01%	0.04%	0.07%	0.07%	0.05%	0.03%	0.01%	0.00%	0.00%
12	0.00%	0.00%	0.00%	0.00%	0.00%	0.00%	0.01%	0.03%	0.03%	0.02%	0.01%	0.01%	0.00%	0.00%
13	0.00%	0.00%	0.00%	0.00%	0.00%	0.00%	0.00%	0.01%	0.01%	0.01%	0.01%	0.00%	0.00%	0.00%
14	0.00%	0.00%	0.00%	0.00%	0.00%	0.00%	0.00%	0.00%	0.01%	0.00%	0.00%	0.00%	0.00%	0.00%
15	0.00%	0.00%	0.00%	0.00%	0.00%	0.00%	0.00%	0.00%	0.00%	0.00%	0.00%	0.00%	0.00%	0.00%
16	0.00%	0.00%	0.00%	0.00%	0.00%	0.00%	0.00%	0.00%	0.00%	0.00%	0.00%	0.00%	0.00%	0.00%
17	0.00%	0.00%	0.00%	0.00%	0.00%	0.00%	0.00%	0.00%	0.00%	0.00%	0.00%	0.00%	0.00%	0.00%

Figure 5.6: All sea states in the scatter diagram and the corresponding probabilities. T_z is the mean wave period on the horizontal axis, and H_s is the significant wave height on the vertical axis. The white cells are zero cells. The coloured ones have a nonzero value. Yellow indicates a low value; green indicates a higher value. The frame highlights T_z and H_s combinations, which highlight the most frequent load cases, with a combined probability of 91% concerning the total scatter diagram.

5.2.2. Damage

Figure 5.7 shows the normalized fatigue mooring line damage according to time domain simulations, waves from a Jonswap spectrum with a $\gamma_{peak} = 3.3$ and a lifetime of 25 years. The total damage normalizes the values. As expected from section 5.1.3, the most contributing load cases are H_s: 3.5 - 6.5 m with T_z: 8.5 - 10.5 s and contribute for 42% to the total damage. Since these load cases consist of resonance periods combined with a relatively high probability of occurrence, these combinations become the most critical for fatigue damage.

The periods above 11.5 s (12.5 - 16.5 s) cumulatively comprise only 3% of the total probability of sea state occurrence. Despite the low probability of occurrence, these periods contribute 12% to the total damage. This example shows the relevance of correctly calculating load cases with wave periods above 11.5 s. The reverse effect happens for the short wave periods, 3.5 - 7.5 s, which have a probability of occurrence around 30% and a contribution of 12% to the total damage. This emphasizes the presumption of a significant impact for damage caused by long wave periods.

Hs \ Tz	3.5	4.5	5.5	6.5	7.5	8.5	9.5	10.5	11.5	12.5	13.5	14.5	15.5	16.5
0.5	0.00%	0.00%	0.00%	0.00%	0.00%	0.00%	0.00%	0.00%	0.00%	0.00%	0.00%	0.00%	0.00%	0.00%
1.5	0.00%	0.00%	0.07%	0.26%	0.43%	0.27%	0.09%	0.02%	0.00%	0.00%	0.00%	0.00%	0.00%	0.00%
2.5	0.00%	0.00%	0.08%	0.66%	1.59%	1.68%	0.88%	0.25%	0.05%	0.01%	0.00%	0.00%	0.00%	0.00%
3.5	0.00%	0.00%	0.04%	0.61%	2.45%	3.64%	2.54%	0.95%	0.24%	0.05%	0.01%	0.00%	0.00%	0.00%
4.5	0.00%	0.00%	0.02%	0.38%	2.28%	4.79%	4.31%	2.01%	0.62%	0.16%	0.04%	0.01%	0.01%	0.00%
5.5	0.00%	0.00%	0.01%	0.20%	1.54%	4.38%	5.08%	2.88%	1.08%	0.34%	0.10%	0.03%	0.02%	0.01%
6.5	0.00%	0.00%	0.00%	0.09%	0.87%	3.16%	4.66%	3.19%	1.42%	0.52%	0.19%	0.08%	0.04%	0.02%
7.5	0.00%	0.00%	0.00%	0.04%	0.43%	1.94%	3.54%	2.93%	1.54%	0.66%	0.29%	0.13%	0.08%	0.05%
8.5	0.00%	0.00%	0.00%	0.01%	0.05%	1.07%	2.30%	2.30%	1.41%	0.72%	0.36%	0.19%	0.13%	0.08%
9.5	0.00%	0.00%	0.00%	0.01%	0.02%	0.53%	1.34%	1.60%	1.14%	0.68%	0.40%	0.23%	0.17%	0.11%
10.5	0.00%	0.00%	0.00%	0.00%	0.01%	0.25%	0.72%	1.01%	0.84%	0.57%	0.38%	0.24%	0.19%	0.13%
11.5	0.00%	0.00%	0.00%	0.00%	0.00%	0.11%	0.36%	0.59%	0.56%	0.44%	0.32%	0.22%	0.18%	0.12%
12.5	0.00%	0.00%	0.00%	0.00%	0.00%	0.04%	0.17%	0.32%	0.34%	0.30%	0.24%	0.18%	0.15%	0.12%
13.5	0.00%	0.00%	0.00%	0.00%	0.00%	0.02%	0.07%	0.17%	0.20%	0.19%	0.17%	0.13%	0.13%	0.10%
14.5	0.00%	0.00%	0.00%	0.00%	0.00%	0.01%	0.03%	0.08%	0.11%	0.11%	0.11%	0.09%	0.09%	0.07%
15.5	0.00%	0.00%	0.00%	0.00%	0.00%	0.00%	0.01%	0.04%	0.05%	0.07%	0.06%	0.06%	0.05%	0.11%
16.5	0.00%	0.00%	0.00%	0.00%	0.00%	0.00%	0.00%	0.01%	0.02%	0.03%	0.04%	0.03%	0.07%	0.00%

Figure 5.7: Normalized damage per sea state for mooring line 1, with a $\gamma_{peak} = 3.3$. Sea states H_s: 3.5 - 6.5 with T_z: 8.5 - 10.5 contribute 41.60% to the total damage. The white cells are zero cells. The coloured ones have a nonzero value. Yellow indicates a low value; green indicates a higher value. The absolute values for the damage are for γ_{peak} 1, 3.3, 6, respectively: 0.0097, 0.0089 and 0.0098.

This thesis focuses on the impact of the different γ_{peak} in the Jonswap spectrum, where $\gamma_{peak} = 1$ represents a broad ocean spectrum, 3.3 a regular North Sea spectrum and 6 a narrow-banded spectrum. Figure 5.7 shows the absolute damage of the different peak enhancement factors in the subscript. The absolute fatigue damage, in reality, would be higher since the assumptions reduce the environmental forces and only the wave-induced responses are considered in these results.

The values for the damage fit the expectation and are in the right order of magnitude. Besides, the fatigue damage for $\gamma_{peak} = 3.3$ is significantly lower than $\gamma_{peak} = 1$ and 6. In general, the broadest spectrum accounts for the highest total damage. However, due to the high probability of occurrence for resonance periods, the damage for $\gamma_{peak} = 6$ is slightly higher, which is explained by table 5.1.

Table 5.1 shows short wave periods, 3.5 s - 5.5 s, have increasing relative damage for an increasing γ_{peak}. The middle wave periods, 8.5 s - 10.5 s which include the resonance frequencies, show increasing relative damage for a rising γ_{peak}. In the case of long-wave periods, 14.5 s - 16.5 s, the opposite effect arises, meaning the long-wave periods get more relevant when the wave spectrum broadens. This finding aligns with the theory and is caused by a higher degree of extremes at $\gamma_{peak} = 1$, which shows the system's behaviour for extremes in wavelength. Moreover, these results indicate the high wave periods as relevant for the total damage. The sharper peak for $\gamma_{peak} = 6$ explains the relatively high damage as more waves around the resonance arise.

The relative damage due to the wave height has an equal distribution as the wave period in terms of focus in the scatter diagram. $\gamma_{peak} = 1$ has the lowest relative damage for the low wave heights. For the high wave heights, the opposite distribution counts. The difference between wave height and length is the equal distribution between the low, middle and high waves since the resonance periods have an equal spread over the wave heights.

Table 5.1: γ_{peak} and the relative damage ordered for short, medium and long wave periods and low, medium and high wave heights. The relative damage is the damage concerning the total damage. Resonance occurs for the middle wave periods. The 'relative damage' column gives the damage for all the wave heights in the indicated wave period range and vice versa the wave height.

γ_{peak}	Wave period (s)	Relative damage	Wave height (m)	Relative damage
1	3.5 - 5.5 (Short)	0.20%	2.5 - 4.5 (Low)	27%
3.3	3.5 - 5.5 (Short)	0.22%	2.5 - 4.5 (Low)	30%
6	3.5 - 5.5 (Short)	0.27%	2.5 - 4.5 (Low)	31%
1	8.5 - 10.5 (Middle)	56%	5.5 - 7.5 (Middle)	39%
3.3	8.5 - 10.5 (Middle)	66%	5.5 - 7.5 (Middle)	42%
6	8.5 - 10.5 (Middle)	70%	5.5 - 7.5 (Middle)	43%
1	14.5 -16.5 (Long)	6.2%	12.5 - 14.5 (High)	5.8%
3.3	14.5 -16.5 (Long)	4.3%	12.5 - 14.5 (High)	3.9%
6	14.5 -16.5 (Long)	2.5%	12.5 - 14.5 (High)	3.2%

5.3. Lumping block method

This lumping block method is characterized by factors ζ and β_j. This section determines both parameters for the UMaine VolturnUS-S Semi-submersible Platform. Moreover, ζ depends mainly on the floater's shape, not the environmental conditions.

5.3.1. Zeta, ζ

ζ links the spectral wave energy to the cumulative damage and equation 5.1 shows how. The factor is of great relevance for the lumped values and affects the accuracy of the method to a great extent. Figure 5.8 shows ζ as an empirical parameter, which is the best-fitted regression line for the equation in the left corner of this figure when plotting the cumulative fatigue damage to the spectral wave energy on a logarithmic scale. m is the slope of the t - n curve, and for this floating system, 3.

$$\begin{aligned} D_{a_k} &= m_{0k}^{\zeta m} \\ D_{a_j} &= \sum_{k=1}^{n_j} D_{a_k}\, p_k = \sum_{k=1}^{n_j} m_{0k}^{\zeta m}\, p_k \end{aligned} \tag{5.1}$$

The lumping block method would be compelling if ζ is constant for every floating system. Song sets $\zeta = 0.67$, for a square floater [48]. Simulating with this value overestimates the fatigue results by 15% (section 5.4.1 gives more details), meaning ζ must differ for every floating system to overestimate the damage with a maximum of 5%. Fitting ζ for each specific floater is a time-consuming task. Important to mention is the perfect fit of ζ's trendline in the article of Song.

An extensive series of time-domain simulations are plotted against the corresponding spectral wave energy to determine ζ for the UMaine VolturnUS-S Reference Platform. Figure 5.8 shows this logarithmic relationship and solution, resulting in $\zeta = 1.3774/3 = 0.46$ with an error of $R^2 = 0.600$. This value of ζ will be used to determine the lumped fatigue damage in section 5.4.1. The values for mooring line 2 are almost the same: 0.464 for line 1 and 0.468 for line 2.

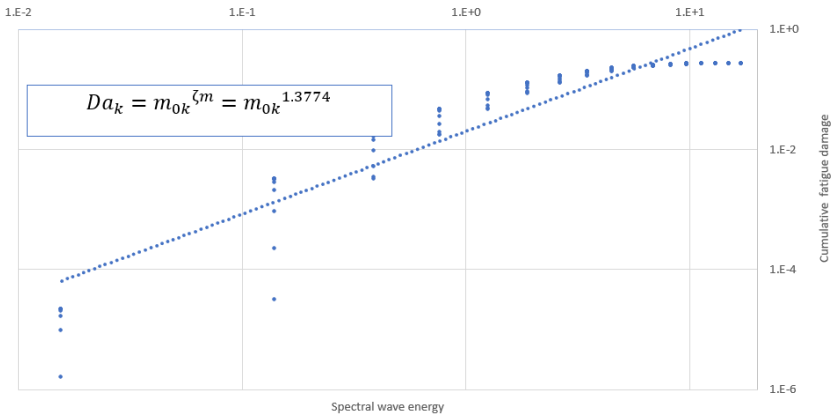

Figure 5.8: Emperical determination of ζ, based on time domain simulations. $\zeta = 1.3774/m = 0.46$, for $m = 3$. For all cases, for a $\gamma_{peak} = 3.3$ and mooring line 1, $R^2 = 0.600$.

Because of the low regression factor R^2, this thesis will also test the impact of a better-fitted trend line. Since the spectral density energy depends on H_s, the H_s values with the highest contribution to the total damage are considered. Section 5.2 shows H_s 2.5 to 9.5 m as the most governing cases responsible for 87% of the total damage. Figure 5.9 shows the corresponding fit, resulting in $\zeta = 1.1247/3 = 0.375$. Moreover, the corresponding error decreases to $R^2 = 0.901$.

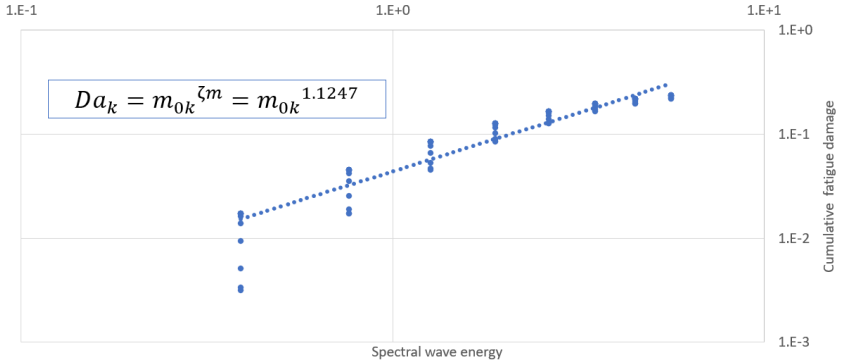

Figure 5.9: Emperical determination of ζ, based on time domain simulations. $\zeta = 1.1247/m = 0.375$, for $m = 3$. $H_s = 2.5 - 9.5$ m, for a $\gamma_{peak} = 3.3$ and mooring line 1, $R^2 = 0.901$.

With the primary goal of constructing a robust and efficient lumping block method applicable for all sea states, including varying γ_{peak}, looking for a constant ζ in all cases is essential. Otherwise, the lumping block method does not save time.

Table 5.2: Overview of all empirical ζ-values simulated for different γ_{peak}. The line in bold is the used values for the simulations in the next part of this thesis. Although the ζ fits different data points, the values are more or less similar.

γ_{peak}	Line	$\zeta_{allcases}$	R^2	$\zeta_{H_s 2.5-9.5}$	R^2
1	1	0.46	0.65	0.38	0.92
1	2	0.47	0.58	0.38	0.91
3.3	**1**	**0.46**	**0.60**	**0.37**	**0.90**
3.3	2	0.47	0.58	0.37	0.91
6	1	0.48	0.61	0.38	0.90
6	2	0.48	0.58	0.38	0.91

Table 5.2 shows for different γ_{peak} the corresponding ζ. Only minor differences in ζ occur for the different mooring lines and γ_{peak}. This makes the hypothesis to construct a robust and accurate method with a single ζ more plausible. Although the ζ for the mooring line 2 is similar to mooring line 1 in the three cases, the regression factor is slightly lower. The line in bold will be used in the next sections for the lumped damage simulations, where it is first determined which of the two values for ζ is used. In addition, this table indicates ζ depends mostly on the shape of the floater since the square-shaped floater results in a $\zeta = 0.67$ [48], and this triangle-shaped floater in $\zeta = 0.46$ [2]. While different environmental conditions, like in table 5.2, keep ζ almost the same.

5.3.2. Beta

As the theory in section 2.3.3 mentions, β_j is a correction factor for the representative wave height and makes the method of Song a bit more conservative. Equation 5.2 shows β_j as a multiplication factor for H_{srj}. Figure 5.10 indicates the order of magnitude for β_j, with a theoretical maximum of 1.031 for $m = 3$, and asymptotic progress to 1. β_j depends on the number of nonzero original sea states in a lumping block and therefore could differ for each block. This case study has a maximum of 196 nonzero cells for one lumping block resulting in β_j being 1.002. So this factor increases the representative wave height between 0.2% and 3.1%.

$$H_{srj} = 4.00\beta_j\sqrt{m_{0rj}} \tag{5.2}$$

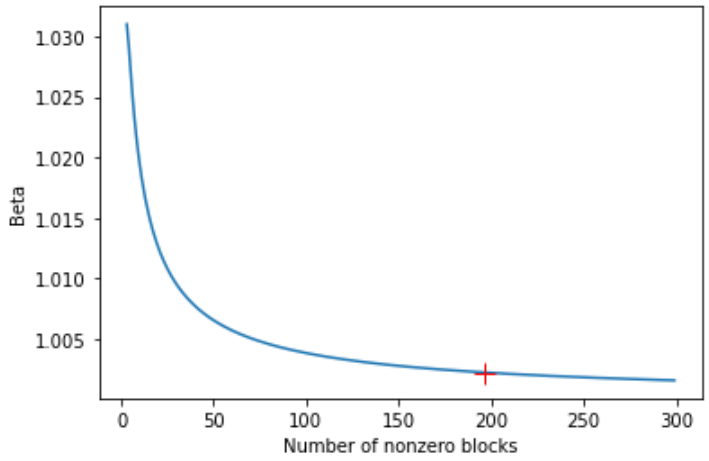

Figure 5.10: β_j against the number of nonzero cells in a lumping block. The red cross indicates the number of 196, the total of nonzero cells in the scatter diagram. The used values of β_j in this case study are all left of the red cross.

5.4. Accuracy of the method

This chapter summarizes the most important results of this thesis. Figure 5.11 and 5.12 conclude using $\zeta = 0.46$, which will be used during the simulations. Besides, these figures show the similarities between lines 1 and 2. Figure 5.13 indicates the reliability of the lumping method for different peak enhancement factors. Next, the reliability of the resonance blocks is determined. With this knowledge, the pitfalls of the method are explained. This shows that the lumping block method gives unreliable results for broad wave spectra.

5.4.1. Lumped values

All the damage results are visualized relative to the base case: a full-time-domain damage calculation of the scatter diagram. ζ does not influence the base case, but the γ_{peak} does. Therefore, three different base cases exist for γ_{peak} 1, 3.3 and 6. Dividing the lumped block damage by the base case damage gives the normalized damage. A normalized value of 1 is the same as the original time domain simulation. Everything below 1 is an underestimation, and above is an overestimation of fatigue damage. This thesis aims for a slight overestimation of the normalized value.

Determination of ζ

Figure 5.11 shows the reliability of the lumping block method for mooring lines 1 and 2 when the scatter diagram is divided into 57 blocks for different values of ζ. $\zeta = 1$ shows the effect of leaving the factor out and overestimating the damage by 17%, $\zeta = 0.67$ is the value for a square floater and overestimates the fatigue damage by 13%. The previous section justifies $\zeta = 0.46$ and $\zeta = 0.375$, with normalized lumped values of 11% and 10%, respectively.

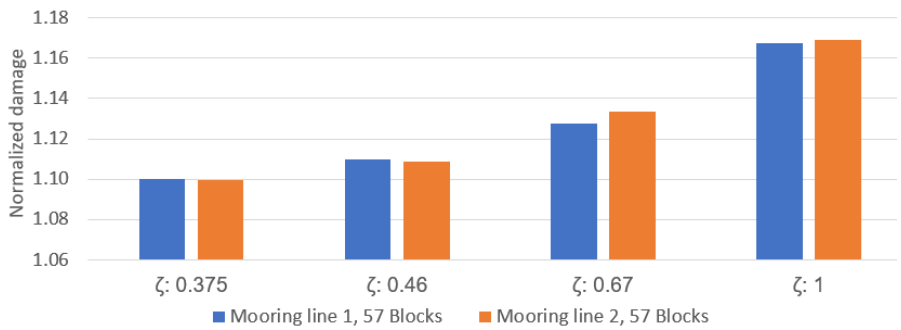

Figure 5.11: Impact of $\zeta = 1,\ 0.67,\ 0.46,\ 0.375$, for a $\gamma_{peak} = 3.3$. The blue blocks show mooring line 1 and the orange ones line 2. This is a visualization of 57 blocks. In conclusion, the reliability increases with a better fit of ζ. In addition, the accuracy for mooring lines 1 and 2 are comparable.

In conclusion, the impact of zeta is significant for the method's accuracy with an improvement of 7% compared to the situation without ζ. In addition, a ζ determined for a square floater overestimates the damage by 2-3% compared to the damage calculation with ζ for a tringle-shaped floater. With a difference of 1%, it is unclear whether $\zeta = 0.46$ or 0.375 is better to use. Besides, this graph visualizes the minimal difference between lines 1 and 2, which applies to all situations. Therefore the following charts show only line 1.

Figure 5.12 enlarges the differences between $\zeta = 0.375$ and 0.46. $\zeta = 0.375$ shows better reliability for the small block sizes: 57, 29 and 14. However, the accuracy for 4 lumping blocks drops to a normalized value of 0.85. While $\zeta = 0.46$ has normalized damage values of 1.11, 1.07, 1.04 and 0.95. In conclusion, $\zeta = 0.46$ gives better-lumped values than $\zeta = 0.375$ and will be used in the rest of the study. The next paragraph indicates the differences between both.

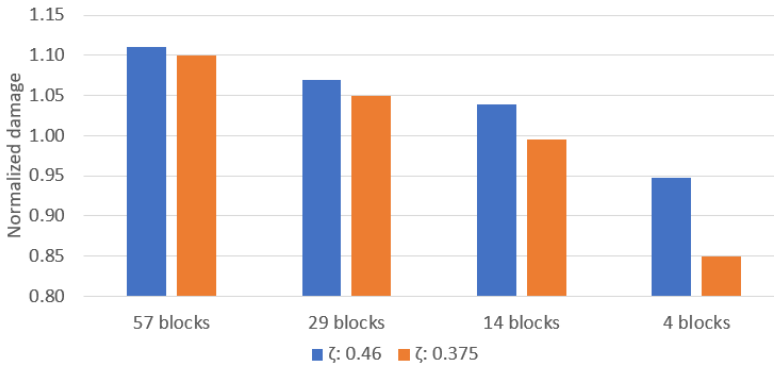

Figure 5.12: Difference between $\zeta = 0.46$ and $\zeta = 0.375$. Mooring line 1, $\gamma_{peak} = 3.3$.

Reliability per block for different ζ
By disregarding the wave height above 9.5 m to better fit the dominant load cases, the representative values H_{srj} and T_{zrj} differ. Table 5.3 shows the impact per block and the differences in H_{srj} and T_{zrj}. Surprisingly, the newly fitted ζ underestimates H_{srj} for the part included in the fit of ζ. Figure 5.9 shows an error for 8.5 and 9.5 m, the misfit in these load cases is too significant, leading to an underestimation of H_{srj}, and subsequently an underestimation of the damage shown in the relative damage column.

Table 5.3: The first two columns expresses the H_{srj} and T_{zrj} for the lumping blocks for $\zeta = 0.375$ and $\zeta = 0.46$. The third gives the difference between the first and the second column. The damage column shows the relative damage of the lumping block compared to the original time-domain simulations of the cells in the corresponding block. The last column gives the probability for a block. In conclusion, the difference in H_{srj} leads to the difference in relative damage. Block_{11} and block_{21} cover the resonance frequencies. The names of the different blocks are shown in figure 5.16. A high first number indicates a large wave height, H_s, and a high second number indicates a long wave period, T_z.

	$\zeta = 0.375$		$\zeta = 0.46$		Difference		Damage		Probability
	H_{srj}	T_{zrj}	H_{srj}	T_{zrj}	H_{srj}	T_{zrj}	$\zeta = 0.375$	$\zeta = 0.46$	
Block 11	3.70	8.93	3.90	9.00	-0.20	-0.07	0.88	1.03	89.9%
Block 12	5.73	12.03	5.88	12.04	-0.15	0.00	0.66	0.72	9.6%
Block 21	11.23	9.94	11.25	9.93	-0.02	0.01	1.04	1.05	0.2%
Block 22	11.42	12.43	11.44	12.42	-0.03	0.02	0.84	0.96	0.3%

The lower ζ ensures too low values for the representative H_{srj}. The 'damage' column in table 5.3 shows $\zeta = 0.46$ gives a good estimation for the most critical damage load case, block_{11}. Subsequently, the underestimation of damage of total damage could be attributed to the difference in block_{11}. This result shows that the miscalculation in H_{srj} contributes to underestimating the total damage. In addition, the difference in H_{srj} for block_{21} and block_{22} is almost none since these blocks have a low probability of occurrence.

The equations for representative spectral wave energy in section 2.3.3 show the multiplication of the probability of sea state k by the spectral wave energy. Since the chance of a wave height above 9.5 m

is 5% of the total, the effect on the total damage is almost not measurable. Although the reliability for $block_{12}$ is better for $\zeta = 0.46$, the accuracy is poor. Section 5.4.3 explains why.

The reliability of the lumping block method for different γ_{peak}
Figure 5.13 shows the reliability of the damage calculation for the γ_{peak} 1, 3.3 and 6 and a changing number of lumping blocks. For a peak enhancement factor of 1, the reliability decreases from 1.11 for 57 blocks to 0.78 for one lumping block. The reliability for γ_{peak} 3.3 starts at 1.11 and decreases to 0.90 for a single lumping block. The method is reliable for a peak enhancement factor of 6, as the relative damage stays at or above 1: 1.12, 1.08, 1.07, 1.01, 1.00 and 1.01. With $H_{srj} = 4.26\ m$ and $T_{zrj} = 9.59\ s$ for 1 block.

This graph shows that the reliability improves for an increasing γ_{peak}. Moreover, the lumping block method for $\gamma_{peak} = 1$ is unreliable, caused by the decreasing pattern of the reliability with a decreasing number of blocks, visualized by the blue bars in figure 5.13. The reliability decreases linearly and does not become asymptotic. This conclusion also remains if the method is extended by adding a parameter β as Song proposed. For $\gamma_{peak} = 3.3$, the lumping method slightly underestimates the fatigue damage, especially for 1, 4 and 8 blocks.

Song focuses on a $\gamma_{peak} = 3.3$ and does receive reliable results [48], while this study slightly underestimates the damage. This study's slight underestimation of the damage is due to the worse fit for ζ, as explained in section 5.3.1. For this specific floater, it is possible to make the results reliable by increasing ζ. However, it is not an elegant way to improve reliability by reverse engineering. However, it could be helpful in engineering practice about this specific floater.

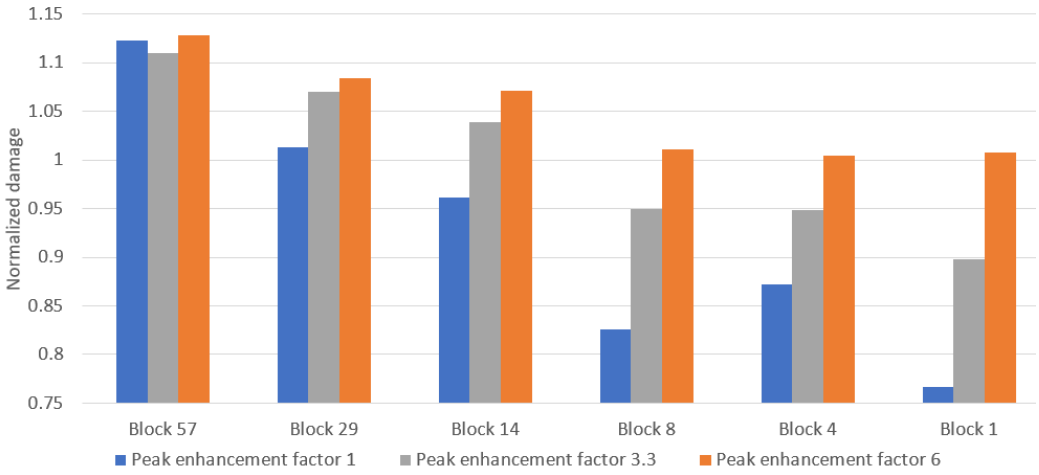

Figure 5.13: The fatigue damage calculation reliability of a lumping block method for γ_{peak}: 1, 3.3 and 6 for different numbers of blocks, relative to time domain calculations of the scatter diagram. "1" at the x-axis corresponds to the same fatigue damage as the time-domain fatigue calculation. The lumping block methods underestimate the fatigue damage below one and overestimate above 1. The figure shows good reliability for a γ_{peak} of 6 and poor accuracy for a γ_{peak} of 1.

Reliability per block for different γ_{peak}
The reliability for this lumping block method relies on a high extent to ζ. The last section shows accurate results for $\gamma_{peak} = 6$, but poor results for $\gamma_{peak} = 1$. Differences in ζ cannot explain this difference in reliability since the fitted values are the same and the regression of the data points have the same error for all γ_{peak}, as shown in table 5.1. To clarify the difference, this section focuses on the difference per block leading to the underestimation of the model, and section 5.4.3 relates the physics to the lumping block model.

Table 5.4 indicates the accuracy for 8 lumping blocks per lumping block. The "time-domain" column expresses the fatigue of the cells from the original scatter diagram that fall in a given lumping block relative to the total time-domain fatigue damage. In the "lumped" column, the lumped damage values of a lumping block are given relative to the fatigue damage of the corresponding original cells in the scatter diagram.

Table 5.4: The lumping block values for γ_{peak} 1, 3.3 and 6, $block_{31}$ only has zero values and are not shown. The "time-domain" column expresses the damage of the cells from the original scatter diagram that fall in a given lumping block relative to the total time-domain fatigue damage. In the "lumped" column, the lumped damage values of a lumping block are given relative to the fatigue damage of the corresponding cells in the original scatter diagram. The lines in bold highlight the main difference between γ_{peak} 1 and 6. $Block_{12}$, $block_{22}$ and $block_{32}$ cover the resonance frequencies. The names of the different blocks are shown in figure 5.16. A high first number indicates a large wave height, H_s, and a high second number indicates a long wave period, T_z.

γ_{peak}:	1		3.3		6	
Relative damage to:	Time-domain	Lumped	Time-domain	Lumped	Time-domain	Lumped
block11	0.11	0.92	0.12	0.93	0.11	0.91
block12	**0.44**	**0.95**	0.50	0.99	**0.52**	**1.07**
block13	0.00	0.89	0.00	0.94	0.00	0.89
block21	0.01	1.07	0.01	1.11	0.01	1.00
block22	**0.40**	**0.67**	0.34	0.91	**0.34**	**0.96**
block23	0.02	0.73	0.02	0.77	0.01	0.68
block32	0.02	0.70	0.01	0.85	0.01	1.07
block33	0.00	0.97	0.00	1.14	0.00	1.08

Section 5.2 explains a higher relative contribution for higher wave periods to total damage when the γ_{peak} decreases. In addition, table 5.3 and 5.4 emphasize the lumping block method's low reliability for calculating the representative fatigue damage for lumping blocks with long wave periods, especially for a $\gamma_{peak} = 1$. The "lumped" column indicates the reliability for $\gamma_{peak} = 1$, $block_{22}$ is 0.3 lower compared to this block with $\gamma_{peak} = 6$ and highlights why the lumping method is unreliable for $\gamma_{peak} = 1$. Or the other way around, the lumping block method shows better results for the blocks with short wave periods than those with long wave periods. While in contrast, the long wave period blocks contribute more and more to the total damage for a decreasing peak enhancement factor. Figure 5.16 shows the configuration of different amounts of blocks.

This difference is visualized in figure 5.14 and 5.15. Instead of the lumped values, the error is plotted: '1 - relative lumped damage'. These figures demonstrate the increasing error for more relevant blocks for a $\gamma_{peak} = 1$, compared to a $\gamma_{peak} = 6$. Where blue is the contribution to the damage, a higher bar contributes more to the damage. The red bars indicate the error, and a more significant error corresponds to a high bar.

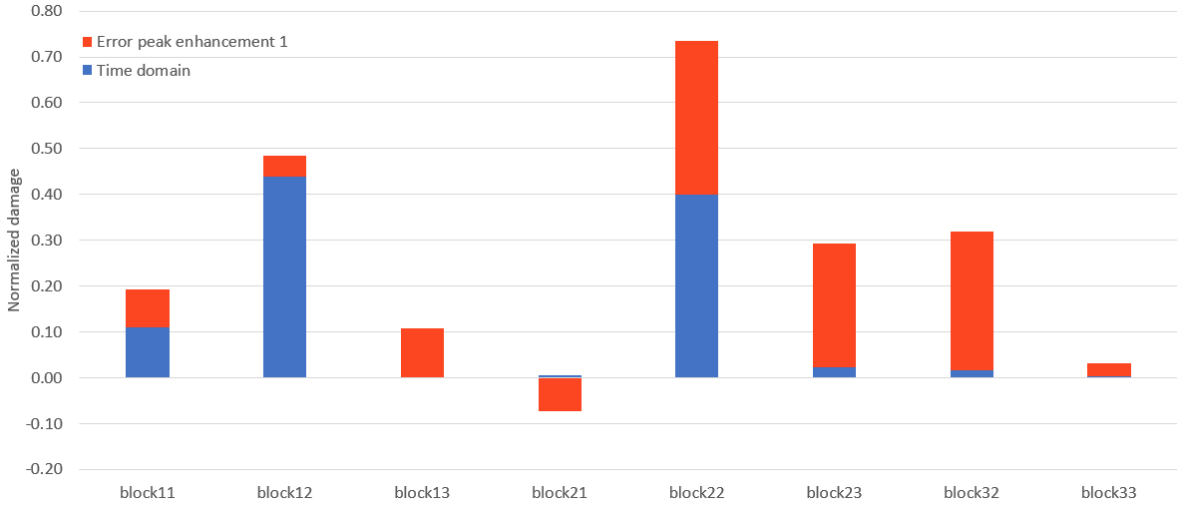

Figure 5.14: Damage relative to the total time-domain in blue and the error of the lumped damage relative to the corresponding damage from the cells in the original scatter diagram in red, a negative error means an overestimation of the damage. $Block_{12}$, $block_{22}$ and $block_{32}$ cover the resonance frequencies. The contribution to the damage of $block_{22}$ increases. Furthermore, the error compared to the $\gamma_{peak} = 6$ increases, resulting in an unreliable lumping block method for $\gamma_{peak} = 1$.

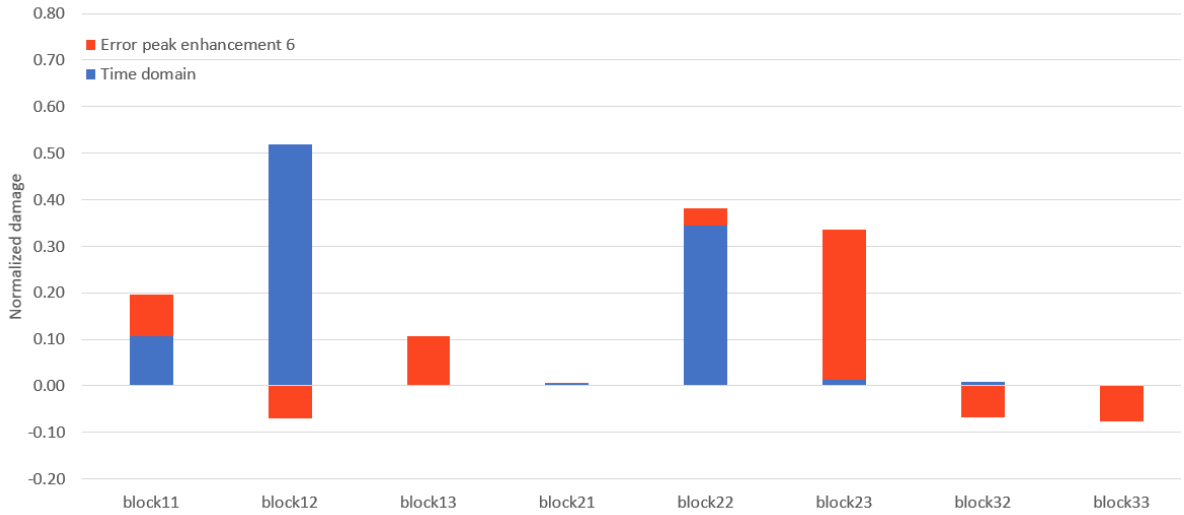

Figure 5.15: Damage relative to the total time-domain damage in blue and the error of the lumped damage relative to the corresponding damage from the cells in the original scatter diagram in red, a negative error means an overestimation of the damage. Block_{12}, block_{22} and block_{32} cover the resonance frequencies. The impact of block_{22} decreases compared to $\gamma_{peak} = 1$, and more importantly, the error decreases, resulting in a reliable lumping block method for $\gamma_{peak} = 6$.

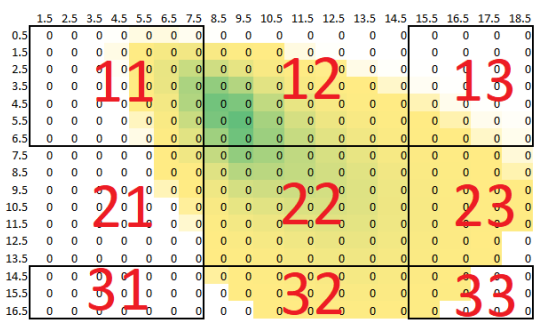

(a) The names for 8 different blocks.

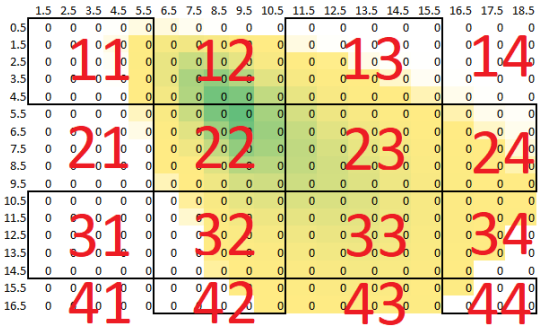

(b) The names for 14 different blocks.

Figure 5.16: The names and layout of the different blocks. The first digit indicates the row, and the second number indicates the column. A high first number indicates a large wave height, H_s, and a high second number indicates a long wave period, T_z. The coloured ones have a nonzero value. Yellow indicates a low value; green indicates a higher value.

5.4.2. Resonance and lumping methods

This section expresses the reliability of the lumping block methods around the resonance peaks for the mooring lines. Section 5.1.3 shows resonance peaks for 9 and 10 s. Lumping the scatter diagram in 57 blocks, the 5^{th} block of every row encloses the resonance periods. Figure 5.17 and 5.18 visualize the difference between the reliability of the damage for the "resonance blocks" and the other blocks normalized with the damage from the scatter diagram for the γ_{peak} 1 and 6. The blue bars in figure 5.17 correspond to the resonance blocks only, and the orange bars to the average reliability of the other blocks in the row. So the average of the first row encloses block_{11} to block_{14} and block_{16} to block_{19}, and disregards the zero-blocks.

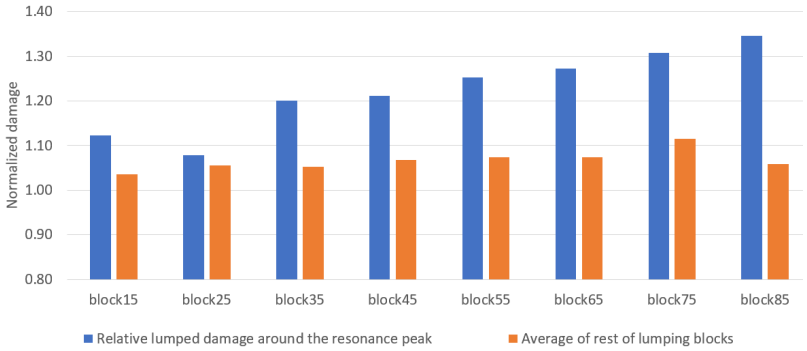

Figure 5.17: Relative damage for 57 lumping blocks and a $\gamma_{peak} = 1$, normalized by the damage from the original sea states. Blue shows the relative damage for every resonance block. The orange bars express the average reliability of the other lumping blocks in the row. So the average of the first row encloses $block_{11}$ to $block_{14}$ and $block_{16}$ to $block_{19}$, and disregards the zero-blocks.

These figures show the lumping block method for the resonance blocks overestimates the lumped damage up to 30%. Furthermore, the difference between the average and resonance blocks is significant and increases for an increasing H_s. Both figures show a similar course of the overestimation of the damage. The blocks with a low wave height, $block_{15}$ to $block_{35}$, overestimate the fatigue damage less than the blocks with an increasing wave height. The overestimation of both peak enhancement factors is comparable.

The overestimation for the resonance periods explains the overestimation in the 57 and 29 blocks results in figure 5.13. Since these configurations isolate the resonance frequencies leading to too conservative lumping damage results.

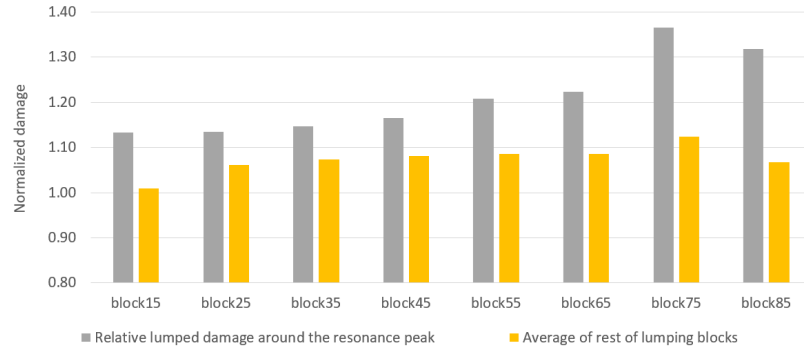

Figure 5.18: Relative damage for 57 lumping blocks and a $\gamma_{peak} = 6$, normalized by the damage from the original sea states. Grew shows the relative damage for every resonance block. The yellow bars express the average reliability of the other lumping blocks in the named row. So the average of the first row encloses $block_{11}$ to $block_{14}$ and $block_{16}$ to $block_{19}$, and disregards the zero-blocks.

The overestimation of the damage around the resonance blocks is due to the determination of H_{srj} in the lumping block method. The lumping method overestimates the representative wave height to aim for a slight overestimation of the damage. Since the damage is positively correlated to H, an increasing H always results in higher damage. Moreover, the non-Gaussianity of the mooring line response caused by non-linear waves is positively related to the wave height [55]. Meaning an increasing wave height results in a higher level of non-Gaussian response. Subsequently, the increasing wave height results in more fatigue damage. This results in additional overestimation at higher wave heights or non-linear character of damage at resonance. Thus a slight overestimation of H leads to a substantial overestimation of the corresponding damage, resulting in an increasing overestimation for $block_{55}$ to $block_{85}$ since H_s is higher for these blocks.

5.4.3. Pitfall lumping method

Section 5.4.1 and specifically figure 5.13 indicates the lumping methods for a peak enhancement factor 6 as reliable and with a factor of 1 unreliable. This section explains this difference by relating the physics to the lumping block model. Table 5.4 zooms in on the differences per block for 8 lumping blocks. In particular, the blocks from the second column ($block_{22}$ and $block_{32}$) have poor reliability for $\gamma_{peak} = 1$. Table 5.5 overviews 29, 14 and 8 blocks for the specified blocks that enclose 11.5 - 15.5 s and the corresponding relative damage. The damage for these wave periods significantly differs between γ_{peak} 1 and 6. Especially the blocks with a wave height above 6 m have an unreliable pattern for $\gamma_{peak} = 1$. These lines are highlighted in bold.

The poor reliability for the resonance blocks cannot declare these unreliable results, especially not the difference between γ_{peak} 1 and 6 since both have the same poor pattern, as shown in section 5.4.2. Moreover, the resonance wave periods are seconds below these cases.

Table 5.5: For a different amount of lumping blocks, the reliability for the blocks which enclose wave period 11.5 - 15.5 s. The values are normalized by the damage for the cells in the original scatter diagram. The bold lines have a H_s above 6 m and show an unreliable pattern. The names of the different blocks are shown in figure 5.16. A high first number indicates a large wave height, H_s, and a high second number indicates a long wave period, T_z.

29 blocks			14 blocks			8 blocks		
	Lumped 1	Lumped 6		Lumped 1	Lumped 6		Lumped 1	Lumped 6
$block_{14}$	1.05	1.07	$block_{13}$	0.95	1.00	$block_{12}$	0.95	1.07
$block_{24}$	1.01	1.06	**$block_{23}$**	**0.77**	0.91	**$block_{22}$**	**0.67**	0.96
$block_{34}$	**0.93**	1.07	**$block_{33}$**	**0.79**	0.92	**$block_{32}$**	**0.70**	1.07
$block_{44}$	**0.92**	1.06	**$block_{43}$**	**0.83**	1.04			
$block_{54}$	**0.95**	1.14						
$block_{64}$	**1.06**	1.13						

For the explanation of the difference, damage-increasing environmental circumstances are critical. Firstly, combining long-wave period and wave height is essential for underestimating the damage and is visible in the first row of table 5.5. $Block_{14}$, $block_{13}$, and $block_{12}$ give good representations of the damage, while the accuracy decreases for a higher H_s. The unreliable results for a broad wave spectrum are caused since $\gamma_{peak} = 1$ contains more non-linear waves than $\gamma_{peak} = 6$. For increasing H_s and non-linear sea states, the skewness and kurtosis of the mooring line response spectrum increase [55], creating more outliers in tension which results in greater fatigue damage and explaining the differences in the accuracy of the lumping block method between γ_{peak} 1 and 6.

In addition, two other wave spectrum parameters increase the misfit in the lumping block method's reliability. Table 5.1 shows the large wavelengths and heights increase in relevance for fatigue calculation with a decreasing γ_{peak}, section 5.4 concludes with the method's poor reliability for long wavelengths. In addition, the damage increases with a growing number of frequencies in the wave spectrum, caused by more non-linearities of the waves. These environmental circumstances happen for a $\gamma_{peak} = 1$ spectrum. Since these conditions increase the damage compared to a narrow wave spectrum, the proposed method underestimates the representative wave height and period. Therefore the model underestimates the damage above the resonance frequencies.

This leads to the conclusion that the used lumping block method has unreliable results for a spectrum with a large frequency spread, such as a spectrum with a $\gamma_{peak} = 1$. Generally, the model decreases in reliability when the broadening of a wave spectrum causes damage-increasing conditions.

The blocks in table 5.4 are not those with the longest wavelengths. Moreover, the blocks with the longest wavelength score better on reliability. These blocks at the end of the scatter diagram are more likely to have a small number of original cells since these blocks enclose a lot of sea states with zero probability. This is visible in figure 5.16. If a lumping block consists of a few original sea states, like 1, 2 or 3, the accuracy is around 100%. Since the representative values are (almost) the same as the original time domain simulations, the damage calculation from the model will be the same. Moreover, these blocks have less impact on the total damage due to the low probability of occurrence.

In conclusion, the relatively high likelihood of events for waves between 11.5 - 15.5 s, their increasing relevance for a low γ_{peak} and the shortcomings of the lumping method at these spectral parameters ensure that not the longest wavelengths but the wavelengths just above resonance underestimate the fatigue damage and ensure the method is not reliable in those cases.

5.5. Assumptions

This section indicates the assumptions for the case study, with the primary goal to focus and conclude only on the reliability of the lumping block method. Moreover, the results can be assigned to a single wave-induced load case. Firstly, the only environmental force is wave-induced, so no wind and current forces are exposed to the wind turbine. In addition, only a one-directional wave spectrum is used for the wave input, so there is no directional spreading. Besides, the wave spectrum only consists of wind waves, so there is no swell, and the environmental conditions besides wind are constant and zero. Lastly, the turbine is parked. This section explains the impact of these assumptions.

Wind and waves

The surge response of the floater is the main contributor to mooring line damage. Waves, wind and currents will contribute to this movement. Since the wind and current are constant and zero in the simulations, the corresponding calculations underestimate the damage compared to reality. This chapter gives insights into the effects of these assumptions.

Below rated wind speed, the surge motions are mainly dominated by the wind, and waves barely contribute to the motions. However, these low wind speed fatigue contribution from wind-dominated load cases is minimal compared to the wave-dominated load cases. At rated wind speed, the total thrust force is maximal. Subsequently, the surge motion is the highest wind-wave combination and is mainly surge resonance induced. The low-frequency waves are dominant for the wave-induced force at rated wind speed. The motions are wave-induced for wind speed above rated wind speed, with the extreme wave and the surge resonance as most critical for damage. The fatigue is wave dominated, resulting in greater damage if the wave height increases [55] [27].

Generally, the corresponding wind damage is mainly dominated by the low-frequency turbulent wind-induced response for wind speed closest to the rated wind speed. Compared to rated wind speed during operational conditions, the mooring line damage caused by wind becomes smaller for both lower and higher wind speeds when waves stay constant [55].

In general, when exposed to wave-only conditions, the fatigue damage of the mooring line is proportional to wave height. For any load case with constant windspeed, fatigue damage increases with increasing wave height. Increasing wind speed above the rated windspeed for a given wave height and period decreases fatigue damage [51].

In conclusion, wind-induced movements contribute significantly to the damage of the mooring lines. Disregarding the wind forces leads to an underestimation of the total fatigue. However, the majority of the wind-induced motions are approximately Gaussian. Leading to fewer outliers caused by wind, meaning the wind-induced motions are better predictable than the non-Gaussian wave-induced responses [27].

Multi-directional wave spectrum and swell

The case study of this thesis considers frequencies corresponding to the Jonswap spectrum with waves from one direction. Meaning wave frequencies (WF) and some low frequencies (LF) are considered. However, this thesis disregards swell (extremely low frequencies) and the multi-directional wave spectrum. By disregarding the directional spreading, the damage in the lines can be assigned to a single wave load case. This thesis does not include swell since almost no swell exists in large parts of the North Sea [6]. This section will explain the impact of those assumptions.

Comparing multi-directional waves with a single-directional wave for 6-DOFs, generally concludes the single-directional wave is over-predictive for the resulting responses. However, in some movement directions, the damage increases for a multi-directional wave spectrum like the yaw direction. Though

the damage to mooring lines mainly depends on surge response, a single-directional wave spectrum will turn into larges responses and, subsequently, greater damage. This is because more extremes occur when the waves come from a single direction. Considering only single-directional waves is, therefore, an overestimation of reality. [1]

WF and the LF both add to the total damage. If the associated damage is separated, it turns out that the WF-induced damage in most directions is dominant for mooring line fatigue when considering waves from a Jonswap spectrum. However, the LF provides a greater damage contribution for all rotational movements and the heave direction. The WF is dominant in the leading damage directions, like the surge response, caused by the higher probability. Despite the total damage is reduced by excluding swell. The most contributing frequencies are included. Considering the Jonswap spectrum for the case study means low-frequency waves exist but no swell. Changing the peak enhancement factor of the Jonswap from 1 to 3.3 leads to a reduction of 20% in low-frequency waves and goes up to 40% for the extreme cases of γ_{peak} = 6 or 7. Concerning only one-wave direction is a conservative assumption for total damage [1].

Current
This section indicates the effects of disregarding the current forces. Fatigue in the mooring lines due to current is partially caused by the (constant) force of the flow but mainly caused by the Vortex-Induced Motion (VIM) from current eddies [54]. As the draft of a floater increases, the contribution from VIM fatigue damage can become a governing factor for mooring design.

Current could be a governing design criterion for places like the Gulf of Mexico and Offshore West Africa. However, for North Sea practices, the fatigue corresponding to the current force is minimal since the current flows are negligible. Subsequently, the VIM is not present. Therefore disregarding the current in this thesis has little impact on the results [54].

Rotor movement
In addition to disregarding the wind and current force, the turbine is parked. This section indicates the impact of the nonrotating blades. A rotating turbine ensures damping in the surge direction. Section 5.1.1 explains the missing damping for the parked turbine, resulting in less surge movement and, thus, mooring line damage.

In addition to the motion damping, the tower expires damage due to the blade passing (3P) effect in operational conditions. For tower damage, this is a critical factor in the total damage. However, the blade passing effect does not affect the damage in the mooring lines. Also, the 1P blade effects impact the damage in the tower but have no impact on the floater and mooring line dynamics [4]. Therefore, this assumption does not affect the mooring line damage.

5.6. Relevance for fatigue modelling

The results of this thesis conclude on the accuracy bounds of Song's lumping block method. It turns out that the model's reliability decreases when the broadening of a wave spectrum causes damage-increasing conditions, like outliers in wave period and non-linear and irregular waves. Besides the proposed method of Song, there are many other methods to simplify and speed up fatigue calculations. Based on studies and this thesis, this chapter indicates the most critical parts for simplifying a fatigue calculation method in general. The main points are the response's Gaussianity and the waves' non-linear behaviour.

Gausiannity
Skewness and kurtosis characterize the non-Gaussianity of the response. Section 2.5.2 defines those measures and gives the values for a Gaussian distribution. Positive skewness indicates a longer tail on the right side, and positive kurtosis accounts for a peaked course with heavy tails. Both positive values result in a response with many outliers compared to neutral values with the same variance.

Xu et al. describe the Gaussianity of the mooring line response for a semi-submersible floater in different environmental circumstances for linear and non-linear waves [55]. When considering linear waves only, the skewness and kurtosis of the response spectrum will increase slightly for load cases above rated wind speed.

However, including non-linear waves, the skewness and kurtosis factors of the surge response spectrum multiply with a factor of 2 compared to only linear waves. This leads to high non-Gaussianity due to wave non-linearity in combination with increasing wave height, resulting in higher extreme tension from the fully non-linear waves. Therefore, linear wave theory underestimates tension response when the waves become large. Moreover, mooring line tension tends to be quite non-Gaussian at large sea states, while other environmental response processes appear to be quite Gaussian [55].

Nonlinearity
The previous section shows the non-Gaussian behaviour for the non-linear wave-induced surge response. This section explains the connection between the non-Gaussianity of the response and fatigue calculations by comparing purely linear wave and wave spectra with non-linear waves exposed to the FOWT.

For small sea states, the differences between in or excluding non-linear waves are negligible. Both situations result in the same mooring line tension. For increasing wave heights, the linear waves underestimate the fatigue calculation significantly compared to non-linear waves, and the underestimation increases significantly with increasing wave height. When considering only wave force, the surge motion and mooring line tension are underestimated by approximately 25% and 25%, respectively, compared to situations with non-linear waves. Leading to a 50% underestimation in mooring line damage [55].

The non-Gaussiannity of the wave response increases with a higher degree of non-linearity and increasing wave heights. Furthermore, mooring line tension tends to be non-Gaussian at large sea states, with an increasing non-Gaussianity for a rising wave height and non-linearity, leading to more mooring line fatigue damage when the wave height increases. The results are the same for a rotating and parked turbine

In conclusion, considering non-linear wave kinematics is critical for maintaining the correct line tension in designing and analyzing mooring lines for FOWT, especially for high wave heights. Remarkable since other response processes appear to be quite Gaussian, for example, wind-induced motions, leading to primarily linear motions and tensions.

Thesis results
The results of this thesis emphasize the explanation from the literature of the behaviour between (non-)linear waves and the corresponding (non-)Gaussian response. The main differences in this thesis arise as the wave spectrum becomes wider and the waves become higher, both effects producing non-linear waves. The thesis results also show a significant difference in damage calculation for the lumping method, for a higher demand of non-linear waves and an increasing wave height, leading to a significant underestimation of the corresponding fatigue damage.

Table 5.5 shows poor damage calculation results for an increasing wave height and a broad wave spectrum. Both parameters lead to more non-linear waves, resulting in non-Gaussian behaviour of the surge response of the floater. The skewness and kurtosis of the response spectrum increase, which leads to an increased chance of outliers of the response and, thus, the forces in the mooring lines. The outliers significantly influence the fatigue outcome and predictability. Table 5.5 shows the differences between γ_{peak} 1 and 6. The main reason for the underestimation is caused since the proposed lumping block method does not properly consider these outliers, making the method unreliable for broad wave spectra.

This example emphasizes the most important criteria for simplifying mooring line fatigue simulations: the non-linear waves leading to non-Gaussian responses of the mooring lines. Both the reference paper and this thesis show that this can lead to an underestimation in fatigue calculation between 25% and 50% comparing linear to non-linear simulations. While the other environmentally induced forces, like wind and constant current, result in Gaussian mooring line response, the wave-induced tensions lead to non-Gaussian mooring line responses and tensions.

Especially non-linear waves with an increasing wave height, the non-linear wave-induced motions are the most critical parameter to consider for reliable fatigue calculations. They must be taken into account for simplifying fatigue mooring line calculations. Based on this research, it is recommended to calculate the load cases above a specific wave height based on regular time domain simulations and to simplify everything below this wave height and the combination with other environmental forces.

6

Conclusion

This thesis tests a lumping block method on accuracy in broad and narrow wave spectra. The method aims to construct a robust and efficient alternative for the computationally expensive time domain fatigue calculations of mooring lines in the early design stage of a Floating Offshore Wind Turbine. A robust way of modelling must be applicable and reliable in all possible sea states, including extreme wavelengths, non-linear waves, and dynamic amplification caused by the resonance frequencies.

Recent studies show the lumping block method's good accuracy and applicability for a North Sea Jonswap spectrum, which is rather narrow-banded. This thesis varies the broadness of the wave spectrum to investigate the effect on the method's reliability and applicability in all sea states. The method's reliability for different wave spectra is validated by comparing the proposed numerical lumped time-domain simulations with the original numerical time-domain simulations.

As explained in the following paragraphs, the main conclusion of this thesis is that applying the lumping block method in broad wave spectra leads to severe limitations.

Fatigue assessment
The long wavelengths cause relatively more fatigue damage for broad wave spectra than the same waves with a narrow banded spectrum. The long waves barely contribute to the total damage in the narrow-banded wave spectra. The middle wavelengths, which include the resonance frequencies, contribute even more to the total damage compared to the same waves in a broad wave spectrum, as shown in table 5.1.

Generally, the literature indicates a broad wave spectrum will cause more damage to mooring line fatigue than a narrow spectrum, especially for a sea scatter diagram with a high probability for extreme wave periods. On the other hand, damage due to resonance frequencies is larger than in short and long wave periods. Since the likelihood for these frequencies in the narrow-banded wave spectrum is higher, a narrow-band spectrum leads to greater total mooring line damage.

The thesis results show that, in general, one cannot indicate if wave-induced responses from a broad or narrow-banded spectrum cause more total damage since the difference in absolute damage between both spectra depends on the spread in wave periods and the corresponding probability over the scatter diagram.

Resonance and lumping methods
As shown in section 5.4.2, the lumping block method has poor reliability for the resonance frequencies. The method overestimates the corresponding damage from 10% for low wave heights to 30% for high wave heights, caused by the intended overestimation for the representative wave height H_{srj} of the lumping block method and the corresponding increase in non-Gaussian mooring line response, as explained in section 5.6. Although resonance impacts the total fatigue damage in a narrow spectrum more, the lumping method overestimates the damage in a broad and narrow spectrum in the same order of magnitude.

Wave spectrum and lumping methods
The main conclusion of this thesis is that the lumping method's reliability decreases for the broadening of a wave spectrum since it causes damage-increasing conditions, like extreme wave periods, more frequencies in the wave spectrum and non-linear waves. The lumping block method underestimates the damage for a broad wave spectrum. The reliability for a single lumping block is 20% lower for a broad spectrum simulation than the same narrow wave spectrum simulation. Furthermore, for broad wave spectra, the lumping block method systematically underestimates the mooring line's damage for wave periods above the resonance periods by 25% for the 4 and 8 blocked cases.

This is caused by the fact that the lumping block method has more accurate results for the blocks with short wave periods than for those with long wave periods. In contrast, the long wave periods contribute more and more to the total damage for a decreasing peak enhancement factor, leading to a consistent underestimation of the mooring line's structural damage for broad wave spectra. Furthermore, the lumping method poorly simulates the damage for increasing frequencies in the wave spectrum, outliers and non-linear waves. An increasing amount of non-linear waves and increasing wave height causes many outliers in response since the kurtosis and skewness of the tension spectrum increase. This influences the fatigue outcome and the predictability significantly, which explains the differences in the accuracy of the lumping block method between γ_{peak} 1 and 6.

For a decreasing number of lumping blocks, the accuracy decreases linearly for a broad wave spectrum, while the reliability stabilizes for a narrow spectrum. The method has no constant deviation in accuracy. Therefore, the proposed lumping block method is unreliable for a broad wave spectrum. This conclusion also remains if the method is extended by adding a parameter β as Song proposed.

Nevertheless, the lumping method gives accurate results for damage calculation with a corresponding narrow wave spectrum. The proposed method yields accurate but slightly conservative damage results. The method has accurate results for the lines of a floater and is reliable and independent of the number of lumping blocks. Therefore, the lumping block method is robust and efficient in fatigue calculations of mooring lines for sea states corresponding to a narrow spectrum. Also, the results of this thesis conclude that the lumping block method is safe and usable for significant parts of the North Sea since only middle or narrow spectra exist. This confirms the existing literature.

Relevance for fatigue modelling
Besides the accuracy bounds for Song's method, the case study emphasizes the critical parts for reliable mooring line fatigue simulations. When simplifying or speeding up such calculations, correctly calculating the non-Gaussian mooring line response is critical for accurate results. Increasing wave height and non-linear waves increase the skewness and kurtosis of the surge response spectrum of the floater. The increasing non-Gaussian behaviour leads to an increased probability of outliers of the response and, thus, the damage in the mooring lines.

Moreover, environmental forces like wind and constant current result in Gaussian mooring line response. In contrast, the wave-induced tensions for mooring lines lead to non-Gaussian responses and tensions. The resulting response outliers are significant for the total fatigue damage and are difficult to predict. Therefore the non-linear wave-induced motions are the most critical parameter for reliable fatigue calculations and must be considered for simplifying fatigue mooring line calculations.

7

Discussion

This thesis concludes on the accuracy of a lumping block method's applicability in different wave spectra based on a comparison with comprehensive time domain fatigue assessment. Moreover, the assumptions described in section 5.5 frame the results and show the included parts of comprehensive fatigue time-domain simulations. The results of the original time domain simulations align with the expectations since the absolute damage is in the correct order of magnitude, and the damage caused by a varying peak enhancement factor corresponds to the physical change in wave height and period.

In addition, the results of the lumping block method simulations for the different wave spectra are also in line with the theory. Firstly, a narrow spectrum yields accurate results, as described in other studies. Besides, the model's reliability decreases when the broadening of a wave spectrum causes damage-increasing conditions, like outliers in wave periods and irregular waves.

The lumped fatigue results are normalized to compare and generalize the results with the original time domain simulations. The 4 and 8 blocks cases gain the most insight by isolating the frequencies above resonance, which indicates poor reliability for long wavelengths. The simulations are repeatable, although slight differences arise within the Jonswap-generated waves.

To increase repeatability and reliability, more time simulations should be considered to determine ζ, which links the spectral wave energy to the cumulative damage. This thesis only links sea conditions, and the corresponding damage of one scatter diagram to fit ζ. Simulating a broader range of sea conditions would improve the proposed results. This way, the factor becomes more confident, and higher regression factors can be achieved.

Recommandations
Before getting a safe and efficient lumping block method for practical implementation, the method must account for all environmental conditions. The results in this thesis show the method's reliability significantly decreases under extreme wave conditions. However, the results show the method's accuracy for narrow and middle-broad spectra. Several variables must be tested to validate the method under all wave conditions and create a method applicable to all sea states. The following recommendations emerge from this study.

Firstly, change ζ to a parameter with a component that accounts for different wave spectra, such that representative wavelengths above the resonance periods account for the number of frequencies in the wave spectrum and the associated increase in non-Gaussian surge response. At the moment, ζ is of great interest for reliability, while the factor directly and only depends on the spectral wave energy and, thus, on the wave height. Since the proposed method does not consider a changing wavelength parameter, the effects are not included, leading to poor lumping block calculations if significant changes occur. Changing the ζ as proposed may make the method reliable for broad or changing wave spectra.

Secondly, quantifying the non-linear relation between the wave period to the corresponding damage is hard. The outlined problem can be solved by combining the lumping block with the original time domain simulations for the broad wave spectra. Since a misfit in the wave period as input for the simulations leads to enormous and varying errors for the resulting damage. In contrast, a misfit of wave height only causes a constant and less severe error. Moreover, significant lumping method errors occur in load cases with high wave heights and long wave periods. Therefore studying the effects for accuracy and efficiency when calculating the inaccurate lumping load cases based on regular time-domain simulations and lumping beyond and below these load cases is recommended. This combination ensures the critical non-Gaussian motions are included in the fatigue calculation and could still achieve serious efficiency.

The previous paragraph indicates an option to improve the accuracy of the lumping method by combining the lumping block method and original time domain simulations. Of course, many ways of lumping the scatter diagram could be possible to improve the method's accuracy. Instead of blocking based on equal grids, a promising method based on probability appears. This way, the lumping blocks divide the scatter diagram, where each block has an equal probability of occurrence. Although this way of lumping focuses less on the extremes in period and height, a more precise calculation will be made for the most common load cases, which dominate the total fatigue. Generally, the arrangement of the lumping blocks over the scatter diagram is an important recommendation.

In addition, this thesis focuses on a single wave direction without wind. Environmental conditions where wave directions change and wind occurs do exist and change the mooring line damage significantly. Literature indicates wind and wind-wave combination attributes to additional mooring line damage. Although linear, this is a comparative environmental effect as the damage increases through a broader spectrum. Therefore including wind force can lead to the same complications as this study. In addition, an omnidirectional wave spectrum will impact the damage as well. After all, sea states have multi-directional wave spectra, and the wind is usually present. Hence this follow-up study will indicate if and how the lumping block method can be used for practical implementation.

A final check focuses on the parameters that affect the ζ. The results of this study suggest ζ mainly depends on the shape of the floater and not the environmental conditions. Follow-up research should show how easy the lumping block method is to implement for other floaters and concludes on the method's genericity and power to use.

References

[1] Yüksel Ruwad Alkarem and BO Ozbahceci. "A complemental analysis of wave irregularity effect on the hydrodynamic responses of offshore wind turbines with the semi-submersible platform". In: *Applied Ocean Research* 113 (2021), p. 102757.

[2] Christopher Allen et al. *Definition of the UMaine VolturnUS-S reference platform developed for the IEA Wind 15-megawatt offshore reference wind turbine*. Tech. rep. National Renewable Energy Lab.(NREL), Golden, CO (United States); Univ. of . . ., 2020.

[3] Jose Azcona et al. "Impact of mooring lines dynamics on the fatigue and ultimate loads of three offshore floating wind turbines computed with IEC 61400-3 guideline". In: *Wind Energy* 20.5 (2017), pp. 797–813.

[4] Yoon Hyeok Bae, MH Kim, and Q Yu. "The dynamic coupling effects of a MUFOWT (multiple unit floating offshore wind turbine) with partially broken blade". In: *The Twenty-fourth International Ocean and Polar Engineering Conference*. OnePetro. 2014.

[5] Denis Benasciutti and Roberto Tovo. "Spectral methods for lifetime prediction under wide-band stationary random processes". In: *International Journal of fatigue* 27.8 (2005), pp. 867–877.

[6] Antonio Bonaduce et al. "Wave climate change in the North Sea and Baltic Sea". In: *Journal of Marine Science and Engineering* 7.6 (2019), p. 166.

[7] Tony Burton et al. *Wind energy handbook*. John Wiley & Sons, 2011.

[8] DJT Carter. "Estimation of wave spectra from wave height and period". In: (1982).

[9] Anteng Chang et al. "Wave-scatter lumping strategies for fatigue damage assessment". In: *The Eleventh ISOPE Pacific/Asia Offshore Mechanics Symposium*. OnePetro. 2014.

[10] Crown Estate Scotland 2022. *Scotwind*. 2022. URL: `https://www.crownestatescotland.com/our-projects/scotwind` (visited on 09/07/2022).

[11] RC Curi et al. "Application of a Distributed Parameter Filter to Predict Simulated Tidal Induced Shallow Water Flow". In: *Stochastic and Statistical Methods in Hydrology and Environmental Engineering*. Springer, 1994, pp. 211–223.

[12] Jian Dai et al. "Effect of wave inhomogeneity on fatigue damage of mooring lines of a side-anchored floating bridge". In: *Ocean Engineering* 219 (2021), p. 108304.

[13] Ulverston Daltongate. *Orcina Ltd*. 2022. URL: `https://www.orcina.com/` (visited on 05/31/2022).

[14] DHI. *Decode offshore wind engineering challenges at every stage*. 2021. URL: `https://blog.dhigroup.com/2021/10/19/decode-offshore-wind-engineering-challenges-at-every-stage/` (visited on 07/07/2022).

[15] Evan Gaertner et al. *IEA wind TCP task 37: definition of the IEA 15-megawatt offshore reference wind turbine*. Tech. rep. National Renewable Energy Lab.(NREL), Golden, CO (United States), 2020.

[16] Hanbin Ge, Lan Kang, and Yasuhiro Tsumura. "Extremely low-cycle fatigue tests of thick-walled steel bridge piers". In: *Journal of Bridge Engineering* 18.9 (2013), pp. 858–870.

[17] Jun Sik Han et al. "A comparative study on the fatigue life of mooring systems with different composition". In: *Journal of Hydrodynamics* 22.1 (2010), pp. 435–439.

[18] K Hasselmann. "Measurements of wind wave growth and swell decay during the joint North Sea Wave Project (JONSWAP)". In: *Deutsche Hydrographisches Institut, Hamburg, Germany, UDC 551.466.31; ANE Clerman Bight* (1973).

[19] H. Holthuijsen. *Waves in Oceanic and Coastal Waters*. 1st ed. The Edinburgh Building, Cambridge CB2 8RU, UK: Cambridge, 2007.

[20] Hui-Min Hou, Guo-Hai Dong, and Tiao-Jian Xu. "An improved lumping block equivalent method for predicting fatigue damage of mooring system for fish cage". In: *Ocean Engineering* 193 (2019), p. 106567.

[21] Michaela Ibrion, Nicola Paltrinieri, and Amir R. Nejad. "Learning from Failures: Accidents of Marine Structures on Norwegian Continental Shelf over 40 Years Time Period". In: *Engineering Failure Analysis* 111 (Mar. 2020), p. 104487. DOI: 10.1016/j.engfailanal.2020.104487.

[22] Junbo Jia. "An efficient nonlinear dynamic approach for calculating wave induced fatigue damage of offshore structures and its industrial applications for lifetime extension". In: *Applied Ocean Research* 30.3 (2008), pp. 189–198.

[23] Massie W Journee J. *OFFSHORE HYDROMECHANICS*. Tu Delft, 2019.

[24] Garbis H Keulegan, Lloyd H Carpenter, et al. "Forces on cylinders and plates in an oscillating fluid". In: *Journal of research of the National Bureau of Standards* 60.5 (1958), pp. 423–440.

[25] Kolstein. "Fatigue in steel structures". In: (2007).

[26] Marit I Kvittem and Torgeir Moan. "Time domain analysis procedures for fatigue assessment of a semi-submersible wind turbine". In: *Marine Structures* 40 (2015), pp. 38–59.

[27] Marit I Kvittem et al. "Short-term fatigue analysis of semi-submersible wind turbine tower". In: *International Conference on Offshore Mechanics and Arctic Engineering*. Vol. 44342. 2011, pp. 751–759.

[28] Huajun Li et al. "Investigation on the probabilistic distribution of mooring line tension for fatigue damage assessment". In: *Ocean Engineering* 124 (2016), pp. 204–214.

[29] Alexander Lindorf and Manfred Curbach. "S–N curves for fatigue of bond in reinforced concrete structures under transverse tension". In: *Engineering Structures* 32.10 (2010), pp. 3068–3074.

[30] Kai-Tung Ma et al. *Mooring system engineering for offshore structures*. Gulf Professional Publishing, 2019.

[31] Dimitris I Manolas et al. "Hydro-servo-aero-elastic analysis of floating offshore wind turbines". In: *Fluids* 5.4 (2020), p. 200.

[32] Milton A Miner. "Cumulative damage in fatigue". In: (1945).

[33] Kim E Mittendorf. "Joint description methods of wind and waves for the design of offshore wind turbines". In: *Marine Technology Society Journal* 43.3 (2009).

[34] JR Morison, JW Johnson, and SA Schaaf. "The force exerted by surface waves on piles". In: *Journal of Petroleum Technology* 2.05 (1950), pp. 149–154.

[35] Kolja Müller and Po Wen Cheng. "Application of a Monte Carlo procedure for probabilistic fatigue design of floating offshore wind turbines". In: *Wind Energy Science* 3.1 (2018), pp. 149–162.

[36] Y Murakami et al. "Fatigue crack path and threshold in Mode II and Mode III loadings". In: *Engineering Fracture Mechanics* 75.3-4 (2008), pp. 306–318.

[37] Dag Myrhaug and Søren Peter Kjeldsen. "Steepness and asymmetry of extreme waves and the highest waves in deep water". In: *Ocean Engineering* 13.6 (1986), pp. 549–568.

[38] A. Adams N. Barltrop. *Dynamics of fixed marine structures*. 1st ed. Jordan Hill, Oxford Ox2 8DP: Atkins Oil & Gas Engineering Limited, 2007.

[39] John Nicholas Newman. "Second-order slowly varying forces on vessels in irregular waves". In: *Proceedings of the international symposium on dynamics of marine vehicles and structures in waves. London, UK, 1974*. 1974.

[40] Norwegian petroleum. *Norwegian petroleum*. 2022. URL: https://www.norskpetroleum.no/en/interactive-map-quick-downloads/interactive-map/?mapv2ObjType=field&mapv2ObjId=26465170 (visited on 09/07/2022).

[41] Orcina. *Line theory: Line pressure effects*. 2021. URL: https://www.orcina.com/webhelp/OrcaFlex/Content/html/Linetheory,Linepressureeffects.htm (visited on 05/25/2022).

[42] Willard J Pierson Jr. "Wind generated gravity waves". In: *Advances in geophysics*. Vol. 2. Elsevier, 1955, pp. 93–178.

[43] I. Rychlik. “A new definition of the rainflow cycle counting method, International Journal of Fatigue”. In: *International Journal of Fatigue* Volume 9, Issue 2 (1987), pp. 119–121.

[44] M Sakano and Muhammad Abdul Wahab. “Extremely low cycle (ELC) fatigue cracking behaviour in steel bridge rigid frame piers”. In: *Journal of Materials Processing Technology* 118.1-3 (2001), pp. 36–39.

[45] Matthew L Schirmann, Matthew D Collette, and James W Gose. “Significance of wave data source selection for vessel response prediction and fatigue damage estimation”. In: *Ocean Engineering* 216 (2020), p. 107610.

[46] John M Sheehan et al. “Characterizing the wave environment in the fatigue analysis of flexible risers”. In: (2006).

[47] Emanuel PP Soares-Ramos et al. “Current status and future trends of offshore wind power in Europe”. In: *Energy* 202 (2020), p. 117787.

[48] Xiancang Song and Shuqing Wang. “A novel spectral moments equivalence based lumping block method for efficient estimation of offshore structural fatigue damage”. In: *International Journal of Fatigue* 118 (2019), pp. 162–175.

[49] Xiancang Song et al. “An innovative block partition and equivalence method of the wave scatter diagram for offshore structural fatigue assessment”. In: *Applied Ocean Research* 60 (2016), pp. 12–28.

[50] Yupeng Song et al. “Multi-parameter full probabilistic modeling of long-term joint wind-wave actions using multi-source data and applications to fatigue analysis of floating offshore wind turbines”. In: *Ocean Engineering* 247 (2022), p. 110676.

[51] Philipp R Thies et al. “Mooring line fatigue damage evaluation for floating marine energy converters: Field measurements and prediction”. In: *Renewable Energy* 63 (2014), pp. 133–144.

[52] Maura Vaccarelli, Roberto Carapellucci, and Lorena Giordano. “Energy and economic analysis of the CO2 capture from flue gas of combined cycle power plants”. In: *Energy Procedia* 45 (2014), pp. 1165–1174.

[53] Det Norske Veritas. “Riser fatigue”. In: *Recommended Practice DNV-RP-F204, Hovik, Norway* (2005).

[54] Yongyan Wu et al. “Governing factors and locations of fatigue damage on mooring lines of floating structures”. In: *Ocean Engineering* 96 (2015), pp. 109–124.

[55] Kun Xu et al. “Effect of wave nonlinearity on fatigue damage and extreme responses of a semi-submersible floating wind turbine”. In: *Applied Ocean Research* 91 (2019), p. 101879.

[56] Kelvin O Yoro and Michael O Daramola. “CO2 emission sources, greenhouse gases, and the global warming effect”. In: *Advances in carbon capture*. Elsevier, 2020, pp. 3–28.

List of Figures

List of Tables

A

The system

A.1. Damping coefficients

This appendix contains the graphs associated with free decay tests. The first two graphs belong to sway and surge, figure A.3 and A.4 show the values for roll and pitch. The last two graphs belong to the movements for heave.

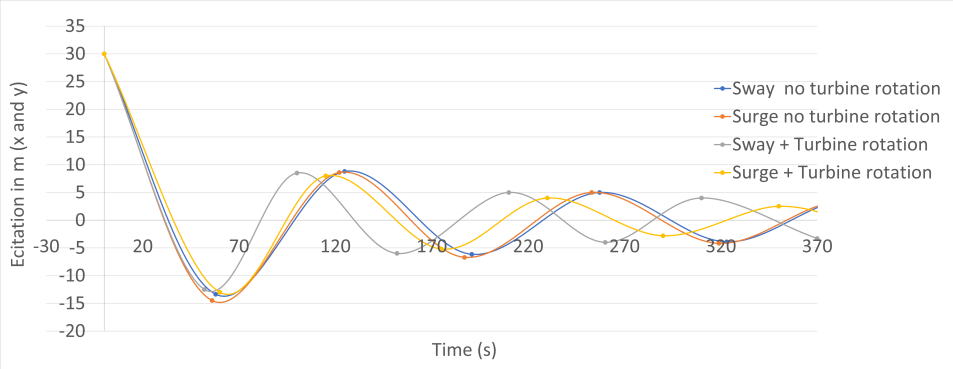

Figure A.1: Damping of sway and surge after a 30 m excitation.

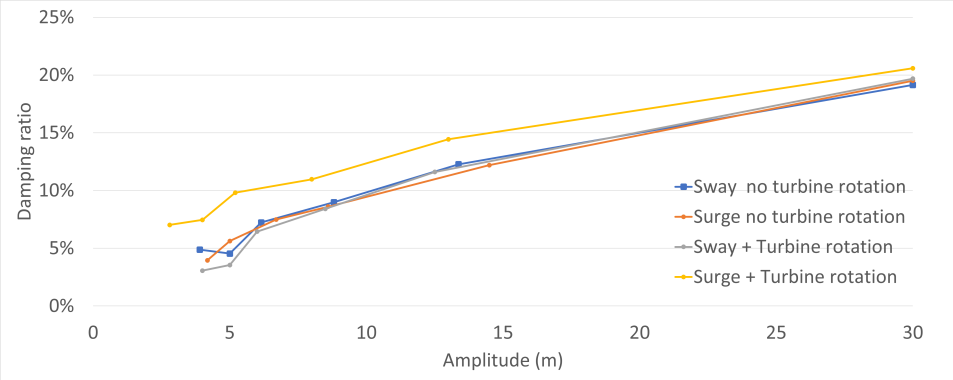

Figure A.2: Damping coefficients of sway and surge after a 30 m excitation.

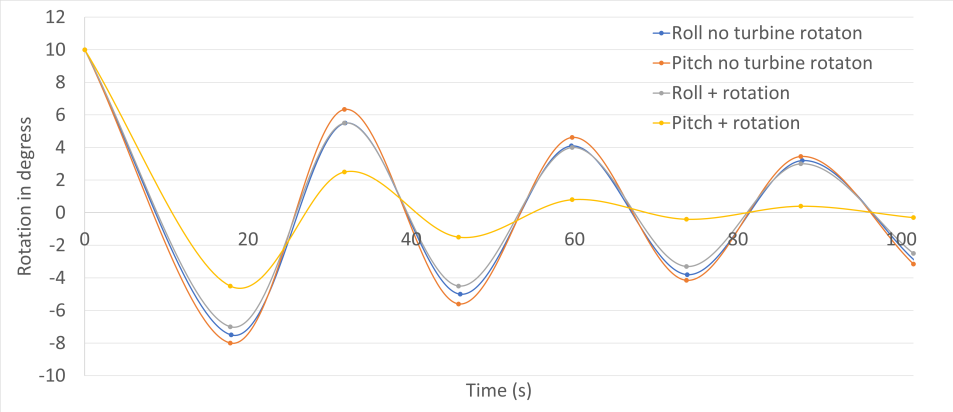

Figure A.3: Damping of roll and pitch after a 10 °.

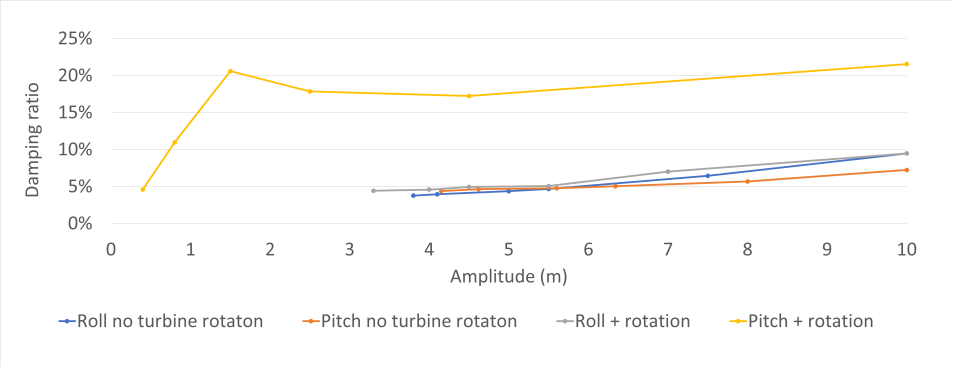

Figure A.4: Damping coefficients of roll and pitch after a 10 °.

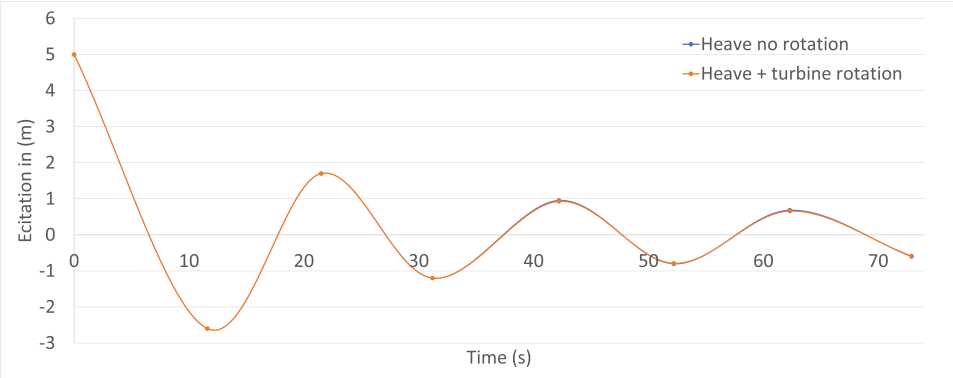

Figure A.5: Damping of heave after a 10 m.

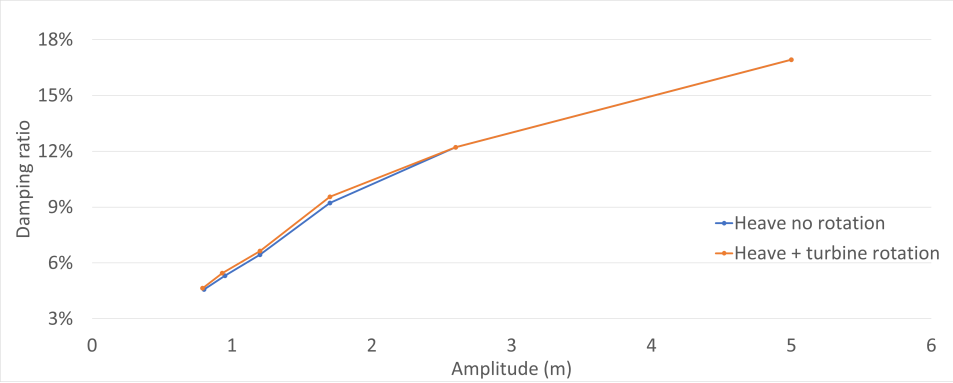

Figure A.6: Damping coefficients of heave after a 10 m.

A.2. Response spectra of the mooring lines

The maximum peaks lay around $120e^3\ Kn^2/Hz$. The peaks from wave period 2-5 s are around $0.5e^3\ Kn^2/Hz$. For the periods 6 - 11 s, the peaks are in the range of $60-90e^3\ Kn^2/Hz$ except for the resonance peaks 9 and 10 s. The peaks above 11 s decrease, for the 12 - 15 s periods the maximum tension lies around $30e^3\ Kn^2/Hz$, and the above 15 s the peaks are in the order of magnitude of $5e^3\ Kn^2/Hz$. The unit means is comparable to an impulse force times the force.

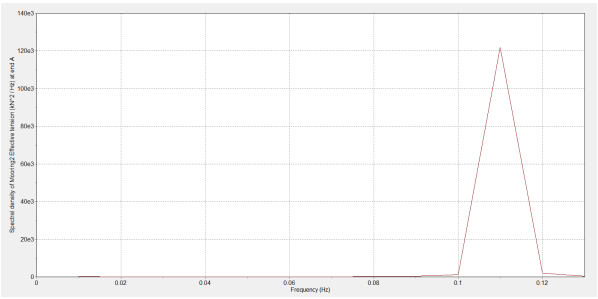

Figure A.7: Tension spectrum for a wave period of 9 seconds, with a peak of 2470 kN^2/Hz at point $f = 0.111Hz$. For mooring line 2.

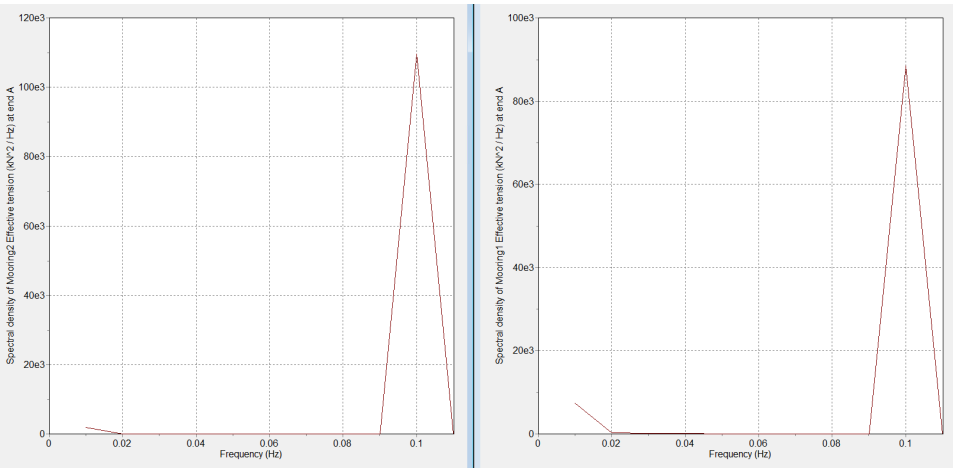

Figure A.8: Tension spectrum for a wave period of 10 seconds, both peaks of 2386 kN^2/Hz at point $f = 0.1Hz$. For mooring lines 1 and 2.